UNIVERSITY OF AGDER

Design and Installation of a Grid-Connected PV System

John Christer Sivertsen
Petter Søyland

Supervisor
Georgi Hristov Yordanov

This master's thesis is carried out as a part of the education at the University of Agder and is therefore approved as a part of this education. However, this does not imply that the University answers for the methods that are used or the conclusions that are drawn.

University of Agder, 2014
Faculty of Engineering and Science
Department of Engineering Sciences

Abstract

As the worlds electrical demand is being more covered by photovoltaic (PV) systems, Germany installed 3.3 GW of the worlds PV systems in 2013 compared to 0.6 MW being installed in Norway. Irradiation measurements done for southern Norway indicates that the conditions for more PV systems being installed are good when comparing irradiation in Grimstad to Hamburg. This thesis addresses the initial steps of planning and building a PV system to analysing how the inverter handles the varying irradiance in southern Norway.

To investigate the opportunities in Grimstad, a Theia HE-t 3.8 string inverter from Eltek was installed along with 23 de-rated PV modules to constitute a PV system of 2.116 kW_p. The PV system was estimated to have a system loss of 20.4 % and a yearly production of 2088 kWh with an average performance ratio of 80 %, which is considered to be good for a small PV system with aged PV modules. From when the system started commissioning to when this thesis was finalized, approximately one month of measurements was recorded, providing information on how the inverter operated on clear and cloudy days as well as days with overirradiance.

Results indicate that the inverter efficiency drops during early and late operating hours on sunny days, as well as during midday on cloudy days. This was found to be a result of the inverter using two different algorithms for low and high irradiance. When the inverter switches algorithms, it could operate at a not optimal efficiency for 10 minutes up to two hours dependent of the available irradiance, the inverter will then operate at a high efficiency for as long as it is operating with one specific algorithm. One day with overirradiance reviled that the inverter responds rapidly to sudden irradiance changes and were able to produce 2.8 kW_{AC} at irradiance close to 1.5 suns. It therefore has good preconditions for handling varying irradiance while operating at an average high efficiency. For the one month of operation the inverter managed to produce 313 kWh, which is more than was estimated for May. With a lack of more months to compare with and from the results recorded for May, the PV system has good prospects for future operation and to produce the expected 2088 kWh/year or more.

Preface

This is a master's thesis submitted in fulfilment of the requirements for the degree of Master in Technology in Renewable Energy at the department of engineering sciences, University of Agder. We would like to thank our supervisor Dr Georgi Hristov Yordanov for good comments, explanations, discussions and help at all aspects during the progress of this thesis.

We would like to thank Bjørn Lindemann, Stein Bergsmark and Kristen Leifsen from UiA who were essential for obtaining approvals, providing electrical services and components, and securing a good communication with Rolf Håkan Josefsen from Agder Energi regarding the grid connection of the inverter. We would also like to thank Kjetil Boysen and Espen Kristensen from Eltek for advices regarding the inverter, providing the PC tool (Theia Analyzer) and the python script for data logging.

An extra thanks is sent to Stein Bergsmark for giving valuable constructive criticism on the content and language of the thesis as well as project funding, giving us the possibility to buy the inverter, execute the grid connection and write a good thesis.

Last but not least we would like to thank Prof. Tor Oskar Sætre from UiA who provided part of the funding for the project's implementation and Steve Schading from UiA who advised on the selection of proper fasteners for mounting the PV modules in order to avoid galvanic corrosion.

Grimstad, June 2014.

John Christer Sivertsen

Petter Søyland

Contents

List of Figures

List of Tables

Abbreviations

AC	**A**lternating **C**urrent
BIPV	**B**uilding-**I**ntegrated **P**hotovoltaics
CAN	**C**ontrol **A**rea **N**etwork
CCC	**C**urrent **C**arrying **C**apacity
DC	**D**irect **C**urrent
DSP	**D**igital **S**ignal **P**rocessor
FoL	**R**egulation of **S**upply **Q**uality in the **P**ower **S**ystem
GSES	**G**lobal **S**ustainable **E**nergy **S**olutions
HF	**H**igh **F**requency
IEA	**I**nternational **E**nergy **A**gency
IGBT	**I**nsulated **G**ate **B**ipolar **T**ransistor
JRC	**J**oint **R**esearch **C**entre (of the European Commission)
LF	**L**ow **F**requency
MOSFET	**M**etal-**O**xide-**S**emiconductor **F**ield-**E**ffect **T**ransistor
MPP	**M**aximum **P**ower **P**oint
MPPT	**M**aximum **P**ower **P**oint **T**racking
NVE	**N**orwegian **W**ater **R**esources and **E**nergy **D**irectorate
PCC	**P**oint of **C**ommon **C**onnection
PR	**P**erformance **R**atio
PVGCS	**P**hotovoltaic **G**rid **C**onnected **S**ystem
PVGIS	**P**hotovoltaic **G**eographical **I**nformation **S**ystem
PWM	**P**ulse **W**idth **M**odulation
RCD	**R**esidual-**C**urrent **D**evice
RMS	**R**oot **M**ean **S**quare
STC	**S**tandard **T**est **C**onditions

THD	**T**otal **H**armonic **D**istortion
UiA	**U**niversity of **A**gder
PR	**P**erformance **R**atio

Chapter 1

Introduction

In this chapter, the background and motivation of this thesis is explained. The project description is presented, with goals, objectives, key assumptions and an outline of the thesis.

1.1 Motivation

By year 2020 the European Union aims to get 20 % of its energy from renewable sources [1]. One of the technologies helping EU reach this goal is photovoltaic (PV) power generation, which has grown rapidly in Europe due to governmental support. PV systems are a competitive alternative to other renewable sources currently because of subsidies and in some countries like Germany they can even compete with building new fossil fuel plants. The International Energy Agency (IEA) PV power systems programme registered that approximately 39.9 GW of PV systems was installed over the world throughout 2013, which was an increase of 7.9 GW compared to the past two years. The PV installations in Europe decreased that year, installing only 10.3 GW compared to 17 GW in 2012. China was the country installing most PV systems in the world in 2013 with its 11.3 GW compared to Germany with 3.3 GW and Norway with 0.6 MW [2]. PV systems in Norway have traditionally been mostly limited to residential housings and boats where connection to the electrical grid is difficult. Grid connected systems have not been widely developed in Norway due to both technical and economic barriers with no support from the government. Getting concession to feed energy into the grid has been a relatively complicated process suited for professional electricity producers. However, in 2010 NVE made an exception to the regulations to make it easier for customers to feed energy into the grid. In the near

future, it is expected that Norway will have a complete framework of regulations making it more beneficial and easier to buy and install a grid-connected PV system, which may give the required boost necessary to create a more healthy and mature PV market in Norway.

1.2 Project Description

The purpose of this master project is to establish and learn the necessary skills and experience required to build a grid-connected PV system. The project involves planning and designing; decide array size, number of strings, circuit breakers and choose modules based on I-V curve measurements; install and connect the PV system to the grid; perform commissioning; operate the PV system and analyse operational data. PV modules from the former National Renewable Energy Centre (Energiparken) will be reused in this project. Some of these PV modules are already mounted on the planned installation site and will be complemented with additional modules if the I-V-characteristics are of good quality.

FIGURE 1.1: Installation site for the PV system.

1.2.1 Goals and Objectives

Goals

The goals of this project are to:

- Plan and design a grid connected PV system.

- Install and if possible (depending on I-V curve measurements) reuse modules already present at the installation site. Wire modules in one or two strings and connect to inverter and grid with help from the certified staff of UiA.
- Perform commissioning of the PV system.
- Analyse inverter performance and operational data.

Objectives

In order to accomplish the goals of this project the following objectives are needed.

- Study the present and the expected Norwegian regulations for feeding power into the AC grid and study the policy of the local grid owner Agder Energi.
- Study the local market for PV inverters and determine the most suitable model(s). Detailed logging on the AC and DC sides is required and the inverter should have a power rating of about 3.5 kW.
- Compare the local tilted irradiation from the years 2011-2013 to the long-term prediction of PVGIS.
- Measure the current-voltage (I-V) characteristics of the available PV modules; identify the modules with drastically reduced current; choose modules with the best characteristics for the PV array.
- Size the PV system with respect to the power rating of the inverter; maximum system voltage of the modules; the no-exceed voltage of the inverter; and available space at the chosen installation site.
- Determine the maximum wind load expected on the PV modules.
- Install PV modules, connect them in strings and label each of the modules according to its position in the PV array.
- Analyse operational data, such as: energy harvest, current and output power.
- Investigate how the inverter performs throughout the day at different irradiance conditions.

If Time Allows

The following objectives will be considered if time allows.

- If there are days with extreme overirradiance events, and if the data logger offers very fine temporal resolution, assess the inverter performance during the strongest bursts.

1.2.2 Key Assumptions

In order to complete the goals and objectives this project is based on the following assumptions:

- Permission will be granted from Agder Energi, the Faculty's administration and the building owner J.B. Ugland Eiendom to connect the PV system to the grid.
- System parts are provided and installed in time.
- Access to necessary software and licences.
- The link between the inverter and the AC grid will be made timely by certified staff of UiA.

1.3 Thesis Outline

The objectives state that an inverter has to be chosen for the PV system. Chapter 2 will explain the basics on how a full-bridge voltage source inverter works and the different kinds of grid connected inverters existing on the market.

Chapter 3 explains the different principles of grid connection, like islanding, microgrid, phase-current, etc. Then, a review of the application process for connecting the PV system to a local utility grid is conducted and explained stepwise.

Chapter 4 presents an introduction to solar irradiance and the basic principles of measuring irradiance. Estimated irradiation from PVGIS is studied and compared with local measurements in Grimstad. External factors like temperature, wind load, temporary shading, corrosion, grounding and fire hazard are also explained in this chapter.

Chapter 5 is the most important part of the thesis and includes the results, discussion and issues. The selected inverters are compared and discussed before a decision is made for what inverter to select as well as the local regulations for grid connection of a private production plant given by Agder Energi, which the inverter must comply with. The information is evaluated and cited in Section 5.2 and 5.3, giving restrictions for the required inverter power quality and disconnection times in case of a grid fault. Factors with a direct influence on the performance and causing losses in the PV system are discussed in Section 5.5. Chapter 5 also contains a full guideline on how to design a PV system from the array- and cable sizing to calculating losses and system protection. In Section 5.6 it is explained how the available PV modules from the former National Renewable Energy Centre (Energiparken) are connected and tested. The I-V curves for each module are measured by using a computer-controlled electronic load. Prior to the mechanical and electrical installation process, a list of the best PV modules is made by analysing the measured I-V curves. The installation process is presented in Section 5.7 and covers the mechanical and electrical installation together with the inverter installation, commissioning of the PV system and thermal imaging. In addition, operational data from the PV system with one-second resolution from a few days of operation are analysed and discussed in Section 5.8 explaining how the inverter is performing at low-, high- and over-irradiance.

How to design a PV system is explained in detail in the Australian manual "Grid-connected PV systems Design and Installation" [3] and the German manual "Planning and Installing Photovoltaic Systems, a guide for installers, architects and engineers" [4]. These manuals are used throughout the whole project as guidelines to design the array size, cable size and protection devices (lightning and earthing). The German manual was at some times hard to come by from the library, since it was often on loan to other groups. The Australian manual is therefore mostly used. This did however, not cause an issue since the two manuals are very alike and the Australian manual is even referring to the German manual. The largest difference between the two is the extent they explain methods and different concepts. The German manual is more detailed and is explaining around a concept and sub-concepts. The Australian manual is more basic, giving easy explanations and more step-by-step procedures, which are easy to understand and follow when designing the system.

Chapter 2

PV Inverters

DC power cannot be fed directly into the utility grid. Power electronic circuits in the inverter are therefore essential to produce the maximum amount of power (MPP). The DC power produced in the PV array is converted to AC power with the required output voltage and frequency by the inverter, making it ready to be used by electrical appliances or exported to the electrical grid [5], [6]. This chapter presents the basic topology for a full-bridge voltage source inverter and the different types of inverters available on the market.

2.1 The Basic Inverter

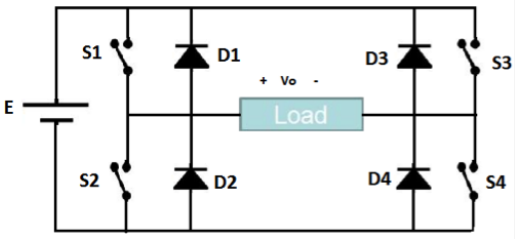

FIGURE 2.1: Full-bridge voltage source inverter [5].

The full-bridge voltage source inverter in Figure 2.1 consists of four switches and four freewheeling diodes. The four switches are turned "ON" and "OFF" so that only the diagonal switches are on at each half-cycle (e.g. S1 and S4). The load is then alternately connected to the DC source in each direction. The system operates with a time period between 0 and T. Between 0 and $T/2$ two switches are "ON" and $V_0 = +E$, between $T/2$ and T the other two switches

are turned "ON" and $V_0 = -E$. The output voltage is a square wave AC waveform with a frequency $f = 1/T$ as shown in Figure 2.2. The frequency is controlled by the on- and off- rate of the switches and gives a square wave voltage with E as its amplitude [5]. By turning the switches "ON" and "OFF" several times in a cycle, it is possible to create an harmonic profile similar to a sinusoidal.

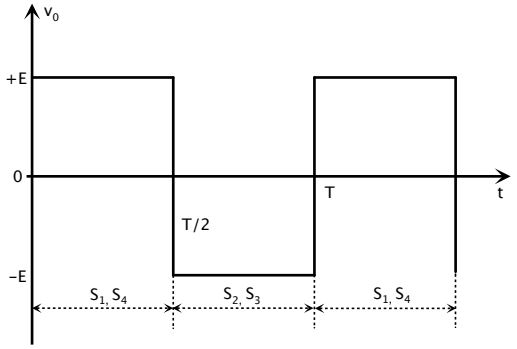

FIGURE 2.2: Output square waveform from the full-bridge voltage source inverter [5].

The switches in Figure 2.1 can be replaced by semiconductor switches as seen in Figure 2.4. There are several types of semiconductor switches used in general electronic circuits, but the majority of them are rarely used. Semiconductors mostly used in modern inverters are usually MOSFETs, which are used at smaller power ratings, and IGBTs which are used at larger power ratings [7], [8]. A semiconductor switch can be turned "ON" and "OFF" by using a comparator that compares an input voltage to a reference signal and thereby turn the semiconductor switches "ON" or "OFF", depending on the results from the compared signals. Figure 2.3 illustrates two comparators and how comparison of the input voltages determines if the IGBTs in Figure 2.4 are turned "ON" or "OFF" [9].

Pulse Width Modulation (PWM) is an efficient method to control the output of the inverter and ensure stable RMS output value. By using PWM, the output voltage of the inverter can be controlled by modifying the width of the pulses. A small control signal in direct proportion with the pulses controls the width as a higher or lower control voltage increases or decreases the width of the pulses, respectively. The control voltage can consist of a sinusoid of the desired frequency and thereby produce a waveform where the average voltage varies sinusoidally. If the control voltage to the IGBTs in Figure 2.4 is 0 V, then v_u and v_v are identical and v_{load} is 0 V. By assuming there is a constant positive input voltage v_{in}, which is equal to $\frac{1}{2}$ of the peak reference voltage v_x and v_y, then v_{load} will be a train of pulses with the same width i.e. 50 %

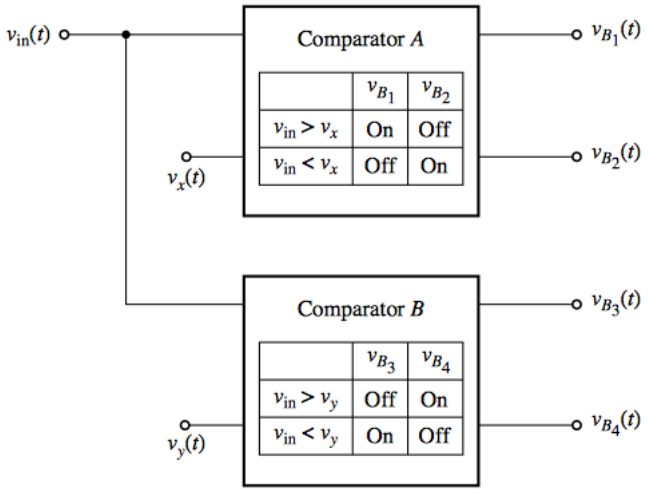

FIGURE 2.3: Comparators used to control the IGBTs [9].

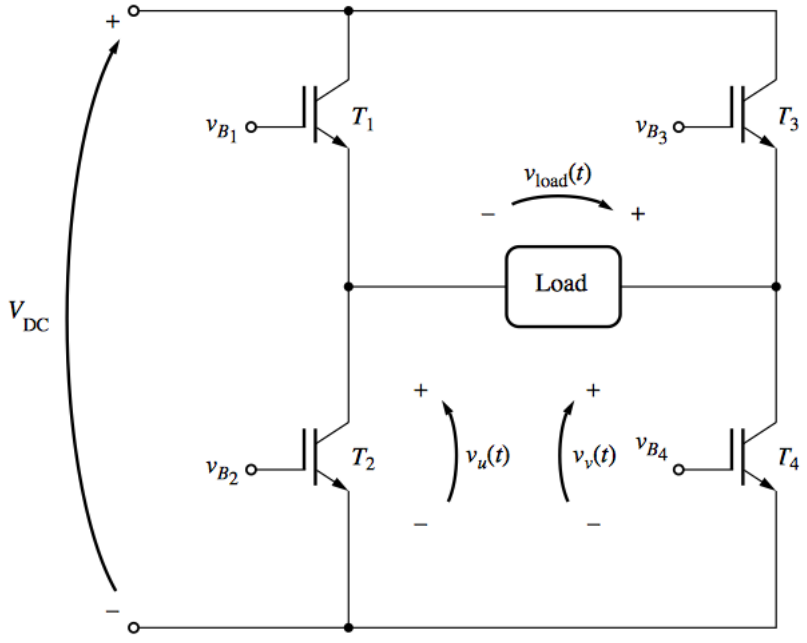

FIGURE 2.4: Full-bridge voltage source inverter with IGBTs [9].

duty cycle. If the input voltage v_{in} is a sinusoidal voltage, the width of the train pulses will vary sinusoidally with v_{in} and produce an output voltage v_{load} as seen in Figure 2.5 [9].

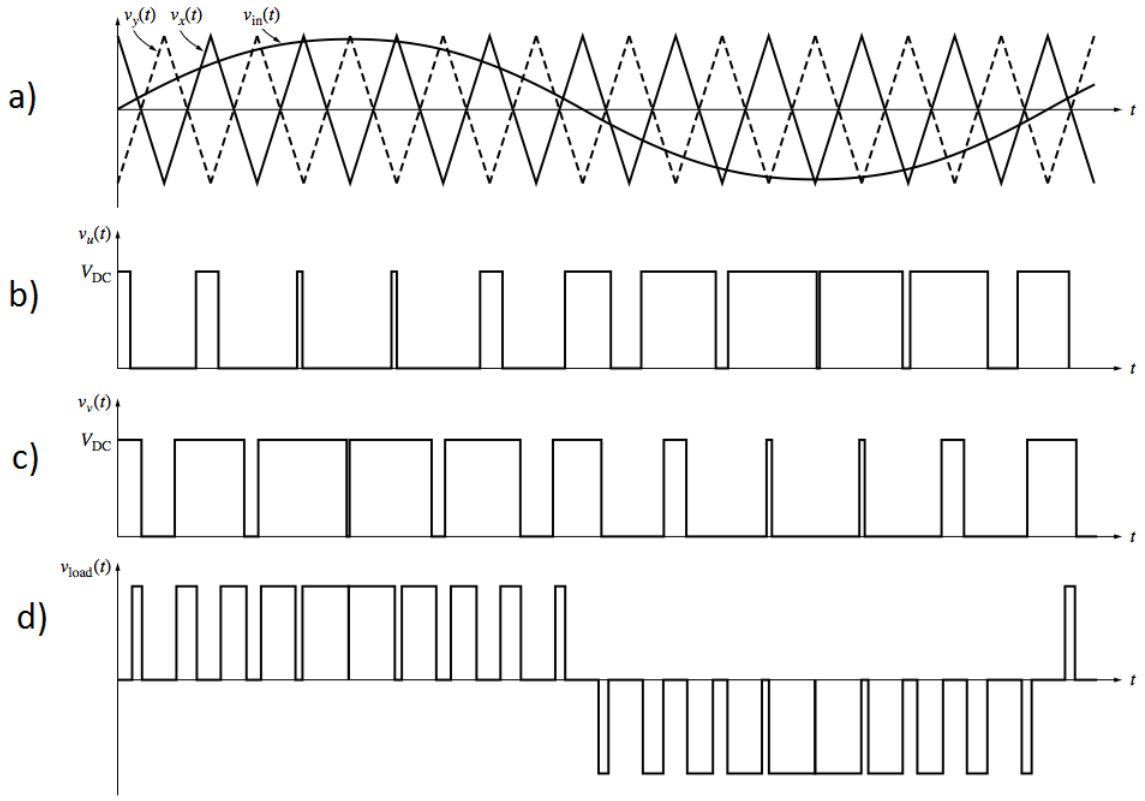

FIGURE 2.5: The output of the full-bridge voltage source inverter with a sinusoidal control voltage applied. a) is the voltage input to the comparator, b) is the voltage pulse from T_2 and T_3 in Figure 2.4, c) is the voltage pulse from T_1 and T_4 and d) is the output voltage pulse over the load [9].

Figure 2.6 illustrates how the DC voltage (flat) runs through the full-bridge inverter and by using PWM can achieve an approximate sine-wave output from pulse waves provided by the switches [3]. As seen from "180 V_{AC} raw," the PWM is a source of harmonic distortion, which need to be filtered through an inductor. All of the harmonics is, however, not always filtered out and a capacitor is often added (to create an LC-filter) to reduce the remaining harmonics [8].

2.2 Inverter Transformers

Grid Connected inverters can be divided into three basic concepts and technologies: With a low frequency (LF) transformer, high frequency (HF) transformer and transformer-less inverter [10]. The LF and HF transformer electrically isolates the DC circuit from the grid (galvanic

isolation). Galvanic isolation is an expression for a topology in which the output circuit and the input circuit are isolated or separated both physically and electrically, removing the connection between output wires and input wires [11]. The advantages of using a LF or a HF transformer are therefore the electrical isolation between the AC and DC side of the transformer and transformer reliability because of few components. The HF transformer operates at higher frequencies and is more compact and lighter than the LF transformer. It also has less transformer losses and therefore a higher degree of efficiency when compared to LF transformer [10], [12].

There are a few inverters on the market with no transformer and they have a higher efficiency than inverters with a transformer (no transformer losses). This does, however, lead to a disadvantage; it has no galvanic isolation. Some extra safety measures must therefore be added, like a residual circuit breaker, for the inverter to be safe for use [10]. A DC-DC boost converter is added in the front of the inverter to provide the DC voltage needed to provide a suitable AC sine wave, like explained in Figure 2.5 [3]. When operating with a transformer-less inverter, there is a risk of supplying small amounts of DC current to the utility grid. A utility transformer is often installed within the switching sub-circuit of the inverter to prevent this and provide the necessary required isolating characteristics [13], [14]. The description of a transformer-less inverter could therefore in practice be changed to a less-transformer (fewer transformers) inverter [13].

2.3 Grid-connected Inverters

On the solar inverter market, manufacturers mainly produce two main types: Grid-connected and Stand-Alone inverters. As shown in Figure 2.6, the grid-connected inverter uses a grid sensing device and a digital signal processor (DSP) to ensure the inverter has a grid to connect to and "copy" its voltage amplitude and frequency. This is to ensure the grid-connected inverter produces exactly the same voltage and frequency as available on the grid, this is also known as *"grid-compatible sine wave AC electricity"* [15]. If the grid sensing device in Figure 2.6 does not find the voltage and frequency to copy, then switches in the inverter will disconnect it from the grid.

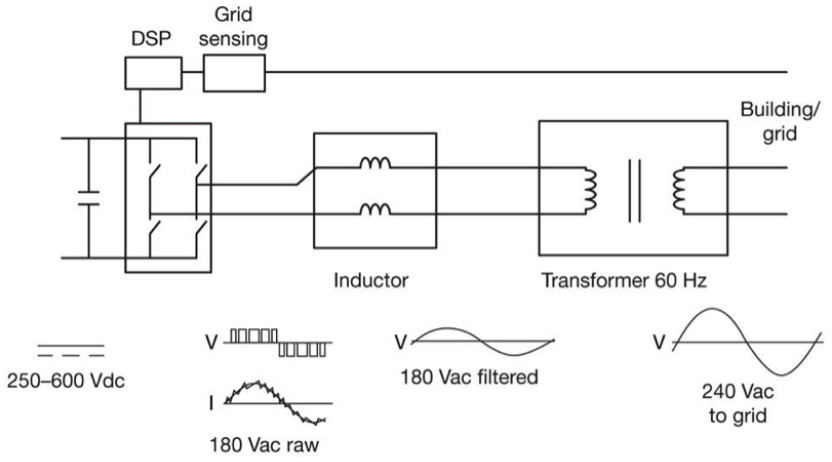

FIGURE 2.6: The basic topology of a grid connected, single phase, transformer-based inverter (at 60 Hz) [16].

2.3.1 MPPT

Grid-connected inverters normally use Maximum Power Point Tracking (MPPT) so the inverter can operate near the maximum power point and keep the output efficiency as high as possible [17]. The MPPT is an electrical system, which uses several different module electrical operating points to optimise the module performance. The tracker searches for the array's MPP at some specific times of the day to ensure that the environmental conditions have not moved the MPP [3]. The basic principle of the MPPT algorithms is the use of $\Delta P/\Delta V = 0$ (from $P = I \cdot V$) to find the array output MPP. The algorithm measures both ΔP and ΔV to find the array's momentary operating region and is using this when increasing or decreasing $V_{reference}$. By doing this, the MPPT algorithm ensures that the PV system operates by the MPP of the array at all time [17]. This method can, however, not track the MPP under rapid and instant changes in irradiance conditions. A more complex method called *"the incremental conductance method"* is an alternative [17], but will only be mentioned in this thesis.

2.3.2 Power Rating of Inverters

Different types of inverters are developed for the market according to their power ratings and depending on how large PV array the customer wants to connect to a single inverter. This varies from small modular inverters (micro inverters in AC PV modules) to large PV-inverters

generating 100 kW or more. An overview of the different inverter options is illustrated in Figure 2.7.

Central Inverters

Central inverters are normally used with a power rating from 30 kW to 1 MW in large grid-connected PV systems [3]. The largest solar power plant in California is located on Harper Dry Lake in the Mojave Desert with a power rating of 80 MW AC. A new solar power plant is under construction in Colorado Desert with an estimated power rating of 550 MW AC [18]. These are all using large central inverters with a high power rating. This system has the advantage of having all the components located at one location for maintenance, good inverter efficiency and lower cost per watt [3].

String Inverters

A string inverter is the most common inverter used in small grid-connected PV-systems. Some string inverters can serve up to two or three strings of PV modules, with an inverter power rating from 1 kW to 12 kW. However, with a single MPPT it is recommended to use a multi-string inverter for arrays over 5 kW [3]. The downside of having multiple strings in one string inverter is that only one MPPT is installed in each inverter. If one string is shaded then this will affect the output of the entire array, instead of just one string. Individual string inverters for each string could be an alternative but would also be more costly [3]. As illustrated in Figure 3.3, PV arrays based on string inverters are more flexible than PV arrays based on central inverters since they are both easier and cheaper to extend.

Multi String Inverters

The multi string inverter is an improvement of the string inverter where multiple MPPT's can be installed in one inverter. Multiple strings can then be controlled independently and the array can be easily extended, providing high efficiency without any troubles for the customer [7]. The multi string inverter is, however, more expensive than a string inverter because of the multiple MPPTs. One of the increased costs is the installation of extra DC protection in each string when multiple strings are using one DC-AC inverter [3].

Modular Inverters (Microinverters in AC-Modules)

The modular inverters only need to convert 100-300 W and are therefore very small. The transformer-less inverter is connected to the back of each module in the array, next to the junction box as a separate module or integrated into the junction box. The advantage of using this inverter is the removal of DC cabling in the array connections [3]. DC cables can carry higher voltages than AC cables, which will have lower voltages but higher currents. AC cables with larger cross section area and a wider isolation is therefore needed. Like in Figure 2.7, cables from AC-modules are connected together in parallel and then fed into the utility grid as a single phase. An array with modular inverters can easily be extended in the future by adding more modules. One disadvantage is if the modular inverter breaks down or need to be serviced, the whole module needs to be removed for it to be fixed. However, this could be compensated by better design for serviceability. The microinverter is also very expensive compared to other inverters in terms of cost per power rating [3]. It also produces more harmonics, which reduces the power quality and because of demanding grid codes could make it harder to be approved for grid connection. It would also be more challenging and costly to integrate an array with microinverters in smart grids, because a communication cable must be added to each PV module [19].

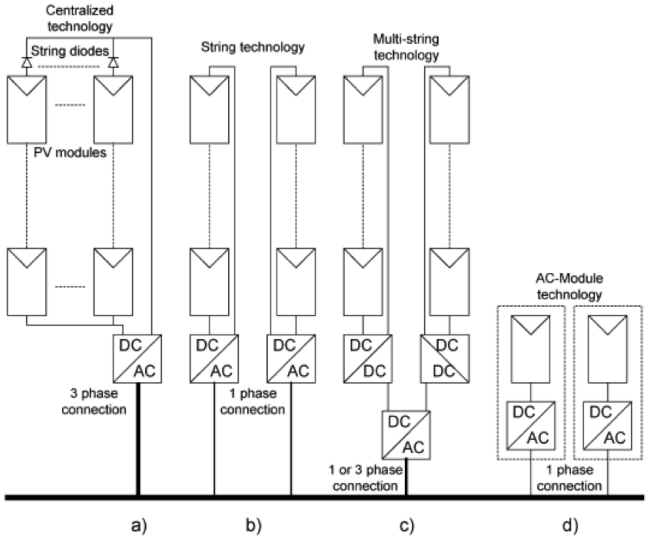

FIGURE 2.7: An overview of the different inverter options: a) Central inverter, b) String inverter, c) Multi string inverter, d) Modular inverter [7].

Chapter 3

Grid Connection

To ensure from whom and how power is being fed into the grid, there exists regulations to control this. These regulations made by NVE and by the government makes sure that the grid is balanced at all times and that no other than utility companies and "plus customers" can feed power into a grid. To get permission to become a "plus customer" an application to Agder Energi needs to be fulfilled according to the given regulations and standards.

3.1 The Plus Customer

The Norwegian water- and energy directorate (NVE) defines a "plus customer" as *"an electrical consumer with a yearly production that usually does not exceed its own consumption, but at some times of the day has an excess production of electrical power that is fed into the grid"* [20]. For the implementation of such a small scale power plant to be possible, NVE gives exemption from some of the requirements larger power utility companies has to sign, such as the balance contract, trading permit and the tariff contract for feeding electricity to the grid. The purpose of this exemption is to make it easier for plus customers to feed and sell their excess power to the utility company. The plus customer still has to sign a grid connection- and grid lease contract with the local utility company to ensure the quality of the power being sold. For the power to be sold, NVE requires the plus customer to install a two-way smart meter in the switchboard [20]. This is however not required if the electrical power produced is intended for private use only, which is the case in the current project where the maximum PV system output will never be greater then the campus consumption [21].

3.2 Grounding Systems

The local grid at UiA Grimstad is using a 400 V three-phase TN-S system. A TN-S configuration is the way a system is grounded and means that the neutral and protective earth are separated. The grid is then grounded at the transformer or generator end (T or Terra is French, meaning Earth) while the neutral conductor at the end user is grounded [22]. A TN-S system is illustrated in Figure 3.1.

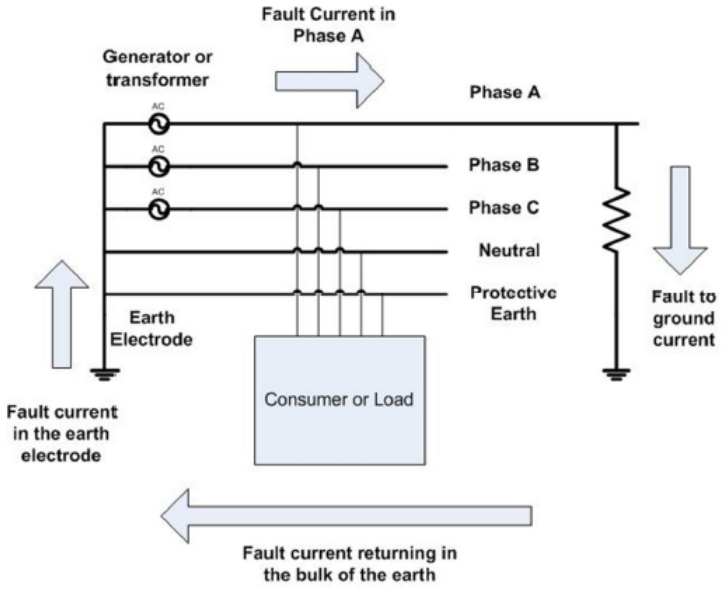

FIGURE 3.1: Configuration of a TN-S grounding system [22].

Inverters with a relatively low power, normally String Inverters, operate as single-phase inverters. Whether or not to use a single-phase- or a three-phase- inverter depends on the size of the system, a decision need to be made before further planning of the PV system is done. As a general rule, PV-systems lower than 5 kWp are built as a single-phase system and larger systems than 5 kWp are built as three-phase systems [4]. Figure 3.2 illustrates the differences when connecting an inverter to the two phase-systems, the inverter in single-phase systems is connected between one phase at the grid and the neutral, for three-phase systems the inverter is connected to each of the three phases of the grid as well as the neutral [4].

It is becoming more common to use multiple single-phase inverters in a PV system [4]. These can be connected to one or three phases, depending of the inverter power. A system cannot feed more than 15 kVA into one phase; the inverters should then be equally divided so that the load on each phase is equal. Figure 3.3 shows a typical configuration where multiple single-phase grid connected inverters are used in an array and connected to one phase via a circuit breaker

(Q4). The design can be used for all kinds of buildings and can be duplicated as many times as necessary [23].

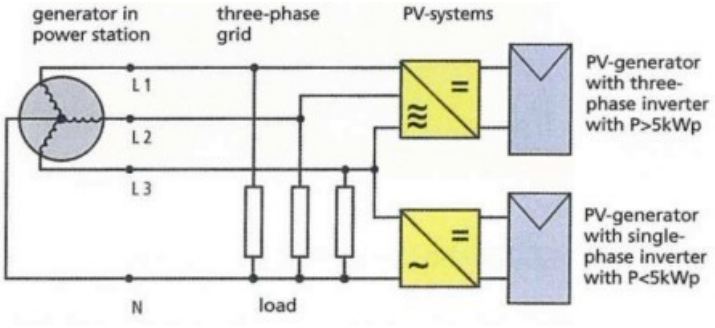

FIGURE 3.2: Configuration of a single-phase inverter connected to one phase, and a three-phase inverter connected to all three phases [4].

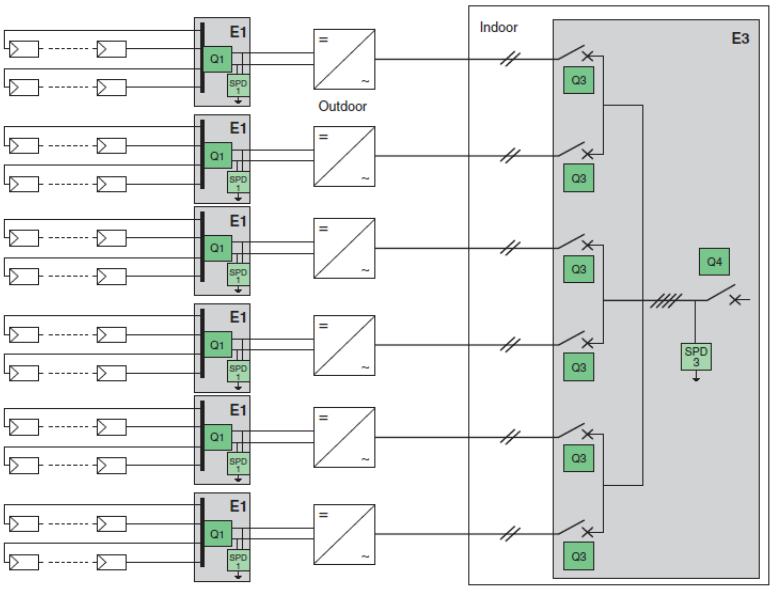

FIGURE 3.3: Illustrating a system with multiple single phase inverters connected to the grid via switch Q4 [23].

Whether or not to use a single- or three-phase system is also determined by what the manufacturer can provide. A look at three inverter manufacturers, Eltek, Danfoss and SMA shows that the smallest grid connected inverter producing 400 V at three-phases was the SMA Tripower 5000 TL-20 producing 5 kW. The smallest three-phase inverter manufactured by Danfoss is the TLX- and FLX-series producing 6 kW, and the smallest three-phase inverter manufactured by Eltek was the Theia TL producing 13 kW. Neither of the three manufacturers has a 400 V three-phase inverter with a transformer, which is recommended by Agder Energi.

The element of uncertainty by installing a single-phase system is the phase balancing. All three-power lines can carry the rated power in both directions. A large voltage source (inverter) on one phase would lead to a change in potential between the three phases. The phases would then be unbalanced and higher currents would flow through the neutral leader. Agder Energi does not, at this time, have regulations for how much power they allow to be fed into one phase. The regulation is under development [21], but Hafslund has set their upper limit for single-phase production to 15 kVA so it can be assumed that this number also applies for Agder Energi [24]. This assumption will result in a maximum allowed phase-current of 65.22 A for a 230 V phase.

3.3 Islanding

Islanding is a critical phenomenon and is at the time not wanted on the utility grid. It occurs when the PV system keeps on feeding electrical power to a utility grid that is isolated from its utility voltage source. The utility grid can be isolated when a grid and a PV-inverter are separated by accident, on purpose or by damage [7]. This is usually divided between wanted- and unwanted islanding, where wanted islanding occurs when renewable energy sources are connected to make a micro grid as shown in Figure 3.4. During islanding, this micro grid is isolated from the utility grid and the renewable sources are used to power it. This micro grid is then called an island [25].

Unwanted islanding can present a high risk for utility workers maintaining the grid as well as causing unwanted incidents on the utility grid. Utility workers arriving to do scheduled maintenance work somewhere on the isolated island might think that it is not energised since the switch (showed as CB1 in Figure 3.4) has to be manually disconnected. Just a few tens of seconds would be lethal if utility workers had commenced maintenance work on the grid immediately after the switch (CB1) was disconnected [26]. Even though the grid is manually disconnected from the micro grid, local production units can produce power a few more seconds until the grid-sensing device cannot find the grid, or until the inverter anti islanding device kicks in. The AC switches (CB1 and CB2) should therefore have an indicator on each side, indicating if AC power is present or not, and to clarify this by an alarm or a light.

Figure 3.4 is an example where the local production unit is the micro grid. PCC is the Point of Common Connection where the micro grid is connected to the main grid, CB1 is the circuit breaker between the main grid and the micro grid and CB2 is the AC circuit breaker between

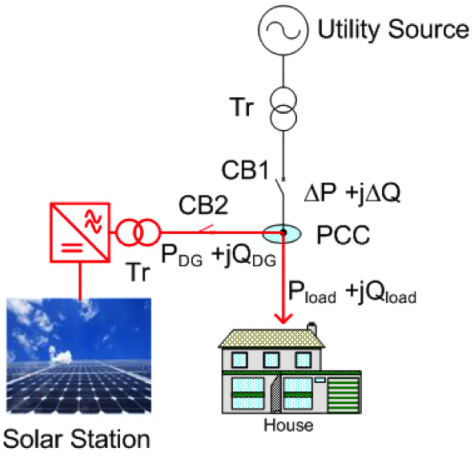

FIGURE 3.4: Solar station disconnected from the utility grid, and operating as an isolated island [27].

the grid connected inverter and the grid it is connected to. In situations where the PV system is placed on the roof, the PCC is situated in the house switchboard where the power $P_{load} + jQ_{load}$ is supplied to the house and a $\Delta P_{load} + j\Delta Q_{load}$ is supplied through a smart meter to the main grid. CB1 is still the circuit breaker connecting or disconnecting the main grid to the micro grid. In cases where the grid needs to be disconnected for maintenance, the switch CB2 must be disconnected prior to disconnecting CB1, and connected after CB1 to avoid islanding. It must, therefore, be possible to remotely control the inverter so this can be done directly by the utility company. Many inverters now have communication terminals e.g. CAN interface (Controller Area Network) that are intended for smart grids or to communicate between a master and several slave inverters. This allows many local PV- or Wind- production units to supply a micro grid and be remotely operated by the local utility company..

3.4 Grid Application Approach

Agder Energi has the sole responsibility for operating, maintaining and ensuring the power quality in the grid. The documentation needed for the application is found on www.aenett.no. The application process can then be divided into five steps found when studying the documentation from Agder Energi. Further discussions of these 5 steps will be done in Chapter 5.7.1.

1. Study the technical guidelines in Appendix J for feeding power into the grid. The chosen inverter must fulfil the restrictions given in Chapter 5.2 and 5.3 for it to be approved by Agder Energi.

2. The contact person for the PV system must complete an application form (Appendix B) made by Rasjonell Elektrisk Nettvirksomhet (REN). For UiA this person is Kristen Leifsen, building manager at UiA campus Grimstad. Required information to fill in is the inverter name and type, the installed power, estimated summer- and winter-production in GWh and development cost of the plant. Agder Energi estimated the time elapsed from the application form was received to a permission was granted to be a few days (in reality it took longer time).

3. After the permission is granted Agder Energi needs to start working on an agreement between them and the customer (UiA) for how the power should be sold regarding price and quantity. In addition, they wanted a preliminary single line diagram (Appendix G) for how the system would be built regarding fuses, circuit breakers, cables, grounding and galvanic isolation. The agreement between the customer and Agder Energi, given in Appendix L, explaining the different parties' rights, different conditions for grid connection and stating that the customer has read all of the additional documents then need to be signed and sent to Agder Energi.

4. A site Acceptance Test must be made of the grid before a PV-system is connected.

5. A documentation form (Appendix K) has to be signed by the installing electrician explaining the protection installed and installations made to ensure that the requirements in FoL are followed (frequency, step voltage, unbalanced loads, flicker, harmonic).

Chapter 4

Factors affecting the PV system

Several factors, external and internal, can affect the PV system both positive and negative. The array is dependent of high irradiance, low temperatures and little losses to operate at optimal performance. When operating at this performance, it is also important that the system is properly grounded and safe regarding to fire. Local measured irradiance is therefore compared with estimated irradiance from the tool PVGIS. A small analysis of the temperature at the site in Grimstad is then conducted to find the module operating temperature and some external and internal factors like wind load, temporary shading, corrosion, grounding schemes and fire hazards are also presented and explained.

4.1 Distribution of Solar Irradiance

The sun is by far the largest energy provider and without it the earth would be yet another dead planet in the universe. Since all energy (with the exception of geothermal energy and nuclear) on earth originally derives from the sun, it should come as no surprise that no other energy source could match the sun's energy potential. The energy in the sunlight reaching the earth's surface is approximately 10,000 times the world's energy requirements, and only 0.01 % of this energy is needed to cover the human's energy need [4]. Solar radiation on earth is influenced by several factors; earth's atmosphere, shadowing, latitude, season and time of the day, etc. The yearly average extra-terrestrial solar irradiance is approximately $G_0 = 1,367\ \frac{W}{m^2}$. This irradiance is reduced in the atmosphere by scattering caused by aerosols, particles and

absorption by atmospheric gases. This reduces the incoming sunlight by around 30 % [28].

$$AM = \frac{1}{\sin \phi} \tag{4.1}$$

Equation (4.1) describes the air mass solar light must pass through in order to reach earth's surface. In other words, cosecant is the ratio between the sun's elevation path and zenith. If the sun is directly overhead the solar light must travel through less air mass then if the sun had a lower zenith angle ϕ [28]. The irradiance on earth's surface changes throughout the year and depends on the geographic location and time of day. The irradiance on a sunny winter day at noon in Grimstad could be $\sim 600\ \frac{W}{m^2}$. On the Equator, at the same time, the irradiance would be in the range of $\sim 1,100$ to $1,200\ \frac{W}{m^2}$. At short periods due to scattering from clouds, solar irradiance can reach up to $1,832\ \frac{W}{m^2}$ near the Equator [29]. The maximum irradiance measured in Southern Norway is $1,600\ \frac{W}{m^2}$ [30]. This was recorded in Grimstad and can be seen in Figure 4.1. A video showing the sky conditions needed to create over-irradiance is available on Youtube™ (`http://www.youtube.com/watch?v=MPo9zjWRjpA`). Due to Norway's

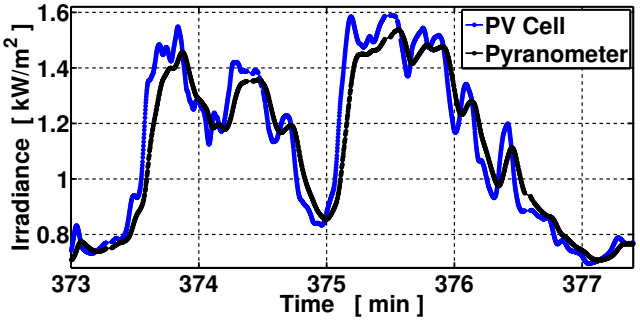

FIGURE 4.1: Overirradiance measured in Grimstad on 24 June 2013 [30].

geographical location in the northern hemisphere there is less solar irradiation [1] than further south in Europe. The solar irradiation in Norway is seasonal and varies substantially throughout the year. Norway's extensive length yields large differences in annual solar irradiation, from 700 $\frac{kWh}{m^2}$ in the far North to 1100 $\frac{kWh}{m^2}$ in the southern parts of Norway [31]. Table 4.1 gives an overview of solar irradiation in five Norwegian cities and Hamburg located in northern Germany. The PV modules are mounted at the optimum tilt angle and orientation (south) as calculated from PVGIS, verifying that Kristiansand in the south has the highest potential for using solar power generation in Norway. It is no surprise that Hamburg receives a higher irradiation than the Norwegian cities since mapping of solar irradiation in Norway is poor when compared to

[1] Solar irradiation is the amount of solar energy falling on unit area over a stated time interval [$\frac{Wh}{m^2}$].

Central Europe, thus the solar irradiation could probably be higher than the estimations given in PVGIS. More on this in Section 4.1.2. These annual irradiations are significantly affected by the cloudy weather, which is common in these regions. According to [32], in 2011 nearly half of the irradiation measured in Grimstad, 1200 $\frac{kWh}{m^2}$ of 2130 $\frac{kWh}{m^2}$, was blocked by clouds and not utilised in the PV modules. Research from Northern Research Institute (NORUT) indicates that the solar power in certain areas in the nordic countries could reach similar energy harvest as Germany [33]. However, in order to accomplish this, the PV modules need to be installed at optimum angle and tracking devices would be needed to ensure maximum incoming irradiance. Adding a tracking device to the PV system would at the moment not be beneficial due to high costs in the small immature PV market in Norway today.

TABLE 4.1: Average sum of global irradiation per square metre received by the modules of the given system ($\frac{kWh}{m^2}$). Mounting position towards south, with optimum inclination. Radiation database: Classic PVGIS (based on ground measurements) [34].

Month	**Oslo**	**Bergen**	**Tr.heim**	**Kr.sand**	**Tromsø**	**Hamburg**
Inclination	40°	33°	43°	38°	45°	36°
January	16.9	5.49	15.1	22.0	0	27.5
February	39.4	27.6	47.2	43.5	25.4	51.2
March	75.7	72.2	94.2	81.7	86.6	79.9
April	115	115	128	120	140	125
May	150	144	153	155	144	159
June	156	158	155	155	144	140
July	151	144	147	154	138	151
August	122	111	121	127	106	141
September	89.3	76.7	81.9	93.4	69.1	101
October	50.7	36.7	49.1	55.7	27.0	69.8
November	23.0	7.92	21.5	26.5	0.548	36.2
December	13.6	3.13	8.16	15.5	0	20.3
Monthly average	**83.5**	**75.1**	**85.1**	**87.4**	**73.4**	**91.8**

4.1.1 Direct and Diffuse Radiation

In order to calculate solar irradiance on inclined surfaces the solar radiation is decomposed into direct beam, sky diffuse and radiation reflected from the ground. Depending on the ground, a coefficient (albedo) is used to represent the diffuse reflections from the ground. The estimated irradiance on the inclined plane can be calculated by using Equation (4.2). The global tilted irradiance (G_t) describes how much solar power per unit area (W/m^2) the solar modules are exposed to.

$$G_t = G_{bt} + G_{dt} + G_{rt} \tag{4.2}$$

The notations used in Equation (4.2) are:

- G_{bt}: Global beam tilted radiation
- G_{dt}: Global diffuse tilted radiation
- G_{rt}: Global reflected tilted radiation

The direct beam (G_{bt}) is the radiation received from within 5° around the sun on a clear day and is the main component of the radiation on a clear-sky day. The sky diffuse radiation component (G_{dt}) is the radiation received after scattering in the atmosphere. Depending on the properties of the ground, reflections can occur and contribute to the global radiation on the tilted surface (G_{rt}) [35]. These reflections, expressed as Albedo values, are shown in Table 4.2 for different

TABLE 4.2: Albedo values for selected surfaces [35].

Surface	**Albedo**
Desert	0.25 - 0.30
Dry sand	0.2 - 0.4
Soils	0.05 - 0.20
Water (high sun)	0.05 - 0.10
Water (low sun)	0.5 - 0.8
Fresh snow	0.75 - 0.95
Melting snow	0.35

surfaces. In Norway, reflections from the many lakes and ponds may give an increased solar energy generation. As seen in Figure 4.2 from the installation site the sea at the distant horizon could reflect and contribute with additional irradiation to the PV system. Although the water has low albedo values ranging from 0.05 to 0.10, it can probably be assumed that the overall size of the reflecting area would compensate for this. Further research and measurements are required on the site to verify and determine how much solar irradiation sea reflections would contribute with. During wintertime, reflections from snow and ice must also be taken into consideration as contributors to the global irradiation.

4.1.2 Solar Radiation Measurements

Solar radiation can be measured by ground sensors or satellite. Typical pyranometers and PV based sensors are used as ground sensors, but there are also other alternatives such as photo-diodes. A pyranometer is built up by one or two hemispherical glass domes with a thermopile-sensing element in the centre, which is encapsulated by the instrument body. The solar radiation is absorbed by a black surface on the thermopile sensor and compared with a white surface (white

FIGURE 4.2: Southern view at the installation site with the sea in the horizon [19].

metallic housing) that reflects the solar radiation. The temperature difference is measured and the thermopile sensor converts this thermal energy into voltage proportional to the temperature difference. The glass dome restricts the field of view to 180° while operating on a spectral range from 300 to 3,000 nm. More expensive pyranometers are equipped with two glass domes to improve thermal insulation and reduce the directional error.

A PV sensor consists of a solar cell and is usually made of crystalline silicon. The sensor operates by delivering a voltage proportional to the measured irradiance. The main benefits when comparing a PV sensor to a pyranometer are low cost, similar reflection losses as in PV modules and fast response (A pyranometer needs longer measurement times due to thermal transients). Disadvantages are limited spectral sensitivity and higher inaccuracy than a pyranometer [4]. The spectral range for a c-Si PV based irradiance sensor is approximately from 300 to 1,100 nm.

Images from geostationary satellites can also be used to derive global irradiance on earth's surface. This is done by using the software Heliosat-II, which converts images from satellites into maps of global irradiation at ground level. This method is described in detail in [36]. The newest operational satellites have a resolution of 1 km x 1 km near the equator below the satellite. This resolution is reduced at high latitudes due to low viewing angle, the satellites are therefore not suitable to map the irradiance north of 58° in Norway [37].

PVGIS

One of the most important factors when deciding on installing a PV system, is to have the available radiation data on the possible installation site. A popular tool for estimating the

potential solar radiation is PVGIS developed by the JRC of the European Commission. Solar irradiation data can from any location in Europe be obtained by using this web-based application. PVGIS utilise interpolated ground station measurement data from the period 1981 to 1990 (PVGIS-3 database), satellite images from 1998 to 2005 and from June 2006 to December 2011 (PVGIS-CMSAF database). Satellite data is used south of 58°N [34], [38] and therefore, only the most southern parts of Norway have irradiance data from satellite images. The ground measurements are retrieved from 566 meteorological stations around Europe. In Norway, data is used from one meteorological station located in Bergen. The measured data from this station is interpolated with other stations in Europe. According to [34], the old database with interpolated ground measurements (PVGIS-3) estimates lower irradiance than the new database, which are based on satellite images. Comparison with newer ground station measurements show that the new database has a higher accuracy than the old database. This is likely caused by wrong measurements in the old database due to shading, frost, snow, dirt, etc. Another factor is the increased solar radiation over Europe in the last 30 years, contributing to higher irradiance in the new database. In Norway, it would therefore be sensible to compare the PVGIS data with local measurements. The company Kjeller Vindteknikk has established a database with data from 68 stations measuring solar irradiance in Norway and local data from this database could then be used as a validation when working with PVGIS in Norway [37].

Local Irradiance

The Photovoltaic Lab at the University of Agder has been logging irradiance data since 2011. The sensors are mounted 7° east from south and with $39° \pm 1°$ tilt angle from the horizontal. The irradiance is measured with a Kipp & Zonen CMP 3 Pyranometer and the PV based sensor 80SPC from Soldata. The results are presented in Table 4.3 together with a long term prediction of PVGIS. Due to little importance in PV power generation, values below 50 $\frac{W}{m^2}$ from the local measurements performed in 2011-2013 are discarded. The monthly average irradiation for each year is slightly higher than given by the PVGIS prediction. The highest monthly average irradiation was 108.8 $\frac{kWh}{m^2}$ in the year 2013, with especially July as a very sunny month with 201.69 $\frac{kWh}{m^2}$. The monthly average irradiation from 2011 to 2013 is 103.3 $\frac{kWh}{m^2}$ which is 16.2 % higher than what PVGIS estimates. This indicates higher irradiance in Grimstad than given by the long-term average in PVGIS. Only the old database was available for Grimstad and some of the reasons explaining the lower irradiance from PVGIS is stated in section 4.1.2. Another possibility could also be as mentioned in section 4.1.1, the albedo effect,

TABLE 4.3: Average monthly global irradiation per square metre received by the modules of a given system ($\frac{kWh}{m^2}$). Mounting position is 7° east from south, with $39° \pm 1°$ tilt angle from the horizontal. Location: Agder Photovoltaic Lab, University of Agder [39].

Month	**2011**	**2012**	**2013**	**PVGIS**
January	48.1	22.14	31.32	21.0
February	28.0	59.77	63.77	43.3
March	118.0	128.29	143.31	80.0
April	166.0	115.59	160.21	119.0
May	156.0	188.52	136.78	152.0
June	169	153.63	164.98	155.0
July	149.0	169.43	201.69	153.0
August	145.0	158.01	161.13	127.0
September	101.0	106.56	109.78	92.7
October	69.4	72.92	60.21	55.1
November	26.8	26.35	51.87	26.0
December	23.2	11.18	20.58	15.4
Monthly average	**100.0**	**101.0**	**108.8**	**86.6**

which would contribute to the globally tilted irradiation due to reflections from the sea, snow and ice. The measurements obtained in Grimstad look promising and show that PV systems in Southern Norway could be a viable energy source with government support, or even without if the current PV prices decrease. However, the information presented here is only an indication, as no final conclusions can be made until there is enough data (7 to 10 years [40]) to support these findings.

4.2 Irradiance and Temperature

The available solar irradiance and the ambient temperature affect the power output. With a nearly linear relation, the current is highly dependent of the solar irradiance incident on the solar cells. If the light intensity is decreased by 50 %, the same reduction can be measured in the current. The short-circuit current also depends on the spectral composition of sunlight. The degree of the dependence varies amongst different PV technologies. The voltage is not affected to the same extent as the current, but there will be a slight increase with higher irradiance [3].

Temperature is the second most important parameter after irradiance affecting the electricity output. If the temperature increases above 25 $°C$ the voltage will decrease and thus reducing the power output. One of the benefits in Northern Europe is the cold climate reducing the ambient temperature of the solar cells. When temperatures are lower than 25 $°C$ the power output increases. This is shown in Figure 4.3(a) which illustrates how the voltage decreases

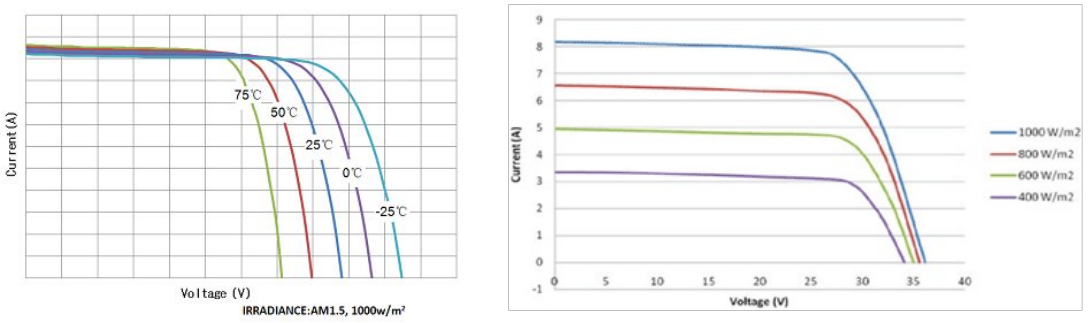

(a) I-V curve at different temperature levels and a fixed irradiance [41].

(b) I-V curve at different irradiance levels and a fixed cell temperature [42].

FIGURE 4.3: Effects of temperature and irradiance on the solar cell performance.

when temperature is rising. Figure 4.3(b) then shows an I-V curve at a constant temperature, indicating how the current and voltage are dependent of the irradiance. Open-circuit voltage V_{OC}, short circuit current I_{SC}, efficiency and fill factor are all temperature dependant. Due to low solar cell efficiency when converting irradiance to electrical energy, typical 9-12 % of the remaining irradiance is either reflected or converted to heat. The generated heat increases the temperature of the PV modules resulting in decreased efficiency.

4.3 Ambient Temperature

The PV array sizing involves the maximum and minimum operating temperatures of the PV cells with the intent of determining the best and worst V_{OC} and V_{MP}. This is dependent of the ambient temperature at the location of the PV system, a temperature that is measured in a shadow so that direct solar radiation does not affect the result. Temperature measurements at UiA Grimstad Campus has only been operating since late 2010 which is not a sufficient number of measurements to be used. The Bioforsk AgroMetBase temperature data for Landvik, a location 5 km from UiA Grimstad, is considered sufficient to use in this thesis. This database can provide data for wind, temperature, air pressure and density in maximum, minimum or average values for every hour, day or month of the year. Maximum and minimum air temperatures at two-metre altitude are used as a starting point to find the operating temperature of the solar cells [43]. The maximum values from Landvik are only registered since 1 January 2006, which is not considered sufficient for good measurements but is still used to give a general idea of the temperatures in the area. From temperature data and Figure 4.4, the maximum ambient air temperature at two-metre altitude for Landvik was 29.4 $°C$ measured on 11 June 2007.

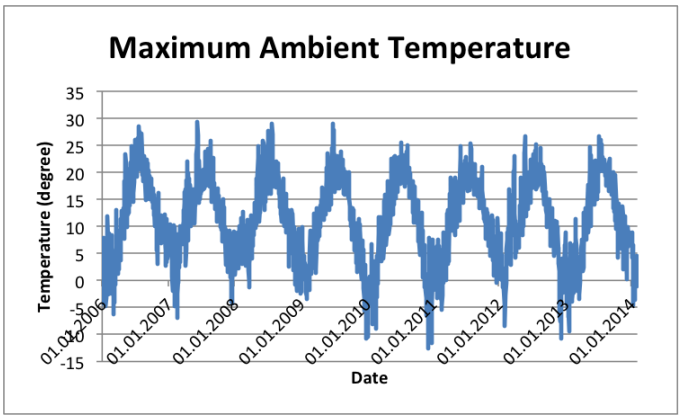

FIGURE 4.4: Maximum ambient temperature of 29.4 $°C$ measured on 11 June 2007 at two metre altitude for Landvik.

The data for the minimum ambient air temperature started logging on 10 April 1987. It is

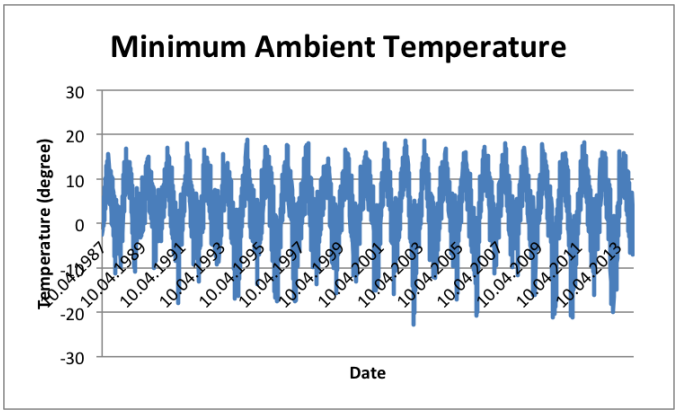

FIGURE 4.5: Minimum ambient temperature of -22.8 $°C$ measured on 31 December 2002 at two metre altitude for Landvik.

considered that 26 years are a sufficient amount of data to paint a good picture of the minimum temperature in the area. It can be seen from Figure 4.5 that the lowest ambient air temperature at two-meter altitude for Landvik was -22.8 $°C$, measured on 31 December 2002.

Module Operating Temperature

The location of UiA campus Grimstad is different from the location at Landvik. The university is located closer to the coast and on a hill where the wind is expected to be stronger than at Landvik. Due to uncertainty, a safety margin of 5 $°C$ is added to the maximum and subtracted from the minimum air temperature before it is used to calculate the initial module temperature. From [34], [44] and [45] it is found that the module's operating temperature at zero wind speed

can be calculated by using Equation (4.3).

$$T = T_A + C_t \cdot G \tag{4.3}$$

T_A is the ambient air temperature, G is the in-plane irradiance and C_t is a constant dependent of the module mounting and ventilation. It is assumed that the ratio between T and T_a is a linear function of the irradiance (G) on a module [44]. It is also assumed that the maximum steady irradiance is approximately 1200 W/m^2 during summer and 800 W/m^2 during winter in Grimstad [34]. When sizing the array, one need to know the highest V_{OC} and lowest V_{MP}. For best and worst case scenario, we need to find the highest and lowest operating temperature which is found by choosing $C_t = 0.035\ °C\left(W/m^2\right)^{-1}$ [45] for the NESTE c-SI modules when put in open-rack configuration during summer and $C_t = 0.0220\ °C\left(W/m^2\right)^{-1}$ during winter [34]. The maximum and minimum module temperature at peak irradiance is calculated to be:

$$T_{max} = (29.4 + 5)\ °C + 0.035\ °C\left(W/m^2\right)^{-1} \cdot 1200\ W/m^2 = \mathbf{76.4\ °C} \tag{4.4}$$

$$T_{min} = (-22.8 - 5)\ °C + 0.022\ °C\left(W/m^2\right)^{-1} \cdot 800\ W/m^2 = \mathbf{-10.2\ °C} \tag{4.5}$$

4.4 Voltage Drop Along the Cables

The voltage drop equals the total resistance times current. The total resistance is dependent of the cross-sectional area of the conductor, the wire length and resistivity. The voltage drop is a loss of voltage in the cable due to resistance and causes a loss in power, expressed as $P = I^2 \cdot R$. The Australian standard AS/NZS5033:2005 is specifying the voltage drop from array to energy meter to be less than 5 %, meaning that the PV string voltage drop plus array voltage drop plus AC cable voltage drop is less than 5 % [32]. This will be explained more in detail when sizing the cables in Section 5.4.2. The voltage drop in the DC cable can be calculated using Equation (4.6).

$$V_{\text{Drop DC}} = \frac{2 \cdot L_{\text{DC cable}} \cdot I_{DC} \cdot \rho}{A_{\text{DC cable}}} \tag{4.6}$$

$L_{\text{DC cable}}$ is the length (m) of the DC cable one way, assuming symmetry in the cable both ways, I_{DC} is the DC current (CCC) in the cable at worst case scenario, ρ is the wire resistivity $\left(\Omega \cdot mm^2/m\right)$ and $A_{DC\ cable}$ is the cross section of the DC conductor $\left(mm^2\right)$ [32]. For the sum

of the voltage drop in the string- and array cable to be less than 5 %, it is assumed that a maximum voltage drop of 2 % is used in the string (module cables) and the array cables.

4.5 Wind load

UiA- Grimstad is located on a hilltop 45 metres above sea level, with a building height of about 15 metres the PV array is located at approximately 60 metres above sea level [19]. This hilltop is exposed to a large variation of wind forces from both sides of the array, creating a windward side of the array with a high-pressure area and a leeward side with a low-pressure area. The wind suction on the leeward side could be strong enough to break the glass or tear the PV modules off its mounting rack if high enough uplift forces are created [4]. The different scenarios are illustrated in Figure 4.6. As illustrated in Figure 4.6(a), the windward will produce forces and

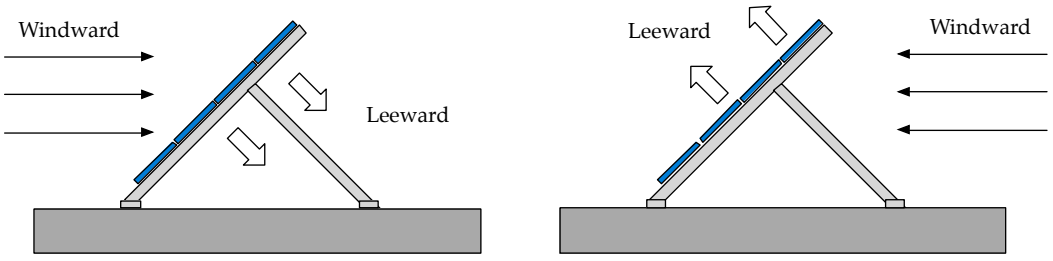

(a) Wind load from the front. (b) Wind load from the rear.

FIGURE 4.6: Illustration of wind forces on the PV array [4].

stresses on both the PV modules and the array structure in addition to a vertical force effect and a fairly high drag. Most of the loads would, however, occur in the vertical direction [46] and effect the supporting beam and PV modules. Figure 4.6(b) illustrates windward forces from the rear working in a vertical direction, lifting the array upwards and inflicting tension to the support beams [46] and PV modules. Forces on the array will be divided between the modules, creating stresses on both supporting beams and PV modules. Because the array is located on the roof of the building, where the wind loads are most intense, building engineers who did the wind load calculations for the university followed the Norwegian standard NS 3479; they did, however, state that a wind load of 1.5 kN/m^2 could be used instead [47]. PV modules used in the array has an area of 0.84 m^2, they would have to withstand a load of 1.5 $kN/m^2 \cdot 0.84\ m^2 =$ **1.26 *kN*** each. As mentioned earlier, wind forces on the array will in general affect the PV modules and the supporting beams. The array is connected to the roof by

steel beams anchored in concrete. Very high forces must therefore be present for the array to lift off. Stainless steel bolts connecting the array to the supporting beam will secure the array. However, one risk is that the PV modules could take off as in Figure 4.7. This will be prevented by fastening the PV modules with four to six nuts and bolts depending on the distance between the beams. This produces another risk; if the module frame is securely fastened the wind could blow through the PV modules and destroy them by creating a large hole or by bending the surfaces so the glass breaks. As seen in Appendix M there has not been done any testing of how much wind load one PV module can resist, and we know that the maximum wind load on each PV module can be as much as 1.26 kN. Depending on how they are mounted, modern PV modules from SunTech are tested for extended wind and snow loads, and sell PV modules certified to withstand wind loads between $2400 - 3800\ N/m^2$ (assumed to be wind from the rear) and snow loads between $2400 - 5400\ N/m^2$ (assumed to be snow on the front glass) [48]. The expected maximum wind load on the roof is much lower than the minimum wind load sustainable by modern PV modules. By comparing the minimum wind load $2400\ N/m^2$ with NAPS (NESTE) PV modules they would be able to withstand $2400\ N/m^2 \cdot 0.84\ m^2 = \mathbf{2\ kN}$. Assuming the NAPS modules can withstand the same as modern PV modules, they would be more than able to withstand the expected wind load of 1.26 kN.

FIGURE 4.7: Illustrates PV modules that got destroyed during a storm [49].

4.6 Temporary Shading

On the installation site, typical temporary shading would come from snow, bird droppings and the surroundings. It can in general be assumed a power loss between 2 % to 5 % due to soiling, but according to [4], this is accepted. The university roof has become a nesting ground for seagulls in the area, so bird droppings on the PV modules like in Figure 4.9 is expected to happen regularly. The PV system is to be mounted on the roof where a fence (roof barrier)

is installed on the roof edges. At a certain time of the day, this roof barrier cast a temporary shadow on the lower PV modules. In Figure 4.8 both shadow from the snow and the fence is projected on the PV modules. Due to the set-up of the rack it is not possible to avoid the temporary shading from the fence. There are many factors contributing on how large effect the shading would have upon a PV system. First of all, it must be determined how many modules that could be shaded simultaneously. By studying Figure 4.8 it can be seen that only the modules on the two lower rows are partly shaded. The array configuration for the PV system in this thesis can be seen in Figure 5.4. Due to limited space on the rack, other test modules and the placement of sensors makes it difficult to completely avoid the temporary shading from the fence. When comparing Figure 4.8 with the module configuration in Figure 5.4 it can be seen that modules 18 to 23 and 1 to 4 is most likely to be affected by temporary shading.

FIGURE 4.8: Partial shading from the fence on previous installed modules. Photo was taken 9:30 on January 2011 [19].

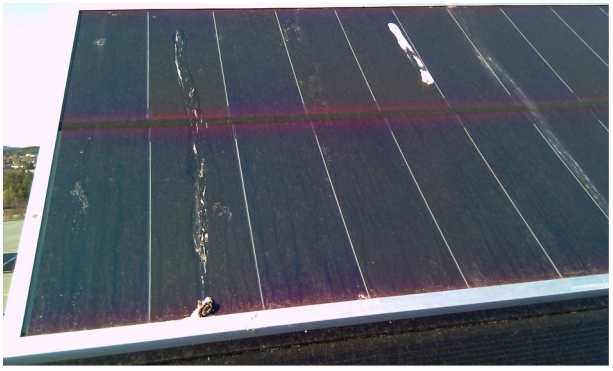

FIGURE 4.9: Bird droppings are expected to occur regularly at the site [19].

4.7 Corrosion

PV modules are designed to operate for more than 25 years in the field, and it is important that the rest of the system target a similar lifespan. Mechanical fittings used on rack mounted PV systems are exposed to different weather conditions. Low steel quality and combinations with different metals in the fittings increases the risk of corrosion [4]. The location plays a large role on how exposed a PV system is to corrosion. Salt from the highways used for de-icing during the Norwegian winter, as well as from the sea and the wet climate are factors needing consideration when designing a PV system. There are several types of corrosion, such as pitting corrosion, stress corrosion cracking, galvanic corrosion, crevice corrosion and erosion corrosion [50]. According to [50], galvanic corrosion is the most relevant corrosion effect as it has often been seen on PV plants. Galvanic corrosion is an electrochemical reaction happening between two pieces of different metallic elements. In order for galvanic corrosion to occur, one element needs to function as an anode and the other one as a cathode, in addition there needs to be an electrolyte and conductivity between the elements [51]. As seen in Table 4.4, elements possess different electrode potential and give an overview on the elements most likely to behave like an anode or cathode when combined. For example by combining zinc and nickel, the zinc would behave like an anode and corrode respectively. Metals in a PV system, such as aluminium,

TABLE 4.4: Galvanic series, showing metallic elements and its corresponding electrode potential [50].

Element	**Electrode Potential [V]**
Magnesium	-2.37
Beryllium	-1.85
Aluminium	-1.67
Zinc	-0.76
Chromium	-0.74
Iron	-0.44
Cadmium	-0.40
Nickel	-0.24
Tin	-0.14
Hydrogen	0.00
Copper	0.34
Silver	0.80
Platinum	1.20
Gold	1.50

stainless steel and copper make up the anode and the cathode. The electrolyte is made of water from rain, moisture, sea, etc. Fixing points is most likely to be affected by corrosion, but can be prevented by following this guideline from [51]:

- When mixing metals, choose metals close together in the galvanic series.
- Minimise contact area between dissimilar metals.
- When mixing metals, small parts (fasteners) and critical components should be of a more noble element.
- Avoid threaded joints for elements far away in the galvanic series.
- Apply coating or insulate dissimilar metals.

Modules already installed on the planned location for this project had some cosmetic corrosion between the washers and the frame of the module, but there were no signs of any physical damage. The frames of the solar modules and the support beams are made of anodized aluminium. By anodizing the aluminium, a thick oxide layer is made to protect it from galvanic corrosion. The bolts, nuts and washers are made of austenitic stainless steel with Type 316 material, which is an alloy of iron, chromium and nickel. This is marine grade stainless steel and has an increased corrosion resistance compared to other types of stainless steel, such as Type 304. The chromium reacts with the atmosphere and form layers of chromium oxide, which protects the steel underneath [51], [52].

Due to the precautions of choosing materials with a protective oxide layer it is unlikely that any galvanic corrosion should develop on the frames of the modules, fasteners or the support beams.

4.8 Grounding

The reasons for connecting the module frames (exposed conductive parts) between the PV system and earth are apparent due to: Bonding in order to avoid floating potentials in the PV system; provide a path for fault current; protection from lightning [3]. Bonding is used to prevent different voltage potential to ground and reduce the risk of electrical shock due to module encapsulation or isolation breakdown. The risk of the array together with the beam support being an extraneous-conductive part is highly unlikely. The PV system will be installed on the roof where there is no direct contact with the earth making it unlikely for the frame of the array together with the beam support to introduce a potential into the installation. However, in this project it is decided to equipotential the beam support and the frames of the PV modules to the fence. This introduces the same potential to all the extraneous-conductive parts on the roof and prevents the hazard of electrical shock. The DC side may be ungrounded or grounded

either on the negative or the positive terminal, but grounding on the DC side can only be done if there is a simple separation (like a transformer) between the DC side and the AC side [53]. The grounding topology of a PVGCS can be seen in Figure 4.10. The NEK 400:2010 preferably

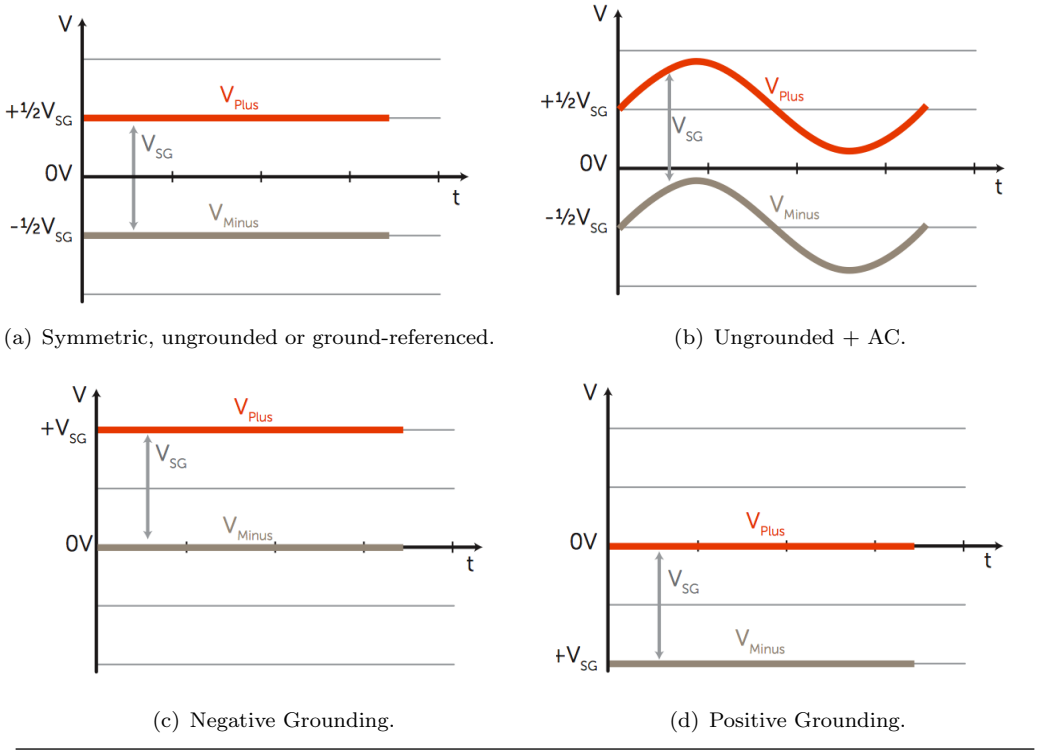

(a) Symmetric, ungrounded or ground-referenced.

(b) Ungrounded + AC.

(c) Negative Grounding.

(d) Positive Grounding.

FIGURE 4.10: Different grounding topologies of a PVGCS [54].

recommends the DC side to be constructed with Class II equipment (double insulation) or similar insulation [55]. If the installation meets these requirements, it is not necessary to ground on the DC side [56]. However, grounding is required on the AC side due to the inverter being a Class I equipment. In this project, it is decided to follow the guidelines of NEK 400:2010. The first topology, ungrounded, seen in Figure 4.10(a) is, therefore, applied to the DC side of the PV system. The PV array is one of the highest points on the roof, including a large metal building and a high tower. It is believed that the metal building is grounded by obvious reasons and a grounded socket which is connected to the metal building is located directly under the array. The university building is, however, not optimised for grounding PV systems. Grounded objects are attracting lightning and it is not desirable to lead high voltages caused by lightning through the building. It is therefore decided not to ground the PV system on the DC side but rather ground it on the AC side, making sure that NEK 400:2010 is fulfilled.

4.9 Fire Hazard

As long as electrical appliances are involved, there is always a risk of fire and PV systems are no exceptions. PV systems do not just present danger to buildings, but also fire-fighters or building occupiers accidentally coming into contact with a live wire [57]. The risk of a building being damaged because of a PV fire is estimated by [58] to be $30 \cdot 10^{-6}$ for German conditions. This risk is based on 30 annual fires for the 1,000,000 PV systems installed in Germany. The risk is, however, higher for PV generators integrated into the roof (BIPV). These systems need extra precautions and risk awareness when being installed. Standoff PV generators are mounted on "hard roof" that acts as a shield between the building and a PV fire. These standoff systems also have the advantage of being cooled down from the wind etc, because of the distance between the PV module and the "hard roof" [58]. Between 1995 and 2012, some 180 fires were caused by PV systems. A study of Figure 4.11 reveals that most of these fires originated in the DC section of the PV system. Most of these fires did, however, originate because of a lack of maintenance and bad practices during installation. Based on Figure 4.11(a) extra care must be taken regarding components with highest counts when installing the PV system, these must also be inspected annually with thermal imaging camera to ensure that no faults are building up with time [58].

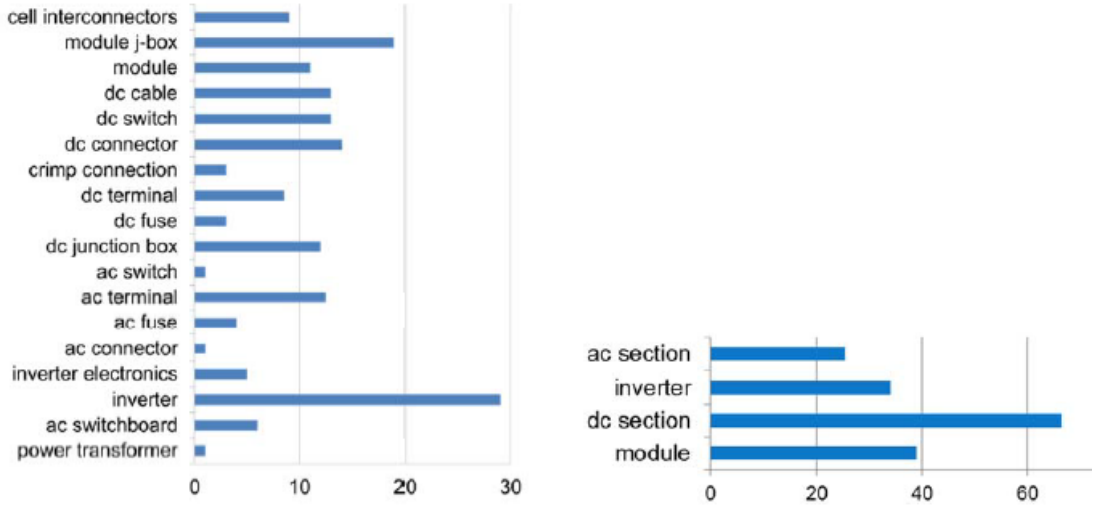

(a) Counts of system component where a fire started.

(b) Counts of system section where a fire started.

FIGURE 4.11: Fire causes in a PVGCS indicating the component and section where most fires start [58].

Chapter 5

Results and Discussion

For the chosen inverter, current and voltage ratings of the PV modules restricts how large the PV array can be. The cable cross section and protection is then decided from the maximum array current entering and leaving the inverter. Many factors are involved in determining how the PV system should be designed, and then installed, these factors are explained and discussed in this chapter. After the system has been installed, results are analysed to ensure that the inverter is fully functional and to see how the inverter handles the varying irradiance in Grimstad.

5.1 Inverter Selection

The type of inverter depends on the size of the solar power plant. It is given that the inverter should have a size of approximately 3.5 kW. This puts some limitations for the inverter type. The two inverters most suitable for this PV array are string inverter and multi string inverter. A multi string inverter would have been a better option if the customer thought about installing multiple strings and maybe expand the solar power plant in the future. This is, however, not an issue at the current location with a total area of 27 m^2 to install a PV array, it would not be very likely to expand the power plant or add more than two strings. The price is also increasing when a multi string inverter is chosen. Even though a string inverter only has one MPPT it is considered the best option for this small system. Most likely a single string will be used, but it has the possibility of adding two more strings if necessary (Appendix A).

One of the criteria for choosing inverter is that a local supplier is used. A search for inverters showed that the relevant inverters were not found close to Grimstad, but distributed over Norway

and Denmark. The design criteria for the inverter size were chosen due to the intention of a long-term investment for the PV lab at UiA-Grimstad. Our supervisor wanted the possibility of connecting modern PV modules with higher current and voltage ratings at a later time [19].

Inverter Types

PVS300-TL is a solar string inverter produced by ABB. This is a single-phase inverter with integrated performance data monitoring and IP55 protection level (dust- and water-proof). It is transformer-less which makes it smaller and lighter than other inverters. The monitoring graphical display is detachable with its own keypad and an EIA-485 interface and Ethernet monitoring protocol. Embedded in the inverter is a DC power switch, DC string fuses, reverse polarity protection, RCD (residual current detection) and grid monitoring with anti islanding [59]. A price quotation is given from ABB for the PVS300-TL to be 12800 NOK plus taxes and transportation costs [60].

Getek in Trondheim distributes the SMA sunny boy S3800. The SMA S3800 has an integrated DC circuit breaker and a maximum input of three strings, designed with a current limit of 16 A. It uses a LF transformer, which provides galvanic isolation, but it does not provide any more information about data logging other than Bluetooth and RS485 interface is optional. Of protective devices, it provides DC reverse polarity protection, AC short-circuit current capability and an optional arc-fault circuit interrupter [61]. However, the datasheet is inadequate when compared with datasheets for the other inverters [62]. It was not possible to get a price quotation for the SMA sunny boy S3800 from Getek.

Eltek in Drammen is supplying the Theia HE-t 3.8. Theia HE-t has a maximum efficiency of 97.3 %, and high efficiency at low irradiation. It is manufactured after the IP65 protection level, meaning that it is dust- and water-proof for installation outdoors or indoors. The inverter uses one MPPT and has three string inputs. The input features reverse polarity protection, ground fault monitoring, optional DC switch and DC string fuses and it is field configurable for ungrounded, positive or negative grounding [63]. Appendix I shows the logging capabilities of the inverter which include input- and output current, voltage and power as well as energy and power produced daily, monthly, yearly and in total. Communication with Eltek explains that Theia HE-t uses two separate log types; an energy log with 365 daily sums and up to 365 monthly sums and a data log containing data from every 15 minutes while the inverter is operating. The data log is easily downloadable from the inverter on a PC via the built-in

Ethernet interface using a PC-tool provided by Eltek, which is normally not provided to end users. However, Eltek is providing UiA-Grimstad with a licence until the end of 2015 [19]. Appendix H shows the full price quotation from Eltek for the Theia HE-t inverter to be 6840 NOK plus taxes and transportation costs.

The DLX 3.8 is produced by Danfoss in Denmark [64]. The DLX 3.8 has a maximum efficiency of 97.3 % and a casing manufactured after the IP65 protection level. It uses an HF transformer, providing galvanic isolation and giving it a total weight of 23 kg. Included in the inverter is reverse PV polarity protection, ground fault monitoring, integrated DC switch and excessive PV power protection. The DLX is a robust inverter that can operate at an ambient temperature range between $-25\ ^{\circ}C$ and $65\ ^{\circ}C$, with a built-in web server for monitoring and a graphical colour display [65]. A quotation was given from a Danish company called Soltek for 9800 DKK, equivalent to approximately 10900 NOK (25/2-14), plus taxes and transport [66].

The Fronius IG plus 35 is also an inverter supplied by Getek. The design of this inverter is an enhancement of other successful inverters with improvements to provide higher efficiency and earnings [67]. A combination of multiple power stages provides maximum power output on cloudy days. It operates with a HF transformer with transformer switchover, resulting in a constant efficiency over a wide range of the input voltage [67]. The Fronius IG plus 35 operates between $-20\ ^{\circ}C$ and $55\ ^{\circ}C$ and has a weight of 23.8 kg. It has protection degree IP54, meaning that it is dust proof and tested against splashing water [68]. The data logging capability of Fronius IG plus 35 is not specified, but an extra data logger/manager can be installed to *"overview how the system operates at all times"* [69]. A price quotation was given by Getek for the Fronius IG plus 35, they offered 10 000 NOK plus taxes and transportation [70].

Appendix C shows the inverters found with the appropriate power rating and the most important parameters for each inverter. For a PV system to be approved and connected to the grid, the local utility company needs to approve the system, inverter and the state of the power output. Agder Energi writes in their regulations [71] that they highly recommend having galvanic isolation in the PV inverter and specifies that it is not allowed to leak any DC current into the grid.

The inverter with no transformer, PVS300 TL 4000 from ABB and SMA 3800 because of a lower maximum DC system voltage and a datasheet that does not give satisfactory information, is ruled out. The three inverters remaining are Theia HE-t 3.8 from Eltek, DLX3.8 from Danfoss and Fronius IG plus 35. The inverters from Eltek and Danfoss have the same technical

properties, and power rating. In addition they have the same protection degree (IP 65), number of string inputs and efficiency. They both have an integrated DC switch, reverse polarity protection and ground fault monitoring. The difference occurs when the price is considered. As explained earlier, the model from Eltek has a price of NOK 6840 before taxes and delivery cost, this is a quotation given especially for UiA Grimstad. Soltek supplies the Danfoss DLX 3.8 for 10900 NOK before taxes and delivery cost. One can assume that the delivery cost will be higher when transporting 21 kg from Denmark than from Drammen, in addition customs and taxes has to be paid when transporting it over the border. The Fronius IG plus 35 has protection degree IP54, meaning that it is less dust- and waterproof than the other two. It also does not have the same protective equipment, it is only equipped with a DC switch, overload behaviour and DC insulation measurement. The data are also only available if an external data manager is bought.

When considering these factors and the fact that Eltek is a local company relatively close to Grimstad, the Theia HE-t 3.8 is considered to be a good and reasonable inverter for this small PV system.

5.2 Inverter Requirements for Power Quality

The power quality requirements are written in the Norwegian law, "Forskrift om Leveringskvalitet i kraftsystemet" (FoL), and give the Norwegian water- and energy directorate authority to impose people or companies that *"fully or partly owns, operates or use electrical installations or electrical utilities which are connected to the Norwegian utility grid and the person that the energy law defines as system operator"* [72], to do the necessary measures to reduce the consequences of short- and long-term power outage [72]. FoL and Agder Energi use different requirements to ensure the power quality, since Agder Energi uses different values to ensure that the requirements in FoL are never broken, their requirements are considered in this thesis. These requirements for power quality as stated from Agder Energi in Appendix J and [71] are also applicable for plus customers and effects the following terms:

- Slow variations in the voltage RMS value
- Step voltage Changes
- Flicker and Flicker Severity
- Harmonic Distortion

5.2.1 Slow Variations in the Voltage RMS Value

Slow variations in voltage are defined as changes in the stationary voltage RMS value over a period of time. To avoid significant voltage variations at the end consumers, it is not allowed to produce a voltage that during an average time of 1 minute exceeds ± 10 % of the nominal RMS voltage [72]. The nominal RMS voltage can therefore only vary between 207 V and 253 V for a 230 V grid, as illustrated in Table 5.1, but cannot exceed these limits for more than 1 minute. This is a limit programmed in the inverter before it is connected to the grid and can be changed dependent of the requirement that apply.

TABLE 5.1: Allowed voltage variations in the grid over 1 minute [72].

Voltage level	**Allowed voltage variation**
230 V	207 V - 253 V
400 V	360 V - 440 V

5.2.2 Step Voltage Changes

The step voltage is defined as rapid changes in the voltage RMS value and is caused by errors and short circuits in the utility grid or big loads at the end user. Step voltage is variations or steps between 207 V and 253 V happening faster than 0.5 % of the agreed voltage level per second [72]. E.g. for 230 V grids, the voltage cannot change more than 1.15 V per second. If this happens, FoL has put limitations shown in Table 5.2 for how often it can happen in grids with a nominal voltage between 230 V and 35 kV.

TABLE 5.2: Number of times the step voltage, expressed as $\Delta U_{stationary}$ and $\Delta U_{maximal}$, can deviate the limits for one 24-hour time period [72].

Step voltage	**Maximum allowed for one 24 hour time period**
	$230\ V < U_N < 35\ kV$
$\Delta U_{stationary} \geq 3$ %	24
$\Delta U_{maximal} \geq 5$ %	24

The step voltages in Table 5.2 are limits for when a step is counted, the value connected to this limit is how many times this can happen during a period of 24 hours. FoL is expressing step voltage as stationary and maximal change in voltage as given:

$$\% \ U_{stationary} = \frac{\Delta U_{stationary}}{U_{agreed}} \cdot 100 \ \% \tag{5.1}$$

$$\% \; U_{maximal} = \frac{\Delta U_{maximal}}{U_{agreed}} \cdot 100 \; \% \tag{5.2}$$

$\Delta U_{stationary}$ is the stationary voltage change as a result of a voltage change characteristic; $\Delta U_{maximal}$ is the maximal voltage difference during a voltage change characteristic; U_{agreed} and U_N is the respective nominal voltage level at the connection point between user and grid [72]. A voltage change characteristic is defined as *"a change in voltage RMS evaluated every half cycle as a function of time, between time periods where the voltage has been stable for minimum one second. The voltage is considered stable when its RMS is located within a voltage interval adequate to 0.5 % of the agreed voltage level"* [72].

5.2.3 Flicker and Flicker Severity

Flicker is defined as *"the visible variation where the luminance (candela/m^2) or the spectral distribution varies with time"* [72]. Flicker is the visible variation of light caused by RMS voltage variations with a frequency between 5 and 20 Hz. The worst frequency for the human eye is statistically 8.4 Hz, this leads to discomfort for people because of intensity variations in light [73]. Flicker severity is the intensity of the flicker discomfort and is defined by the UIE-IEC flicker measuring method. There are two indicators for determining different levels of flicker, according to FoL [72].

i Short term flicker indicator (P_{st}), where the flicker severity is assessed after a time period of 10 minutes.

ii Long term flicker indicator (P_{lt}), where the flicker severity is calculated over a time period of two hours using 12 P_{st} numbers calculated from Equation (5.3).

$$P_{lt} = \sqrt[3]{\sum_{i=1}^{12} \frac{P_{st\ i}^3}{12}} \tag{5.3}$$

where $P_{st\ i}$ is the value of a short-term flicker indicator between $i = 1$ and $i = 12$ [74]. Agder Energi's technical requirements, as illustrated in Table 5.3 from Appendix J, should be followed when choosing an inverter. The inverter makers should have set design limits so the inverter complies with the requirements set in Table 5.3. Only a technician authorised by Eltek can change the parameters [75]. A Type Verification Test Sheet of the Theia HE-t made by Bureau Veritas Consumer Products Services in Germany, states that the inverter complies with standard

TABLE 5.3: Flicker severity limits as set by Agder Energi [71].

	$\mathbf{230\ V \leq U_{nom} \leq 35\ kV}$	**Time interval**
Short term flicker P_{st}	1.0	95 % of the week
Long term flicker P_{lt}	0.8	100 % of the week

EN 61000-3-3 [75]. During the testing at 100 % power a P_{st} and P_{lt} of 0.43 was measured, which is well below the limits required by Agder Energi in Table 5.3.

5.2.4 Harmonic Distortion

If an appliance does not have a linear relationship between current and voltage, then this appliance will be a source of harmonic distortion. The PWM control in an inverter is also a source of harmonic distortion if no extra capacitors have been added to reduce this. If powered by a sinusoidal voltage, like Figure 5.1 shows, and the current is not sinusoidal then harmonic distorted currents will occur. Examples of appliances that create harmonic distortion are power electronic transformers, electric arc furnaces and welding equipment [76]. If these harmonic distortion currents are mixed with large non-linear impedances in the utility grid, then harmonic distorted voltages occur [77]. The inverter will for PV systems be one source of nonlinear current and voltage characteristic, and could cause harmonic distortion in the utility grid. An example of a sinus distortion at third harmonic is shown in Figure 5.1. Harmonic

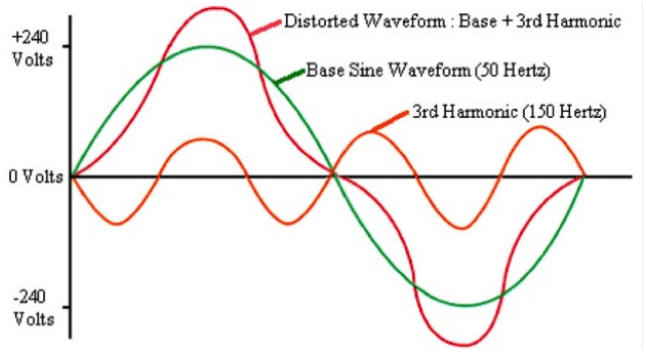

FIGURE 5.1: Harmonic distortion at third harmonic [78].

distortion can be divided into two components:

- Over-harmonic. The frequency is an integer multiple of the nominal frequency ($h \cdot 50\ Hz$, where $h = 2.3.4\ldots$ etc.) [76].
- Inter-harmonic. The frequency is **not** an integer multiple of the nominal frequency ($\mu \cdot 50\ Hz$ where $\mu \neq 2.3.4\ldots$ etc.) [76].

FoL does not set any other requirements to inter-harmonic than providing the Norwegian water- and energy directorate the authority to decide inter-harmonic limits at the connection point. A specific value for this has not been determined and inter-harmonic voltage is therefore not included in this report. There are usually several harmonic components in a grid. A way to put these together is to use the Total Harmonic Distortion (THD) as defined in Equation 5.4.

$$\%THD_h = \frac{\sum_2^{40} U_h^2}{U_1} \cdot 100\ \% \tag{5.4}$$

U_1 is given as the basic harmonic component of the voltage, and the individual harmonic distortion, U_h, for every single multiple of the basic harmonic frequency is defined in Equation 5.5 [72].

$$\%\ U_h = \frac{U_h}{U_1} \cdot 100\ \% \tag{5.5}$$

FoL state that it is the utility company's responsibility to ensure the total harmonic distortion (THD) does not exceed 8 % and 5 %, measured as an average over 10 minutes and one week respectively, at the connection point where the nominal voltage is between 230 V and 35 kV [72]. To comply with this, Agder Energi operates with stricter requirements stating that the THD should not exceed 6 % and 4.5 % as an average over 10 minutes and one week [71], respectively. It is also the utility company's responsibility to ensure that the individual harmonic distortion (U_h) does not exceed the values in Table 5.4, measured as an average over 10 minutes, at the connection point where the nominal voltage is between 230 V and 35 kV [72]. In addition,

TABLE 5.4: Odd- and even-harmonic distortion limits as stated by Agder Energi in Appendix J.

Odd Harmonics				**Even Harmonics**	
Not multiple by 3		Multiple by 3			
Order h	U_h	Order h	U_h	Order h	U_h
5	5.4 %	3	4.5 %	2	1.8%
7	4.5 %	9	1.4 %	4	0.9%
11	3.2 %	15	0.5 %	6	0.5%
13	2.7 %	21	0.5%	> 6	0.3%
17	1.8 %	> 21	0.5 %		
19	1.4 %				
19	1.4 %				
23	1.4 %				
25	1.4 %				
> 25	0.9 %				

Agder Energi has a limit for harmonic currents stating that the PV installation must meet the limit in Table 5.5 for relative harmonic currents given in IEC 61000-3-6 [71].

TABLE 5.5: Limits for relative harmonic currents as stated by Agder Energi in Appendix J.

Over-harmonic order h	**Over-harmonic current $i_h = \frac{I_h i}{I_i}$[%]**
5	5-6 %
7	3-4 %
11	1.5-3 %
13	1-2.5 %
$\sqrt{\sum i_h^2}$	6-8 %

It is Agder Energi's right to impose stricter requirements than stated in FoL. This is done so the requirements in FoL can be fulfilled in grids with several local production units. As shown in Table 5.4 and 5.5, requirements are given for harmonic distortion because hosting several sources of harmonics could cause requirements in FoL to be exceeded.

IEC 61000-3-6, which is a requirement from Agder Energi that the inverter must fulfil, is an *"assessment of emission limits for the connection of distorting installations to **medium voltage, high voltage and extra high voltage power systems**"* [79]. Inverters from Eltek are only connected to low voltage grids ($< 1\ kV$) and are therefore not covered by this standard. The equivalent standards IEC 61000-3-2, *"limits for harmonic current emissions (equipment input current $\leq$16 A per phase)"* [80] and IEC 61000-3-12, *"Limits for harmonic currents produced by equipment connected to **public low-voltage systems** with input current >16 A and $\leq$ 75 A per phase"* [81] cover the requirements for harmonic distortion as listed in EN 50438 [82]. The type test verification sheet [75] also provides data for harmonic distortion, which is well within the limits set by Agder Energi. The Total Harmonic Distortion (THD) of Theia HE-t is measured to be approximately 3.65 % [82], which is within the requirement set by Agder Energi.

5.2.5 Discussion

The testing results of the Theia HE-t 3.8 in [75] provides a value for the requirements given in Appendix J from Agder Energi. The inverter in [75] is tested for UK grid, but some values (like harmonics) are standard for the inverter and therefore common for UK and Norwegian grids. It states that, for the power quality requirements in Appendix J, the inverter from Eltek is sufficient and complies with the required standards for the Norwegian grid. However, this is not surprising since Eltek produce inverters in Norway that complies with European and international standards, it is assumed that they also build inverters for use in Norwegian grids. The main reason why requirements are given for power quality from solar inverters is to ensure the total power quality of the Norwegian utility grid. Deviations from this would result in an

unstable grid, which could destroy the electrical appliances it is meant to supply. Theia HE-t is tested towards these standards, which was made to prevent significant deviations, and is found adequate to be used in both Norwegian and German (and other) utility grids.

5.3 Requirements for Inverter Protection

According to Appendix J, the inverter is required to have a protection so that it is separated from the grid immediately if one of the following events takes place:

- The inverter causes disturbance at the connection point i.e. voltage deviation.
- If unwanted islanding occur (the requirement states that a disconnection must occur within one second after the islanding has occurred)
- If an internal error in the PV system occurs, including the DC side, circuit breakers, etc.

5.3.1 Voltage Dip and Swell

It is called step voltage if the voltage varies between 207 V and 253 V with the limitations explained in Chapter 5.2.1. If the voltage exceeds the ± 10 % nominal voltage limit, it is considered as a **voltage dip** or an undervoltage less than 207 V and **swell** or an overvoltage when the voltage is above 253 V [83] [84]. A voltage dip is explained as a rapid reduction of the nominal RMS voltage to below 90 % and higher than 5 % at a duration between 10 ms and 1 minute. Voltages below 5 % of the nominal voltage are considered as an electrical outage [72]. A voltage dip is mainly caused by short circuits, reconnection when errors occur and when large loads are added to the grid [77]. A voltage swell in an increase of the nominal RMS voltage by more than 110 % of the agreed voltage level within a duration between 10 ms and 1 minute [72]. A voltage swell does not occur often and is mainly caused by rapid disconnection of large loads or wrong transformer stepping [84]. Figure 5.2 illustrates voltage dip a) and voltage swell b). The limits of 253 V and 207 V are illustrated with a red and blue line. If a voltage dip or swell occurs, Agder Energi states that the PV unit must be automatically disconnected within the time frame given in Table 5.6. The table show voltage dip and swell in percentage related to the nominal voltage (U_N). It illustrates that if the voltage deviates within 10 % of the nominal voltage, the inverter can use 60 seconds to disconnect from the grid. If the voltage deviation exceeds 15 %, it must be disconnected within 0.2 seconds [71].

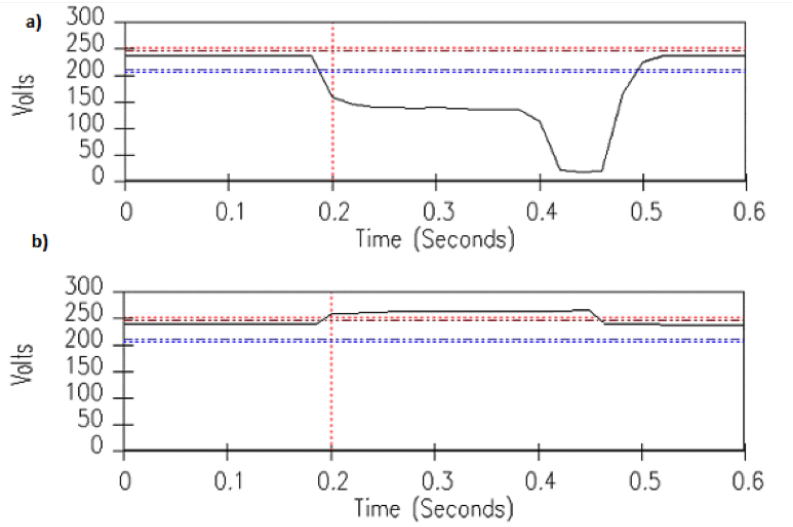

FIGURE 5.2: (a) A voltage dip caused by a short circuit in the grid (b) A voltage swell caused by a disconnection of a large load [83], [84].

TABLE 5.6: Allowed disconnection delay in case of voltage drops or voltage swells as stated in Appendix J.

Voltage area in % of U_N	**Allowed delay [s]**
U>>115 %	0.2
U> 110 %	60
U<90 %	60
U<< 85 %	0.2

5.3.2 Abnormal Frequency

The Norwegian utility grid is very stable and coordinated, the frequency is therefore not the parameter that tends to cause problems. Problems could occur in smaller isolated grids not operated by the utility company (micro grids), or grids that run on generators in general [77]. It is the system operator's responsibility to ensure that the system frequency at all times is within the limitations 50 Hz ± 2 % (49-51 Hz) [72]. If the frequency would go beyond this limit measures like disconnecting generators, frequency control of active production and start of gas generators will be made to control and keep the frequency within these limits [74]. Agder Energi states that if the frequency deviates from the allowed limit, the inverter must be automatically disconnected within the time given in Table 5.7.

TABLE 5.7: The required disconnection time at an abnormal frequency as stated in Appendix J.

Frequency [Hz]	**Maximum disconnection time [s]**
f > 50.2	0.2
f < 47	0.2

5.3.3 Reconnection

The requirements above are given in case a fault occurs and the inverter needs to be disconnected to protect the power quality of the utility grid. The inverter can then be reconnected after the fault is solved; depending on how long the fault lasted. The time frame is given in Table 5.8.

TABLE 5.8: Delay for reconnection of the inverter after a grid failure has occurred, as stated in Appendix J.

Fault duration	**Allowed to be reconnected after:**
< 3 s	5 s
> 3 s	30 s

5.3.4 Discussion

The type verification test sheet [75] tested the inverter for the United Kingdom grid code, which has different tripping times than required from Agder Energi. It is also observed that the over- and under voltage and frequency are different in the UK grid. At first glance, it might look like the inverter does not fulfil the protective requirement from Agder Energi. However, since the tripping times are tested with UK settings it may be assumed that Eltek, a Norwegian company, also has a setting installed for Norwegian grids. The different settings possible to choose are not stated either in the user [53]- or installation manual. If the inverter does not have Norwegian grid settings, then the procedure from page 75 in the user manual is used: "The settings can be changed **within 5 hours** after Start up and feed-in to the grid using the *Owner password*. Thereafter it is only accessible by using the *Installer password*, which will only be available to the installer by contacting *Eltek*" [53]. This gives the impression that the voltage and frequency, as well as its tripping times and reconnection time on page 76 in the user manual, can be changed manually within the first five hours after start up and feed-in. From this, it is assumed that the inverter settings can be manually configured to comply with the protective requirements given by Agder Energi during the installation and set up of the inverter.

5.4 Designing a PV system

Norwegian standards are not completely developed for PV systems since this is still a relatively new phenomenon in Norway. The German [4] and Australian [3] design and installation manuals are therefore used where the Norwegian standards lack guidelines. For the technical standards regarding AC cable CCC, cross section area etc., the Norwegian standard NEK 400:2010 is used. The inverter chosen for this system is Theia HE-t 3.8 from Eltek with the following specifications listed in Table 5.9 from Appendix A. One important factor is the maximum DC system voltage of 600 V, this is the absolute maximum value and must not be exceeded anytime during operation. The maximum PV power is the recommended maximum PV power at STC, a value set by Eltek. If more than 5000 W_p is produced by the PV array, the inverter will only deliver the maximum power and not process the excess power [53]. The PV system will however, be so small that this will not be an issue. The recommended value is therefore used as the maximum input power for this PV plant.

TABLE 5.9: Technical specifications for Theia HE-t 3.8.

THEIA HE-t 3.8	**Specifications**
MPP voltage range	230 V - 480 V
No-exceed DC voltage	600 V
Maximum DC current	18 A
Maximum PV power	5000 W_p
Nominal DC power	4000 W

The PV module chosen to constitute the array is the NAPS (NESTE) NP100G12. These are aged PV modules from the former National Renewable Energy Centre (Energiparken) where the power ratings have been degraded after spending 10-12 years in the field. The approximate de-rated values in Table 5.10 were measured by our supervisor, Dr. Georgi H. Yordanov, from outdoor measurements on a single module and re-used in this thesis. The corresponding temperature coefficients are listed in Table 5.11.

5.4.1 Array Sizing

When designing a grid-connected PV system the properties of both the chosen PV module type and the chosen inverter type have to be taken into account. In order to produce at optimal power output the array has to be matched to the inverter. The following steps are used to size the array [3].

TABLE 5.10: Original and de-rated specifications for the degraded NAPS (NESTE) NP100G12 modules.

NP100G12	**Original specifications**	**De-rated specifications**
Max power	100 $W \pm 10$ %	92 $W \pm 3$ %
Typical I_{MP}	6.0 A	5.48 $A \pm 3$ %
Typical V_{MP}	16.7 V	16.8 V
Typical I_{SC}	6.7 A	6.05 A
Typical V_{OC}	21.6 V	21.7 V
Operating temperature	-40 °C to $+85$ °C	
Maximum system voltage	600 V	
Maximum load [P_a]	N/A	N/A

TABLE 5.11: Temperature coefficients for the degraded NAPS (NESTE) NP100G12 modules.

Temperature coefficients	**Rating**
V_{OC}	-0.075 $V/°C$
V_{MP}	-0.0757 $V/°C$
I_{SC}	$+0.004$ $A/°C$
P_{MAX}	-0.44 $W/°C$

1. Match the array to the inverter voltage specifications
2. Match the array to the inverter current rating
3. Match the array to the inverter power rating

Matching the Array to the Inverter Voltage Specifications

To make sure the array voltage does not exceed the maximum DC voltage of the inverter and PV array, the minimum and maximum modules operating temperature of the location is used to find the PV module voltage for that particular temperature. This is used to find the minimum number of modules in series so that the array V_{MP} does not fall below the minimum inverter voltage. The inverter would then operate away from the MPP and produce lower power. If too many modules are connected to a string the array's open circuit voltage may exceed the maximum allowed input voltage for the inverter or the maximum module system voltage, this could cause an overvoltage and damage both the inverter and the module [3].

Minimum number of modules in a string

Solar modules have the lowest voltage at warm weather. The array has to be designed so the array V_{MP} at the highest operating temperature does not fall below the minimum MPPT voltage of the inverter [3]. The first step is to find the module voltage at the maximum module

temperature by using Equation (5.6):

$$V_{MP\ mod} = V_{MP\ STC} - [\gamma_V \cdot (T - T_0)] \tag{5.6}$$

$V_{MP\ STC}$ is the MPP voltage at standard testing conditions (STC), γ_V is the temperature coefficient of V_{MP}, T is the module temperature at the maximum ambient air temperature and T_0 is the temperature at STC [3].

$$V_{MP\ mod} = 16.8\ V - [0.0757\ A/°C \cdot (76.4\ °C - 25\ °C)] = \mathbf{12.91\ V} \tag{5.7}$$

According to GSES (on page 187), a safety margin of 10 % is added to the minimum inverter voltage due to the following reasons [3]:

1. The inverter may not always be operating at the ideal MPP
2. Allowing for manufacturing tolerances
3. Allowing for lower light conditions (which causes the module voltage to decrease)
4. Allowing a safety margin in case of shading of one or more modules

The module V_{MP} is dependent on temperature, see Equation (5.7), and therefore also irradiance. When a higher irradiance is inflicted upon a module, the temperature rises and the module V_{MP} is slightly reduced due to series resistance. At lower temperatures, the module V_{MP} increases. A safety margin of 10 % is added to count for this variation in array V_{MP}.

The module V_{MP} was calculated by using Equation (5.7), giving 12.91 V. This value must be multiplied by 0.98 to account for a voltage drop of 2 % (will be explained in Section 5.4.2) giving: 12.91 $V \cdot 0.98 =$ **12.65 V**. Second, 10 % is added to the minimum inverter voltage: 230 $V \cdot 1.1 =$ **253 V**. The minimum MPPT voltage of the inverter is then divided by the module V_{MP}:

$$\text{Minimum number of modules} = \frac{V_{\text{inverter}}}{V_{\text{MP}}} = \frac{253\ V}{12.65\ V} = \mathbf{19.99\ modules} \tag{5.8}$$

The value calculated in Equation (5.8) is always rounded up. Since a safety margin is already added, the minimum number of modules allowed in one string for the inverter Theia HE-t 3.8 is **20 modules**.

The "worst-case scenario" happens if the maximum temperature gets higher than the temperature used in the calculations, this will cause the voltage to drop below the minimum inverter voltage. The MPPT is only tracking the V_{MP} of the array within the voltage range specified for

the inverter. If the V_{MP} is outside of this range the MPPT algorithm will find a point within its range that will produce the maximum amount of power. The input current will then be lower than the PV array's I_{MP} and the power will be reduced below P_M as illustrated in Figure 5.3.

Maximum number of modules in a string

The maximum number of modules are calculated with the coldest temperature when the module V_{OC} is at its highest. V_{OC} is used instead of V_{MP} because it is higher and it is the maximum voltage supplied to the inverter when the array is connected or operating. The module V_{OC} is the first value to be calculated by Equation (5.9):

$$V_{OC\ mod} = V_{OC\ STC} + [\beta \cdot (T - T_0)] \tag{5.9}$$

$V_{OC\ STC}$ is the open circuit voltage at STC, β is the temperature coefficient for V_{OC} and T is the lowest expected module temperature at the specified ambient temperature. The module V_{OC} at a given module temperature is found by Equation (5.10):

$$V_{OC\ mod} = 21.7\ V + [-0.075\ V/^{\circ}C \cdot (-10.2 - 25)\ ^{\circ}C] = \mathbf{24.34\ V} \tag{5.10}$$

A safety factor of 5 % is subtracted from the maximum inverter input; this is done to count for manufacturing tolerances and higher voltages than accounted for [3]. The module V_{OC} is given at STC conditions, 1000 W/m^2, to use a standardised value for all of the modules. As mentioned in 4.3, the peak irradiance during winter can reach 800 W/m^2 for Grimstad. The modules V_{OC} would therefore be slightly lower during the winter and slightly higher during summer with a peak irradiance of 1200 W/m^2. Calculations for V_{OC} are not measured for the PV modules during winter or summer, the STC value is therefore used along with a 5 % safety factor to count for higher voltages.

$$V_{\text{inverter}} = V_{\text{max input}} \cdot 0.95 = 600\ V \cdot 0.95 = \mathbf{570\ V} \tag{5.11}$$

The maximum number of modules is calculated by dividing this more conservative no-exceed voltage by module open-circuit voltage:

$$\text{Number of modules} = \frac{V_{\text{inverter}}}{V_{\text{OC mod}}} = \frac{570\ V}{24.34\ V} = \mathbf{23.418\ modules} \tag{5.12}$$

This number is always rounded down to avoid producing over the maximum input voltage. The maximum number of modules allowed in the string is therefore **23 modules**.

Matching the Array to the Inverter Current Rating

It is important to ensure that the maximum current produced by the array is lower than the inverter maximum DC current input. The number of parallel strings the array can consist of is calculated by using the short circuit current (I_{SC}) [3]:

$$I_{SC\ mod} = I_{SC\ STC} + [\alpha \cdot (T - T_0)] \tag{5.13}$$

$I_{SC\ STC}$ is the short-circuit current at STC, α is the I_{SC} temperature coefficient, T is the module temperature at a specified temperature.

$$I_{SC\ mod} = 6.05\ A + [0.004\,(A/^\circ C) \cdot (76.4\ ^\circ C - 25\ ^\circ C)] = \mathbf{6.25\ A} \tag{5.14}$$

This is the module short circuit current at STC irradiance conditions and a high module temperature. It is possible to exceed the extra-terrestrial irradiance in the southern parts of Norway. A research paper published by UiA [30] states that the maximum expected overirradiance in short bursts for Grimstad is 1600 W/m^2.

$$I_{SC\ mod} = 6.05\ A \cdot 1.6 + [0.004\,(A/^\circ C) \cdot (76.4\ ^\circ C - 25\ ^\circ C)] = \mathbf{9.89\ A} \tag{5.15}$$

A higher overirradiance in Grimstad would provide a higher module short circuit current of 9.89 A. If this system was to be designed for operation at the Equator, a short term irradiance of 2000 W/m^2 could be possible, which would give a module short circuit current of 13.5 A. This would increase the array current and reduce the number of strings possible to attach to the inverter as well as affecting the cross section of the chosen cables. The German design manual [4] states the maximal values for the irradiance in central Europe to be 1500 W/m^2, which is a pessimistic number when the overirradiance in Grimstad could reach 1600 W/m^2. It is well known that the irradiance increases at lower latitudes. The German manual lacks to investigate how overirradiance at lower latitudes both in Europe and by the Equator would increase the module short circuit current at short intervals of time, like in Figure 4.1. The consequence of not counting for these overirradiance peaks would be the loss of power when the current exceeds

the MPPT-range.

$$\text{Number of strings} = \frac{I_{\text{max DC input}}}{I_{\text{SC mod}}} = \frac{18\ A}{6.25\ A} = \mathbf{2.88} \tag{5.16}$$

The I_{SCmod} of 6.25 A is used further because this is instructed in the manuals, and because the PV system is relatively small. The maximum number of strings is calculated by Equation 5.16 and is always rounded down to avoid over current in the inverter, the maximum number of strings allowed in the array is two strings. This is not consistent to the number of string input of the inverter given in Appendix A, which is three strings. It seems like the inverter's DC current rating is optimised for two strings of PV modules with higher I_{SC} up to 8.5 A (equals 2.1 strings) and 3 strings of PV modules with a lower I_{SC} down to 5.8 A (equals 3.1 strings). Other PV modules with an even higher I_{SC} could also be installed if only one string is used.

Matching the array to the inverter power rating

When matching an array to an inverter, calculations for current, voltage and power need to be made to ensure the correct sizing of the PV system. The calculations for current and voltage done in this Section give a specific value so the array can be sized with a number of strings and modules in a string. The power calculations are done to find the maximum number of modules allowed in the system [3]. With the chosen inverter and module, the maximum number of modules in the array is:

$$\text{Array size} = \frac{\text{Maximum inverter rated power}}{\text{Module power}} = \frac{5000\ W}{92\ W} = \mathbf{54.34\ modules} \tag{5.17}$$

This is rounded down and means that 54 modules can be connected to the inverter. Current and voltage calculations show that this is not possible, a maximum value of 23 modules in a string and maximum 2 strings give a maximum number of 46 modules in the array. The power calculations are necessary to ensure that a PV system is not oversized. If that happens, the inverter will not be able to process the power shown in Figure 5.3 and will instead limit the produced array power by creating a gap between the array's MPP and the operational range of the MPPT [3].

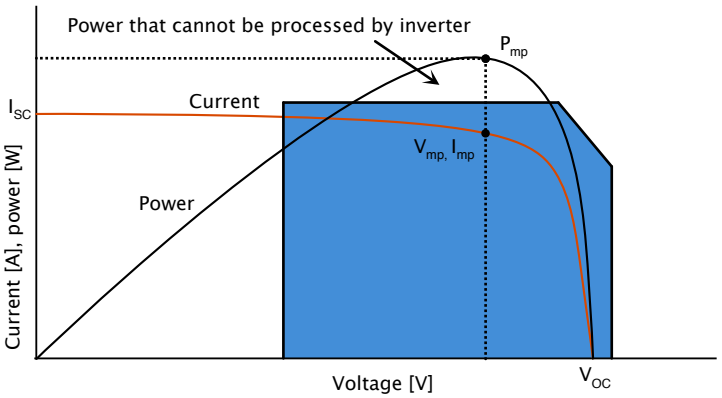

FIGURE 5.3: Illustrates how some of the array's power cannot be processed because it is outside the MPPT range of the inverter [3].

Discussion

Calculations done above are guidelines on how the array should be sized when following the design manuals. It is therefore chosen to follow this and not count for overirradiance, since it is not specified in the manuals, even though it is known that overirradance of 1.6 suns can occur. The system will be oversized, so further results when the inverter starts commissioning will explain how overirradiance affects the system. Because of limited space, the mounting system on the roof of UiA Grimstad can only fit about 32 modules. With the calculated limitations of a string containing between 20 and 23 modules and a maximal number of two strings, it can be concluded that there will be no room for two strings with 20 modules each. The best option would be to install one string with 23 modules in series to make the most out of one string. This will give a rated system power of 2.1 kW_p before system losses in Section (5.5) are accounted for. The 23 modules will be arranged in the configuration given in Figure 5.4 to minimize losses due to shading from the fence and expose as much of the array as possible to the sun. This figure illustrates the order of how the modules are mounted, the polarity, how they are connected to each other in series and will be used later in the thesis. The figure also give an equation for calculating the length of the shadow from the fence in the plane of the PV array at sunrise and sunset, as height of fence/sin(40).

5.4.2 Cable Sizing

Wiring is an important part of the PV system design, both for safety- and efficiency reasons. It is important that the conductor and the electrical insulation is correctly sized since undersized

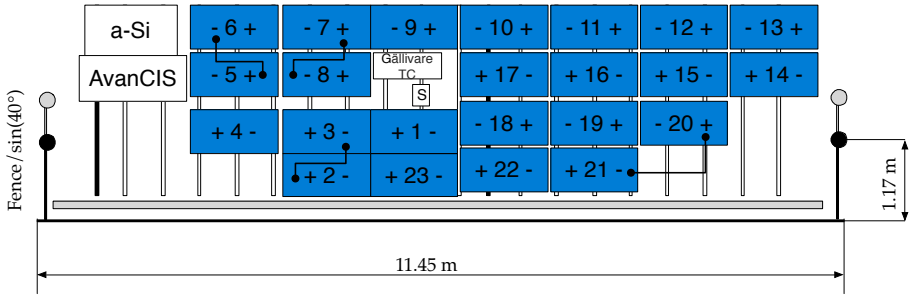

FIGURE 5.4: PV array configuration as it was installed on the roof, showing the order and polarity of the PV modules as well as the four elongated string cables.

cables could cause a fire hazard. If cables are correctly sized, the voltage drop will be minimal and current in cables will never be greater than the cable safe current handling capability. There are different currents and voltages in different parts of the PV system. PV system cables are therefore divided into string-, array- and AC- cables [3].

The voltage drop in these cables can not be so large that the electrical appliances do not get the power it is rated for at normal operation [85]. AS/NZS5033:2005 states the DC voltage drop to be less than 4 % to allow for an AC voltage drop of 1 % [3], while the Norwegian standard NEK 400-5-52:2010 paragraph 525 states that the total voltage drop should be between 5 % to 8 %. The Australian standard, which was made for PV systems, is therefore applied. The 4 % DC voltage drop is divided into 2 % for the string cables and 2 % for the array cables.

Cables with steel or aluminium conductor are sometimes used in electrical plants [19], but copper has the best conductivity. The cable used in this PV system is a 6 mm^2 solar cable with copper conductor, a DC rating of 1.8 kV and a rated current of 32 A [86]. UiA has this cable in storage and we will use this when extra cable length is needed instead of buying a new cable.

Current Carrying Capacity

The current carrying capacity (CCC) is the maximum current that can flow continuously through a conductor without causing any damage to the conductor or the cable insulation due to high temperatures [85]. The resistance in the conductor creates heat, while the insulation set the temperature limitations, and cables carrying more current than the CCC rating will overheat [85]. An overheated cable will result in energy loss and inefficiency, but could also melt the cable insulation, cause a short circuit or a fire. Equation (5.18) and (5.19) is used to

find the maximum allowed current in the array conductor [4]:

$$CCC \geq 1.25 \cdot I_{\text{SC Array}} \tag{5.18}$$

$$CCC \geq 1.25 \cdot 6.25\ A \rightarrow CCC \geq \mathbf{7.81\ A} \tag{5.19}$$

In this section it was decided that only one string is to be used, the array current given as $I_{\text{SC Array}}$ equals one module's rated current, which equals the string current. The peak continuous irradiance measured in Grimstad is about 1200 W/m^2, which can last for tens of minutes [19]. It is therefore assumed that a CCC of 1.25 times I_{SC} can be used [4]. The array CCC found with Equation (5.18) is therefore the same as for the string cables. The current carrying capacity for the AC cable is found in table 52B-2 to 52B-13 in the Norwegian standard NEK 400-5-52:2010 for a chosen cable cross section assuming an air temperature of 30 $°C$.

PV String Cable

The PV modules are delivered with string cables built in from the factory. These cables are already dimensioned with the module current to be 2.5 mm^2 with a total length of 0.9 m both ways for the series cables between the modules and are therefore not necessary to resize. However, it is desirable to minimise the loop area of the array as illustrated in Figure 5.5. To reduce lightning induced voltage spikes it is recommended by the Australian standard AS/NZS5033:2005 to wire the array so that the area of conductive loops is minimal [3]. To ensure this, string cables should be installed as shown in Figure 5.5(a), where the negative and positive string cable are at different lengths. This would result in a negative string cable length of 25 metres one way. Copper cables with 6 mm^2 in dimension intended to use as array cables, is used as negative cable and would give an additional voltage drop as calculated in Equation (4.6).

The wiring loop cable consists of a copper conductor. The resistivity for copper at 20 $°C$ is found to be approximately 0.0168 $\Omega \cdot mm^2/m$ [87], with a temperature coefficient of approximately 0.43 $\%/°C$ in the range between -50 $°C$ to 90 $°C$ [88]. It is assumed that the temperature behind the PV modules can reach up to 70 $°C$.

$$\rho_{loop} = 0.0168\ \Omega\frac{mm^2}{m} \cdot \left(1 + \frac{0.43}{100}\frac{\%}{°C}\,(70 - 20)\ °C\right) = \mathbf{0.020412\ \Omega\frac{mm^2}{m}} \tag{5.20}$$

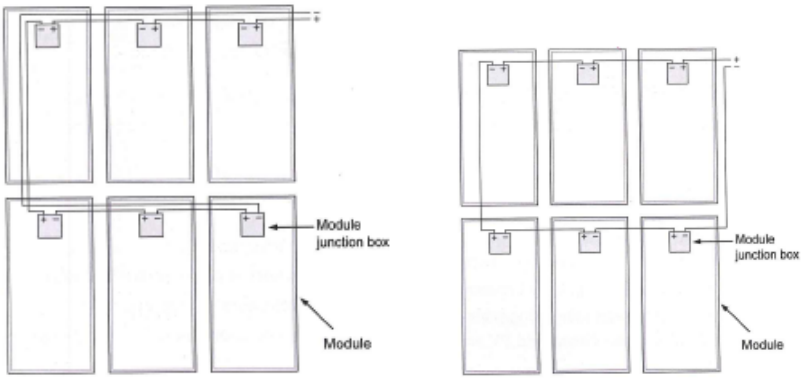

(a) PV string with minimised loop. (b) PV string with incorrect wiring.

FIGURE 5.5: Correct and incorrect wiring of the string cables with regards to minimizing the wiring loop [3].

The voltage drop over the string cables is then calculated to be:

$$V_{drop\ DC} = \frac{0.9\ m \cdot 7.81\ A \cdot 0.020412\ \Omega\frac{mm^2}{m}}{2.5\ mm^2} = \mathbf{0.06\ V} \tag{5.21}$$

The calculated voltage drop for the series cables already installed between each module of 0.06 V is equivalent to a voltage loss of 0.01 %. The distance of 0.9 m occurs between each module, the voltage drop is then multiplied with the number of modules to find the voltage drop of all the 0.9 m cable distance together. Figure 5.4 indicates that four elongated cables must be added between some modules, these elongated cables are made out of 6 mm^2 cables with a distance of 0.8 m and must be added to the total string cable voltage drop, which is calculated to be: $(0.06\ V \cdot 23) + (0.02\ V \cdot 4) = \mathbf{1.46\ V}$ which equals a voltage loss of 0.38 %.

$$V_{drop\ DC} = \frac{25\ m \cdot 7.81\ A \cdot 0.020412\ \Omega\frac{mm^2}{m}}{6\ mm^2} = \mathbf{0.66\ V} \tag{5.22}$$

The negative cable length added to minimise the conductive loops results in an additional voltage drop of 0.66 V, equivalent to a voltage loss of 0.17 %. The total voltage drop for the string cables is **2.12 V** or **0.55 %**, when it is assumed no loss in the MC3 string connectors, which is lower than the recommended value of 2 %.

PV Array Cable

The PV array cable is the connection between the string and the inverter and is often the longest cable in the system. The voltage drop over the array cable is also assumed to be 2 %,

the MPP of the string at STC is expressed as the number of modules times module V_{MP}, $23 \cdot 16.8\ V = \mathbf{386.4\ V}$ [3]. The array cable will be installed through a duct from the array on the roof to the inverter located in the PV lab. The total length of the array cable is assumed to be 50 metres both ways, where 6 metres of the cable is located in open with the sun heating up the black insulation. It is assumed that the exposed cable temperature can reach 75 $°C$. The copper resistivity for the exposed 6 metres is then calculated in Equation (5.23).

$$\rho_{exposed} = 0.0168\ \Omega\frac{mm^2}{m} \cdot \left(1 + \frac{0.43}{100}\frac{\%}{°C}(75 - 20)\ °C\right) = \mathbf{0.0207732\ \Omega\frac{mm^2}{m}} \tag{5.23}$$

It is assumed that the temperature for the remaining 44 metre of the array cable, located in a duct, can get up to 30 $°C$. The resistivity is calculated with Equation (5.24).

$$\rho_{array} = 0.0168\ \Omega\frac{mm^2}{m} \cdot \left(1 + \frac{0.43}{100}\frac{\%}{°C}(30 - 20)\ °C\right) = \mathbf{0.0175224\ \Omega\frac{mm^2}{m}} \tag{5.24}$$

The difference in resistivity between the exposed cable and the enclosed cable is not very large and is almost negligible. If $\rho_{exposed}$ were to be used to calculate the minimum cross-section area, the difference would also be very small. Even though six metres of the array cable is exposed to 75 $°C$, 30 $°C$ is still used as cable temperature because of the small difference and since 6 mm^2 (explained below) is a lot thicker than the calculated minimum cross section area in Equation (5.16).

$$A_{DC\ array} = \frac{2 \cdot 25\ m \cdot 7.81\ A \cdot 0.0175224\ \Omega\frac{mm^2}{m}}{0.02 \cdot 386.4\ V} = \mathbf{0.886\ mm^2} \tag{5.25}$$

By using the two different temperatures, a minimum cross-section of 1.032 mm^2 is reached when 75 $°C$ is used and 0.886 mm^2 when 30 $°C$ is used. The difference is minimal, especially because an array cable with a cross section of 6 mm^2 is already installed between the mounting rack and the PV lab, which has been used for other research projects. Since the minimum cable size is 0.886 mm^2, the 6 mm^2 array cable is both oversized and sufficient to supply the array current to the inverter. A new array cable will therefore not be installed. With the array cable cross section selected, the voltage drop can be calculated with Equation (5.26).

$$V_{drop\ DC} = \frac{2 \cdot 25\ m \cdot 7.81\ A \cdot 0.0175224\ \Omega\frac{mm^2}{m}}{6.0\ mm^2} = \mathbf{1.14\ V} \tag{5.26}$$

A voltage drop of 1.10 V over 50 metres is equivalent to a voltage drop of **0.3 %** this is also less than the recommended maximum voltage drop of 2 %.

AC Cable

The AC cable length from inverter to electrical switchboard is measured to be 22 metres, the maximum output current from the inverter is 19.7 A_{RMS} (Appendix A), the AC phase voltage is 240 V_{RMS} and the power factor ($\cos\phi$) of 1.0 is used in the case when current and voltage are in phase [19]. It is assumed a temperature around the AC cable of 30 $°C$ since it is located inside a building. The resistivity of the AC cable is the same as calculated in Equation (5.24) [3]. The minimum theoretical AC cable cross section is expressed with Equation (5.27):

$$A_{AC\ cable} = \frac{L_{\text{AC cable}} \cdot I_{AC} \cdot \rho \cdot \cos\phi}{Loss \cdot V_{AC}} \tag{5.27}$$

$L_{AC\ cable}$ is the length of the AC cable, I_{AC} is the AC current (expressed as the maximum inverter output current), ρ is the resistivity, $Loss$ is the allowed voltage loss in percentage written as a decimal and V_{AC} is the AC phase voltage of the grid [3]. The minimum AC cable cross section is calculated to be:

$$A_{AC\ cable} = \frac{22\ m \cdot 19.7\ A \cdot 0.0175224\ \Omega\frac{mm^2}{m} \cdot 1.0}{0.01 \cdot 240\ V} = \mathbf{3.164\ mm^2} \tag{5.28}$$

The actual AC cable cross-section is selected to be 6 mm^2, almost double of the minimum AC cable cross section calculated in Equation 5.28. The cross section was chosen after method A2 in NEK 400:2010 assuming two conductors in table 52B-2, giving the AC cable a CCC of 32 A [55]. According to NEK 400:2010, the minimum AC cross section is 4 mm^2 [55] which also meets the calculated cross section in Equation 5.28, but 6 mm^2 is used in case a system with a higher peak continuous current is installed at a later time. The voltage drop in the AC cable can then be calculated by transposing Equation (5.27) [85].

$$V_{Drop\ AC} = \frac{22\ m \cdot 19.7\ A \cdot 0.0175224\ \Omega\frac{mm^2}{m} \cdot 1.0}{6\ mm^2} = \mathbf{1.27\ V} \tag{5.29}$$

A voltage drop of 1.27 V over 22 metres is equivalent to a voltage loss of **0.53 %**. The total voltage loss between the array and the kWh-meter is 0.55 %+0.3 %+0.53 % = **1.38 % < 5 %**. The requirements in AS/NZS5033:2005 and NEK 400:2010 has been fulfilled.

Discussion

It is fairly easy to reduce the voltage loss in the system cables. The solution is to choose a conductor with a larger cross-section than needed, the voltage loss is then reduced and an extra safety factor is added when a thicker conductor can carry a higher current. In addition to this, an extra safety factor was also added when the CCC was found by using 1.25 times $I_{SC\ STC}$. For this thesis, UiA has already decided the cross section area of the DC and AC side and bought the cables to be used. An important part of this chapter is then to assure the quality of the chosen cables, to ensure a sufficient cross section area for the current it is going to carry and to ensure the total voltage loss is within the acceptable limits. The calculations done in chapter 5.4.2 states that the cables chosen for this PV system is more than sufficient to carry both the current produced in the PV string and a higher current for a future upgrade of the PV system. The AC cable is dimensioned to carry more than the maximum current possible for the inverter to produce and is also dimensioned with the intention of a future upgrade.

5.4.3 PV System Protection

One of the most important aspects when designing a safe and reliable PV system is the sizing of fuses and circuit breakers. System protection is needed to minimise the risk of damage to system components such as cables and modules. A PV system normally requires two types of protection [3]:

- Over-current protection on the DC and AC sides
- Disconnect/isolator switches on the DC and AC sides

According to NEK 400-7-712:2010, a disconnect/isolator switch is needed on both sides of the inverter. This makes it easy and safe to perform maintenance on the inverter. Over-current protection is used to protect components and cables from short-circuits or overload currents and is based on the array current (I_{SC}). However, on the DC side NEK 400-7-712:2010 states that over-current protection is not needed if the current-capacity of the conductors is larger or equal to $1.25 \cdot I_{SC}$.

An isolator switch is included in the inverter for isolating the DC side and using fuses could fulfil the overcurrent protection. However, it is decided to use a circuit breaker, which does not need to be replaced when tripped. Both types of protection listed above are included in

a circuit breaker. The DC side of the PV system will be protected by a circuit breaker from manufacturer Eaton and a circuit breaker from ABB will be used on the AC side.

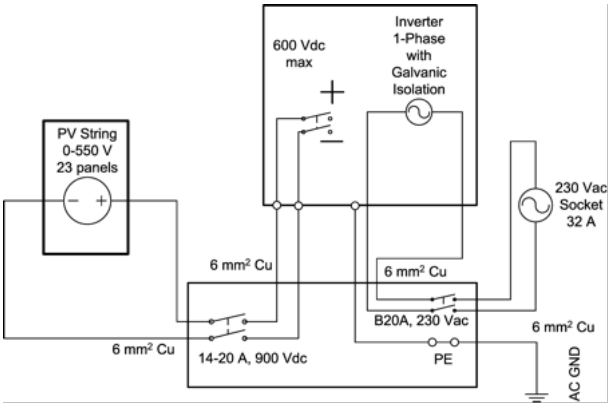

FIGURE 5.6: 2-line diagram of the PV system [19].

From NEK 400-4-43:2010, two requirements must be fulfilled in order for a circuit breaker to protect a conductor from over-current: $I_{SC\ \text{Array}} \leq I_n \leq CCC$ and $I_2 \leq 1.45 \cdot CCC$. I_n is the rated current of the circuit breaker. I_2 is the overload-current ensuring that the circuit breaker trips. On the DC side, 6 mm^2 Cu conductors will be used. According to NEK 400:2010, a 6 mm^2 conductor can carry up to 32 A at an ambient temperature of 30 $°C$. Installation method A2 in table 52B-2 (NEK 400-5-52:2010) is used assuming a single-conductor cable installed in a pipe in a thermic isolated wall. The CCC of the DC cable when using 1.25 x $I_{SC\ array}$ is 7.81 A, while the chosen oversized cable has a CCC of 32 A. Currents of this magnitude is not assumed to occur in the PV system, so the circuit breaker chosen from Eaton is 20 A but the CCC of 32 A is used further. The thermal tripping characteristic is from 1.05 to $1.3 \cdot I_n$ and is found in the technical data in Appendix D. The thermal tripping characteristic is preferably set to 1.3, allowing higher overload-current before the circuit breaker trips. $I_2 = 1.3 \cdot I_n = 1.3 \cdot 20\ A = \mathbf{26\ A}$. The specifications are summarised in Table 5.12.

$$I_{SC\ \text{Array}} \leq I_n \leq CCC \rightarrow 6.25\ A \leq 20\ A \leq 32\ A \tag{5.30}$$

$$I_2 \leq 1.45 \cdot CCC \rightarrow 26\ A \leq 46.4\ A \tag{5.31}$$

TABLE 5.12: Sizing on the DC side.

Maximum DC current ($1.25 \cdot I_{SC}$)	**Circuit breaker**	**Conductor size**
7.81 A	20 A	6 mm^2 Cu

On the AC side, the maximum possible current load from the inverter is 19.7 A (I_B) and the conductor size is set to 6 mm^2 Cu. Installation method A2 (NEK 400-5-52:2010) is used assuming a multi-conductor cable installed in a pipe within a thermic isolated wall. The conductor can carry up to 32 A, which is used as CCC in Equation 5.32. The common B characteristic is used for the circuit breaker (ABB) where $I_2 = 1.45 \cdot I_n = 1.45 \cdot 20\ A = \mathbf{29\ A}$. The specifications on the AC side are summarised in Table 5.13.

$$I_B \leq I_n \leq CCC \rightarrow 19.7\ A \leq 20\ A \leq 32\ A \tag{5.32}$$

$$I_2 \leq 1.45 \cdot CCC \rightarrow 29\ A \leq 46.4\ A \tag{5.33}$$

TABLE 5.13: Sizing on AC side.

Maximum AC current	**Circuit breaker**	**Conductor size**
19.7 A	20 A	6 mm^2 Cu

Discussion

The Eaton circuit breaker, for the DC side, is constructed for PV systems and also for the varying currents. Characteristics for this circuit breaker are given in Appendix D and provides both the tripping characteristic curve and the adjustment tool. The Eaton PKZ-SOL20 can vary its setting value between 14 A and 20 A dependent of the I_{SC}. The lowest value 14 A is therefore used as the setting value since this is the lowest possible. The circuit breaker is therefore rated for 2.2 suns x I_{SC} which is considered more than what is needed when the highest irradiance is 1.6 suns. Since I_{SC} is considered never to exceed 14 A, the circuit breaker will not trip at overirradiance conditions and the inverter will therefore be able to utilise this power.

The cables are oversized and over-current protection should not be necessary on the DC side, due to CCC being larger than $1.25 \cdot I_{SC}$. However, a circuit breaker will be installed due to possible future upgrades on the PV system. The modules can then be replaced in the future with newer more efficient modules without needing to upgrade cables and the circuit breaker.

5.5 Losses in the PV system

Theoretical systems may have 100 % efficiency, but this is not the case when installing a real, physical system. A PV array has several factors that may cause losses in the system. The factors mentioned underneath provides an estimate of losses on a yearly basis, which will be deducted from the total power rating [3].

- Temperature and irradiance losses
- Dirt and soil losses
- Manufacturer's tolerance
- Shading losses
- PV module orientation
- PV module tilt angle
- Voltage drop through System Cabling
- Inverter efficiency
- Angular reflectance effects
- Spectral gain

5.5.1 Temperature and Irradiance Losses

The module voltage is dependent of the module temperature, as the temperature rises the voltage drops. From $P = I \cdot V$, the module power also decreases as the voltage drops. Figure 4.3(a) in Section 4 explains how the I-V curve of a PV module is changing with temperature variations. Wind is also a factor affecting the temperature, no wind data are measured at the site and will therefore not be taken into account.

To calculate these losses the relative efficiency (η_{REL}) is used, which is a factor dependent of temperature and irradiance at a location. The relative efficiency decreases with the latitudes as the temperature increases at southern locations [45]. Since the module energy yield is strongly dependent of temperature irradiance, which is varying, the relative efficiency is used to cover losses due to these factors. This is calculated with Equation 5.34 with respect to STC for lower irradiances, assuming a constant temperature of 25 $°C$, which gives Figure 5.7(a). Figure 5.7(a) explains how the relative efficiency of an aged multicrystalline silicon module changes with lower irradiances. It also illustrates the difference between an aged module and newer modules with higher curves and better efficiencies. Figure 5.7(b) shows the energy contribution in percentage

for each irradiance measured over Grimstad in 2011, indicating that Figure 5.7(a) is calculated for the most common irradiances at this location. The relative efficiency and module STC efficiency is calculated with Equations 5.34 and 5.35. η_{REL} is calculated over several irradiances with respect to STC and constant temperature, the results for this calculation over different irradiances is illustrated in Figure 5.7(a).

$$\eta_{REL}(G,T) = \frac{\eta(G,T)}{\eta_0} = \frac{P_M(G,T)}{G}\frac{G_0}{P_0} \tag{5.34}$$

$$\eta_0 = \frac{P_0}{A \cdot G_0} \tag{5.35}$$

where P_0 is the module STC power rating, η_0 is the module STC efficiency, G_0 is the irradiance during STC while the maximum power P_M and efficiency η is related to the in-plane irradiance G, at any time, and the module temperature T [89].

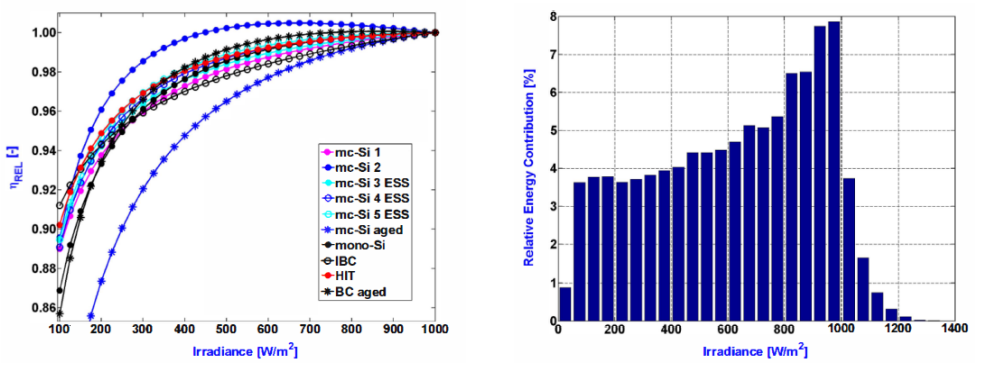

(a) Relative efficiencies with respect to STC, assuming a STC temperature of 25 $°C$.

(b) Relative Energy Contribution with respect to irradiance measured over Grimstad in 2011.

FIGURE 5.7: The relative efficiency is calculated with respect to STC, covering the most measured irradiances over Grimstad in 2011 [89].

From Equation 5.34 and Figure 5.7(a), [89] calculated that an average relative efficiency for aged mc-Si modules of 0.93 can be used.

5.5.2 Dirt- and Soil losses

Dirt or soil can build up on the PV module if it is not regularly cleaned, this could reduce the output power by preventing some of the sunlight from reaching the cells. A dirt de-rating factor, f_{dirt}, is added to the total equation depending on the site and operator. From Figures

(a) Gathering of soil on the edge of a module on site.

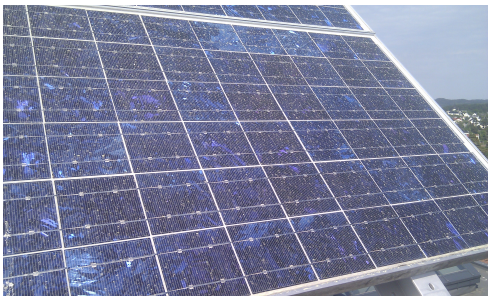

(b) PV modules can be exposed to dust and dirt which would cover the glass plate. Pollen was very prominent in May.

FIGURE 5.8: Soil and dirt de-rating examples of the PV system.

4.9, 5.8(a) and 5.8(b), examples are given from the location of the PV array illustrating that the array gets quite dirty over time, this can be prevented by regularly cleaning by the operator. Figure 5.8(b) shows that the array gets covered by pollen in May, which could affect the power output if not cleaned. Grimstad is a place exposed to a relatively high amount of rain and it can be assumed that the PV array will be cleaned after a rainy day, but soiling and bird droppings need to be manually removed. It is assumed that a PV system operator wants as small losses from dirt as possible and is therefore cleaning the array when needed. The dirt factor is therefore assumed to be 0.98.

5.5.3 Manufacturer's Tolerance

A manufacturer's tolerance is usually showed as a ± percentage after the module power rating on the module specification sheet. The tolerance given in the specification sheet is ±10 %, though the calculated de-rated tolerance found by [19] in Table 5.10 indicates a tolerance of ±3 %. The manufacturer's tolerance should be based on the minimum module power which is 92 W -3 %. A tolerance of -3 % (0.97) is used when doing energy calculations for the PV array.

5.5.4 Shading

Shading is a factor with a significant potential of affecting the output power of the module. This is a hard value to predict and has unique values for every location, dependent of the surroundings. If an accurate value for the shading loss is wanted, then detailed analyses should be made on the roof for at least one year to count for summer and winter conditions. This is however, not done in this thesis. It is observed that in April, the fence in Figure 4.8 will

only shade on the bottom right corner of module number 20 in Figure 5.4 for 30 minutes in the morning when the irradiance is low. More shading factors during the summer occur because of birds flying past or landing on the modules, as shown in Figure 5.9(b). During winter, low sun exposes the array to other shading factors. Figure 4.8 shows shading from both the fence and snow covering the modules. It is also observed that the telecom tower in Figure 5.9(a) can provide shading early in the morning for two weeks in spring and autumn. This report uses approximately numbers, assumed over a year for an ideal system with no fence, telecom tower or trees to shade the array. It is assumed that these losses will be 3 % (0.97).

(a) The telecom tower could shade the array early in the morning.

(b) Birds landing on the modules are a shading factor.

FIGURE 5.9: Illustration of some of the shading factors [19].

5.5.5 Module Orientation and Tilt Angle

Solar systems in Germany and Australia are often mounted on rooftops and are therefore not always mounted with the optimal tilt angle and orientation. For the location in Grimstad, PVGIS calculated the optimal tilt angle to 38° from the horizontal with orientation towards south. The support beams for the PV modules are mounted 7° east from south with $39° \pm 1°$ tilt angle from the horizontal [32]. The exact tilt of the array is uncertain, the margin of error is therefore used to account for the possibility of the array to have a lower or higher tilt angle. By using PVGIS, the uncertainties due to tilt angle are estimated to be the same as the margin of error given as one degree. The uncertainty is estimated by looking at the irradiation in PVGIS for 38° and 40° for then to calculate the difference. The uncertainty factor and possible loss due to tilt and orientation is therefore estimated to be 99.5 % (0.995).

5.5.6 Voltage Drop through System Cabling

The importance of reducing voltage drop is explained in Section 4.4. The important part is keeping the voltage drop within 5 % between the solar array and the AC socket since a voltage drop of 5 % equals a power drop of 5 %. Because solar cables are less expensive than solar arrays, cables with a larger cross sectional area can be chosen to reduce the voltage drop [3]. As explained in section 5.4.2 the total voltage drop of the PV system was calculated to be 1.38 %, which equals to a factor of 0.986.

5.5.7 Inverter Efficiency

In addition to the power losses on the DC side of the PV system, there are losses due to electronics and transformer in the inverter in the form of heating and switching. For the inverter to operate at maximum efficiency it should be installed with sufficient ventilation and not exposed to direct sunlight [3]. It is not believed that the inverter will operate at the maximum efficiency at all time. The Euro efficiency of the chosen inverter, at a specific MPP voltage, of 96.7 % (0.967) is therefore used (Appendix A).

5.5.8 Angular Reflectance Effects

Losses due to sunlight reflecting on the module glass plate need to be added. This factor is dependent on type of module and on the angle of incident, and affects the amount of irradiance entering the module and has an impact on cell temperature and array power output [90]. This factor, $f_{reflection}$, is estimated in PVGIS and given in Appendix N to be 3.1 % (0.969).

5.5.9 Spectral Effects

The spectral effects of the modules vary and are dependent on the meteorological conditions at the site. These effects are often so small and uncertain that they are often negligible, especially when the solar spectra data for overcast conditions are limited [90]. This factor, f_{spec}, is an energy gain to the system and is assumed to be 1 % (1.01) [19].

5.5.10 De-rated Power Rating of the PV System

So far, Section 5.5 in this Chapter explained the different factors that could affect the power output of the PV system. It is calculated in Section 5.4.1 that 23 modules are the maximum number possible to install in one string. With a PV module power rating of 92 W_p, the power rating is 2.116 kW_p for the entire array. When the de-rating factors are determined, the output power of the PV system with no losses can be calculated with Equation 5.36 for an estimate of a year:

$$E_{no\ losses} = \bar{I} \cdot A \cdot \eta_0 \tag{5.36}$$

With the relative efficiency and Table 4.3 giving the average monthly irradiation in Grimstad between 2011 and 2013. The monthly average of the three past years, 103.27 kWh/m^2, which was calculated in Section 4.1.2 is used. In Appendix N, PVGIS assumes a monthly irradiation of 86.6 kWh/m^2 which is lower than the irradiation used. PVGIS uses PVGIS-3 database in Grimstad, which is based on on ground measurements and as mentioned in Section 4.1.2 is known to estimate lower irradiance than the new PVGIS-CMSAF based on satellite data. It is therefore assumed that the irradiation measurements for the past three years in Grimstad can give an idea of the past and future irradiation at this location. The yearly energy when no losses are added is calculated with Equations (5.36) and (5.35), giving η_0, and resulting in Equation (5.37):

$$E_{no\ losses} = \frac{103.27\ \frac{kWh}{m^2 \cdot months} \cdot 12\ \frac{months}{year} \cdot 2.116\ kW}{1\ \frac{kW}{m^2}} = \mathbf{2622.23\ kWh/year} \tag{5.37}$$

Equation (5.37) assumes from Table 4.3 that the radiation must continue at the rate of 1 kW/m^2 for 103.27 hours per average month to produce 103.27 kWh/m^2 [3]. When including other possible losses in the PV system, as explained in this chapter, a more conservative energy yield can be calculated.

$$Energy\ Yield = E_{no\ losses} \cdot f_{rel} \cdot f_{dirt} \cdot f_{man} \cdot f_{shading} \cdot f_{tilt} \cdot f_{Vdrop} \cdot f_{Refl} \cdot f_{spec} \cdot f_{inv} \tag{5.38}$$

$$\begin{aligned} Energy\ Yield = 2622.23\ \frac{kWh}{year} \cdot 0.93 \cdot 0.98 \cdot 0.97 \cdot 0.97 \\ \cdot 0.995 \cdot 0.986 \cdot 0.969 \cdot 1.01 \cdot 0.967 = \mathbf{2087.83\ kWh/year} \end{aligned} \tag{5.39}$$

These calculations assume a system loss of **20.4 %** which is a relative conservative loss regarding that an average value for irradiance and temperature loss is used. This is, however, very close to the total system loss assumed in Appendix N by PVGIS of 22.8 %, while [90] assumed a total system loss of 18 %. Appendix N assumes an irradiance and temperature loss of 7.4 %, other system losses of 14 % and reflection losses of 3.1 %. It is therefore assumed that 20.4 % is an acceptable loss for the PV system which will have less losses on days with colder temperatures on irradiances close to or more than one sun and cleaner arrays. With the assumptions done, an estimated energy yield of **2087.83 *kWh/year*** is calculated.

5.5.11 Performance Ratio

The performance ratio (PR) is calculated to estimate the quality of the PV system and to see how much the de-rating factors affect the total performance of the system. The theoretical maximum energy yield is based upon a system with no losses, which is calculated in Equation 5.37.

$$PR = \frac{System\ yearly\ average\ energy\ yield}{Theoretical\ maximum\ energy\ yield} \tag{5.40}$$

$$PR = \frac{2087.83\ kWh/year}{2622.2\ kWh/year} \cdot 100\ \% = \mathbf{80\ \%} \tag{5.41}$$

The performance ratio for the PV system is calculated to be **80 %** with the system loss assumptions done above. Analyses done by [91] reviewed the performance ratio in 11 countries between 1998 and 2002, where the Performance Ratio data bank had recorded PR between 40 % and 85 %, giving an average mean annual PR of 74 %. From [91] it is concluded that the PR spread of PV systems installed between 1998 and 2002 had significantly increased compared to 1991-1998. The PR values from this report are old, but it still expects that the PR of a well designed PV system will increase in the future. This increase could be a result of better planning, technology and inverters. The average PR value of 74 % was recorded at the same time as the PV modules was made; this value is therefore compliant to the age of the installed

modules. A PR of 80 % is considered a good value for this system considering the age of the PV modules which affects the relative efficiency. This value is variable, and will increase for instance after rainy days, when the PV modules are clean, during the winter when the PV modules are not covered with snow and when the module operating temperature is lower than the constant STC temperature.

5.6 PV modules

Specifications of solar cells and modules are determined by using the following standard test conditions (STC): cell temperature = 25 $°C$; irradiance = 1000 $\frac{W}{m^2}$; air mass = 1.5. Due to lack of a solar simulator it was not possible to perform measurements on the PV modules at a controlled environment with STC conditions. All of the PV modules were therefore tested in outdoor conditions. To find the best 23 modules out of 48 modules, each module was tested with an ESL-solar 500DS electronic load connected to the PV module with a positive (red) and negative (black) cable as shown in Figure 5.11(a). The I-V curve measurements were done on clear sky days, with an irradiance varying between 595 W/m^2 and 1147 W/m^2 (noon) and an ambient temperature varying between 11.2 $°C$ and 32.2 $°C$. The conditions were relatively stable for each module and several of the modules were close to STC temperature. Figure 5.10 shows the temperature variations for module 30. The measurements lasted for approximately 30 minutes for each module.

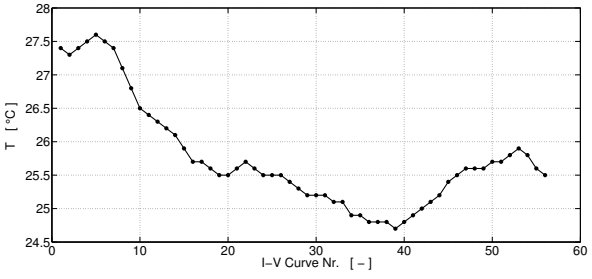

FIGURE 5.10: The temperature for module 30 changes throughout the testing time and is illustrated over the amount of measurements done for this specific module.

5.6.1 Testing Equipment

When the Electronic Load ESL-Solar 500DS is connected to the PV module, it uses a load that is working in MPP tracking mode. In order to stay within the MPP the load works in

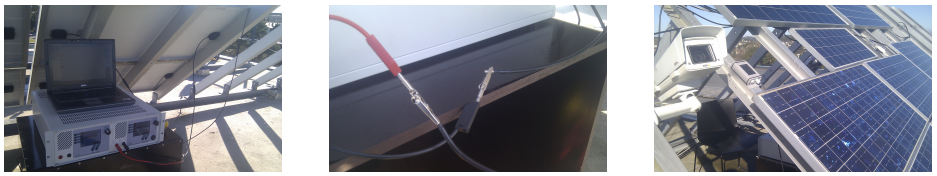

(a) The ELS solar I-V tracker.

(b) The PV module is connected to the I-V tracker with crocodile clamps.

(c) The external temperature and irradiance meter.

FIGURE 5.11: Set-up used when testing the available PV modules with ESL-Solar 500DS.

a continuous mode [53]. To retrieve a good power curve reading, the current and voltage is measured simultaneously in an I-V curve. The data is transferred from the Electronic load to a computer via a USB-port where the ESolar software scans I-V curves and plots the MPP I-V and P-V curve three times every minute. The Electronic Load uses an external sensor for measuring ambient temperature and irradiance, as shown in Figure 5.11(c), to compare with the measurements collected from the PV module. As Figure 5.11(b) shows, the solar string cable is connected to the Electronic Load by using two crocodile clamps, this is one source of error since the increased series resistance from the clamps could result in less accurate data.

5.6.2 Conversion to STC

The modules were rated according to current, voltage and power. Further on, the 23 modules with the highest ratings were then selected and used in the PV system. As seen in Figure 5.12 a high number of I-V curves were measured, approximately 50 curves for each module. The

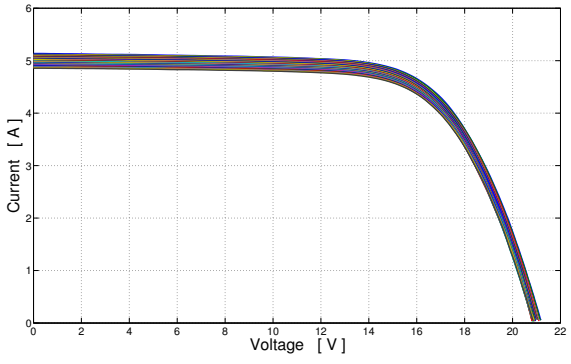

FIGURE 5.12: I-V curves from module 30.

solar irradiance and the ambient temperature varied during the measurement period and in order to compare the PV modules it was necessary to convert the current and the voltage to

STC conditions. The short-circuit current I_{SC} [92] and the maximum power current I_{MP} was converted into STC by using Equations (5.42) and (5.43).

$$I_{SC\ STC} = \frac{I_{SC} \cdot \frac{G_0}{G_S}}{1 + \alpha_{ISC} \cdot (T - T_0)} \tag{5.42}$$

$$I_{MP\ STC} = \frac{I_{MP} \cdot \frac{G_0}{G_S}}{1 + \alpha_{ISC} \cdot (T - T_0)} \tag{5.43}$$

I_{SC}, I_{MP}, G_S and T are the measured values; G_0 is the STC value; α_{ISC} is the relative temperature coefficient; T_0 is the STC value. The relative temperature coefficients of the PV modules were measured in outdoors conditions on one module, by determining the rate of change of current and voltage with temperature. Typically these measurements are done indoor in temperature-controlled environments and by the use of a solar simulator illuminating the PV module [92]. However, such a test fixture is not available at UiA. The relative temperature coefficients are given in Table 5.14.

The open-circuit voltage V_{OC} and the maximum power voltage V_{MP} was converted to STC by using Equations (5.44) [92] and (5.45) [32].

$$V_{OC\ STC} = \frac{V_{OC}}{1 + \beta_{VOC} \cdot (T - T_0)} + \mu \cdot \ln\left(\frac{G_0}{G_S}\right) \tag{5.44}$$

$$V_{MP\ STC} = V_{OC} + n \cdot N_s \cdot V_0 \cdot \ln(1 - \mu_r) + n \cdot N_s \cdot V_0 \cdot \ln\left(\frac{G_0}{G_S}\right) - \mu_r \cdot I_{SC} \cdot R_S \cdot \frac{G_0}{G_S} \tag{5.45}$$

V_{OC} is the measured value; β_{VOC} is the relative temperature coefficient; μ is the irradiance dependency coefficient determined by Equation (5.46); R_S is the series resistance and was retrieved from the I-V curves by using linear regression.

$$\mu = \frac{N_s \cdot n \cdot k \cdot (T + 273.15\ ^\circ C)}{q} \tag{5.46}$$

In Equation (5.46) N_s is the number of solar cells; n is the ideality factor; k is the boltzmann constant; q is the elementary charge. In Equation (5.45) μ_r is the ratio $\frac{I_{MP\ STC}}{I_{SC\ STC}}$.

A large amount of data was collected during the measurements and a MATLAB® script developed by our supervisor was used to perform the STC conversion. Due to asymmetrically distributed data, median values were used. In order to have as high power ratings as possible, modules were compared at the maximum point. When series-connecting modules in a string, the module with the lowest current I_{MP} is operating as the bottleneck of the system. The

TABLE 5.14: Relative PV modules temperature coefficient, number of solar cells in series and ideality factor.

Parameters	Value	Comments
α_{ISC}	$46.61 \cdot 10^{-4}$ $\left[\frac{1}{^\circ C}\right]$	Relative temperature coefficient of I_{SC}
β_{VOC}	$3.46 \cdot 10^{-3}$ $\left[\frac{1}{^\circ C}\right]$	Relative temperature coefficient of V_{OC}
N_S	36	Number of solar cells
n	1.4	Ideality factor

TABLE 5.15: 28 of 48 highest rated PV modules. Red and orange indicates modules with low current, voltage and power values. Yellow highlights the current, which will act as the "bottleneck" of the PV system. PV modules enclosed by the horizontal lines replace the modules with values highlighted in red and orange.

Module	$\tilde{I}_{MP}$ $[A]$	$\tilde{V}_{MP}$ $[V]$	$\tilde{P}_{MP}$ $[W]$	$\dot{V}$ $[V]$	$\dot{P}$ $[W]$	FF
1	5.755	15.689	90.302	16.255	89.013	0.674
18	5.706	16.567	94.644	17.011	93.149	0.692
19	5.690	16.622	94.643	17.071	93.480	0.707
3	5.672	15.278	86.619	15.689	85.909	0.642
37	5.646	16.431	92.701	16.788	91.929	0.695
22	5.610	16.978	95.430	17.260	94.514	0.713
29	5.606	16.786	94.312	17.069	93.466	0.708
35	5.575	16.712	93.132	16.927	92.689	0.701
30	5.570	16.611	92.708	16.822	92.117	0.704
38	5.561	17.211	95.595	17.379	95.167	0.716
23	5.555	16.695	92.761	16.872	92.392	0.704
14	5.550	16.557	91.862	16.720	91.555	0.703
40	5.541	16.799	92.991	16.940	92.764	0.711
20	5.534	16.627	92.000	16.750	91.722	0.692
28	5.533	16.675	92.353	16.810	92.053	0.707
36	5.530	16.802	92.831	16.913	92.614	0.708
42	5.524	16.844	93.060	16.951	92.824	0.710
21	5.514	16.726	92.106	16.806	92.030	0.701
5	5.510	16.181	88.982	16.259	89.034	0.685
43	5.496	16.692	91.725	16.740	91.665	0.709
15	5.492	16.495	90.766	16.532	90.527	0.700
34	5.487	16.480	90.537	16.506	90.386	0.695
31	5.486	16.647	91.357	16.669	91.280	0.695
32	5.485	16.605	91.201	16.626	91.040	0.699
27	5.482	16.791	92.338	16.806	92.028	0.706
24	5.481	16.708	91.487	16.719	91.554	0.705
16	5.480	16.837	92.288	16.848	92.256	0.707
41	5.476	16.770	91.966	16.770	91.830	0.716

modules were therefore arranged in descending order of I_{MP}. By examine Table 5.15 it is seen that sorting by I_{MP} is not enough, due to low power $\tilde{P}_{MP}$ and voltage $\tilde{V}_{MP}$ values on certain modules. 91 W was set as the minimum power value and five of the first 23 modules did not fulfil this criterion. Five additional modules were added to the list, and new conditions were needed to ensure the modules with the highest parameters was chosen. This is done by using

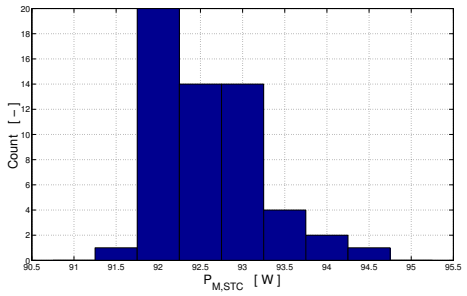

FIGURE 5.13: Histogram of STC power values from module 30, median values are used when ranking the PV modules.

the shunt-free 1 exponential I-V curve model from Equation (5.47).

$$I(V) \approx I_{SC} - I_0 \exp\left(\frac{V + IR_s}{nN_sV_T}\right) \tag{5.47}$$

The differential of I is expressed as:

$$dI = -I_0 \exp\left(\frac{V + IR_s}{nN_sV_T}\right) \cdot \frac{1}{nN_sV_T}\left(dV + R_s dI\right) \tag{5.48}$$

By rearranging Equation (5.48) with respect to dV and integrating between I_{MIN} and I_{MP}, the increments of the output or "new" operating voltage can then be expressed as:

$$\Delta V = R_s\left(I_{MP} - I_{MIN}\right) + nN_SV_T \ln\left(\frac{I_{SC} - I_{MIN}}{I_{SC} - I_{MP}}\right) \tag{5.49}$$

Using the lowest $\tilde{I}_{MP}$ as the string current (highlighted in yellow) will result in a new operating voltage and power for each module. The new operating voltage $\dot{V}$ was calculated by using Equation (5.50), where ΔV determines how sensitive the modules power output is to the "bottleneck" I_{MIN}.

$$\dot{V} = V_{MP} + \Delta V \tag{5.50}$$

By using I_{MIN} the power values $\dot{P}$ was slightly decreased, but the runner-ups have a higher power output than 91 W. In Table 5.15 the modules with parameters in orange and red text was replaced by the five runner-ups enclosed between the lower horizontal lines.

The fill factor (FF) in Equation (5.51) is the ratio of the maximum power and the product of the open-circuit voltage and short-circuit current. We used the FF as an indicator to determine the quality of the PV modules.

$$FF = \frac{V_{mp} I_{mp}}{V_{oc} I_{sc}} \tag{5.51}$$

Parasitic series and shunt resistances (R_P) can affect the fill factor. Any decrease over the lifetime may indicate problems with the PV modules. Bulk resistance of the semiconductor, resistance from the metallic contacts are some of the contributors to the series resistance (R_S). A high series resistance results in power loss within the cell and thereby decreases the fill factor and the power output. Shunt resistance is the resistance across the p-n junction. A low shunt resistance can cause current to leak and hence reducing the fill factor and decreasing the power output from the cell [3], [28]. In addition to revealing the quality of a solar cell and how square an I-V curve is, a high FF is also related with the output voltage $\tilde{V}_{MP}$. A high FF indicates a high output voltage. The relation between FF, $\tilde{V}_{MP}$ and $\dot{V}$ is easily observed in Table 5.15. The modules with the highest FF values also have the highest voltage output. Values between 0.5 to 0.82 are common for solar cells [86]. There are no noticeable deviations except from module three with a FF of 0.642. However, this module is replaced by the runner up due to the low voltage and power values [93].

5.6.3 Discussion

The de-rated P_{MP} and I_{MP} values in Table 5.10 was compared to the converted STC values in Table 5.15 to observe if they are in the same range as the de-rated specifications. The de-rated maximum power is 92 $W \pm 3$ % and have a range from 89.24 W to 94.76 W. All except four modules (3, 5, 22, 28) are within this range when examining the median power $\tilde{P}_{MP}$ of the 28 listed modules in Table 5.15. The de-rated I_{MP} is 5.48 $A \pm 3$ % and have a range from 5.32 to 5.64 and five of the modules (1, 3, 18,19, 37) are not within this range. However, we consider this to be acceptable as the majority 20 of 28 modules are within the de-rated specifications.

The STC conversion methods are based on a shunt-free 1-exponential I-V curve model, given in Equation 5.47. Two assumptions were made in order to derivate the voltage. The shunt resistance is set to $R_{SH} = \infty$, which is an ideal solar cell, but the resistance could be less than $5 - 10\ \Omega$. The next assumption is the ideality factor, which is assumed to be 1.4, but this is probably higher at MPP and also varies with the current. A higher ideality factor degrades the FF and the modules should probably have somewhat lower FF values. The model assumes the cells to be identical, but the shunt resistance can vary by nearly two orders of magnitude [19],

[93]. Although the model is not 100 % accurate the new operating power provided additional information to determine the 23 highest ranked modules.

5.7 Installation process

When the circuit breakers, cables, PV modules and inverter are chosen, it is time to do the physical installation of the PV system. An approval is given from Agder Energi to start commissioning before the agreement is finalised, so that the inverter installations required by Agder Energi could be done while the final details of the feed in agreement is made. Preparations of the PV system on the DC side can then commence before the electrical installation and commissioning is initiated. The mechanical installation of the PV modules was done by the authors of this report while all elements of electrical installation was done by certified electrical students and controlled by certified electricians from Agder El Installasjon.

5.7.1 Grid Application Results

The different steps of the grid application process are explained in Chapter 3.4 and are commented here. The time elapsed from the application form was handed in to the installation started was longer then expected. The initial application in Appendix B was e-mailed to Agder Energi on the 24 January, a response was given on the 11 February saying that the application had been received and being processed. Some more time then elapsed before Kristen Leifsen on the 12 March was asked to call Agder Energi to get an estimated time of approval. The call from Leifsen then speeded up the process and a draft of the agreement was sent from Agder Energi on 17 March. On 9 April, approval was given from Agder Energi to finalise the remaining agreements after the PV system had started commissioning. After this date, a steady flow of communication has been present between Rolf Håkan Josefsen in Agder Energi and Bjørn Lindemann for UiA regarding details in the agreement and documentation needed for UiA to proceed forward after commissioning the inverter. At the time when this thesis is handed in, the application process has not been finalised. The documents in Appendix L need to be signed and sent to Agder Energi before a temporary permit is given. This is changed to a permanent permit after a trial period when Agder Energi decides that the PV system is producing power with the required quality.

Comments and updates to the five Grid Connection steps in Section 3.4:

- It is found in Section 5.2 and 5.3 that the chosen inverter complies with the requirements from Agder Energi in Appendix J.
- The required information in the REN application form, given as Appendix B, regarding contact person and "Produksjonsenhet" was filled out by Kristen Leifsen and referred to general information regarding the placement of the PV system. The authors filled out the information under "Tekniske data". The expected numbers for summer- and winter-production were found using PVGIS prediction for March-October (summer) and November- February (winter) which was rounded up and down, respectively. The expected development cost is based on the inverter cost of 6840 kr and expected installation costs of 11 400 kr. Taxes and transportation of the inverter is not included. The expected cost was divided by the expected yearly power production for a 3.8 kW_p system found in PVGIS of 3040 kWh/year and resulted in a development cost of 6 kr/kWh. The expected yearly power production found in PVGIS is for a 3.8 kW_p system, while the system installed is 2.1 kW_p. The installed system of 2.1 kW_p should have been used, but 3.8 kW_p was used instead because this is the maximum possible output from the inverter, giving Agder Energi a total power they could expect when accounting for future upgrades. PVGIS values were used because these were the numbers available at that time, and PVGIS has a larger data set. The expected cost of 18 240 kr is assumed to be too low when considering that taxes and transportation should be added to this cost. The price would be greater for regular customers since UiA got a discount on the inverter from Eltek, and certified electrical students were used to do the electrical connections. A regular customer would also have to buy PV modules. 12 years old down-payed modules were used, no extra costs was therefore added in terms of module price. The development cost of 6 kr/kWh was calculated using the expected yearly production for a 3.8 kW_p system under the assumption that the PV system would only operate for one year, but is too high to be a competitive profitable system. This cost should rather be based on expected production for a 2.1 kW_p system with a lifetime of some 10 more years (assuming that PV module lifetime is approximately 25 years depending on the module and inverter lifetime is approximately 10 years). The new and more competitive development cost, assuming a production of 1680 kWh/year from Appendix N for a 2.1 kW_p system and an increased cost of 20 000 kr, is then calculated:

$$Development\ Cost = \frac{20\ 000\ kr}{1680\ kWh/year \cdot 10\ years} = \mathbf{1.19\ kr/kWh} \tag{5.52}$$

- A site acceptance test was at a later time rejected by Agder Energi, instead we needed to have a mandatory Statement of Compliance form of the electrical installation signed by Agder El Installasjon, as given in Appendix O. Since quality and protection settings in Appendix J can only be set after the inverter is connected to the grid, Agder Energi gave UiA permission to perform commissioning before the grid connection agreement had been finalised.
- After the quality and protection settings has been installed in the inverter, the documentation form in Appendix K needed to be completed explaining who did the electrical installations of the system, and to add a single-line diagram (Appendix G) and the power and protection settings installed.
- As mentioned earlier, a good communication is present between Bjørn Lindemann and Agder Energi finalising the details of the agreement. When this is done, the final document called "Rammeavtalen", given in Appendix L, has to be signed saying that the customer has read all of the documents related to the grid connection and that the system is operating without exceeding the requirements in Appendix J.

5.7.2 Visual Inspection

The 23 chosen modules in Table 5.15 need to pass a visual inspection test before they can be used to ensure they are free of damages. The modules should be inspected under an illumination of no less than 1000 lux for the damages listed [19]:

- Cracked, bent, misaligned or torn surfaces
- Broken and/or cracked cells
- Faulty interconnections or joints
- Cells touching one another or the frame
- Failure or adhesive bonds
- Bubbles or delamination's forming a continuous path between a cell and the edge of the module
- Tacky surfaces of plastic materials
- Faulty terminations or exposed live electrical parts
- Any other conditions which may affect the performance

The PV modules will pass this inspection if they do not have any major visible defects as listed above. The defects found and its severity level for every module are given in Appendix F. It was

observed that some modules had corrosion, as illustrated in Figure 5.14(a), on the cells beneath the glass which could be a result of moisture behind the glass caused by delamination. Many modules also had bent frames, which could be caused by rough handling during transportation or dismounting. These bends could have left open cracks around the module frame allowing water or moist air to reach the cells. It was observed that most of the cells with corrosion was corroded in the corner of the module where water typically would gather.

Nearly all of the PV modules had white dots on the cells, and some of them had something looking like fingerprints on them. This is illustrated in Figure 5.14(b) and is believed to have happened during manufacturing, but is not affecting the safety of the module or the performance. In the PV array, 22 of 23 modules had this phenomenon and it is therefore very common, but it does not seem to affect the array in any way.

Many modules have been degraded to the extent they got brown discoloured lines around the cells, as illustrated in Figure 5.14(d). This is not believed to be a result of corrosion or hot spots, but rather a degradation since the brown lines on some cells could cover all four sides where water typically would not gather. Since the discolouration is located at the edge of the cells where it does not cover any cell-fingers, it does not significantly affect the power output of the modules.

A total of 13 modules had the phenomenon illustrated in Figure 5.14(c), it is not known what this is or how it is caused, but it looks like something had touched the white fingers before the paint dried and then dragged it over the cell. This may look like a fault produced during the manufacturing process along with the white dots, maybe from a faulty machine component.

From Table 5.15, showing the chosen 23 modules, the modules with corrosion, white dots, fingerprints and brown discolouration ends up high enough on the list to be the preferred modules for the array. This indicates that the faults found on these modules does not affect the module I_{MP} or V_{MP} enough to exclude them from the best 23, these are rather the modules with the best I_{MP} and V_{MP}. The faults does not seem to affect the modules, it is therefore concluded that the faults do not pose any danger to the PV array or the building.

5.7.3 Mechanical Installation

The mechanical installation of the PV modules started on 7 April and lasted for 2 days. The 23 modules were connected to the supporting aluminium beams with nuts, bolts and washers at

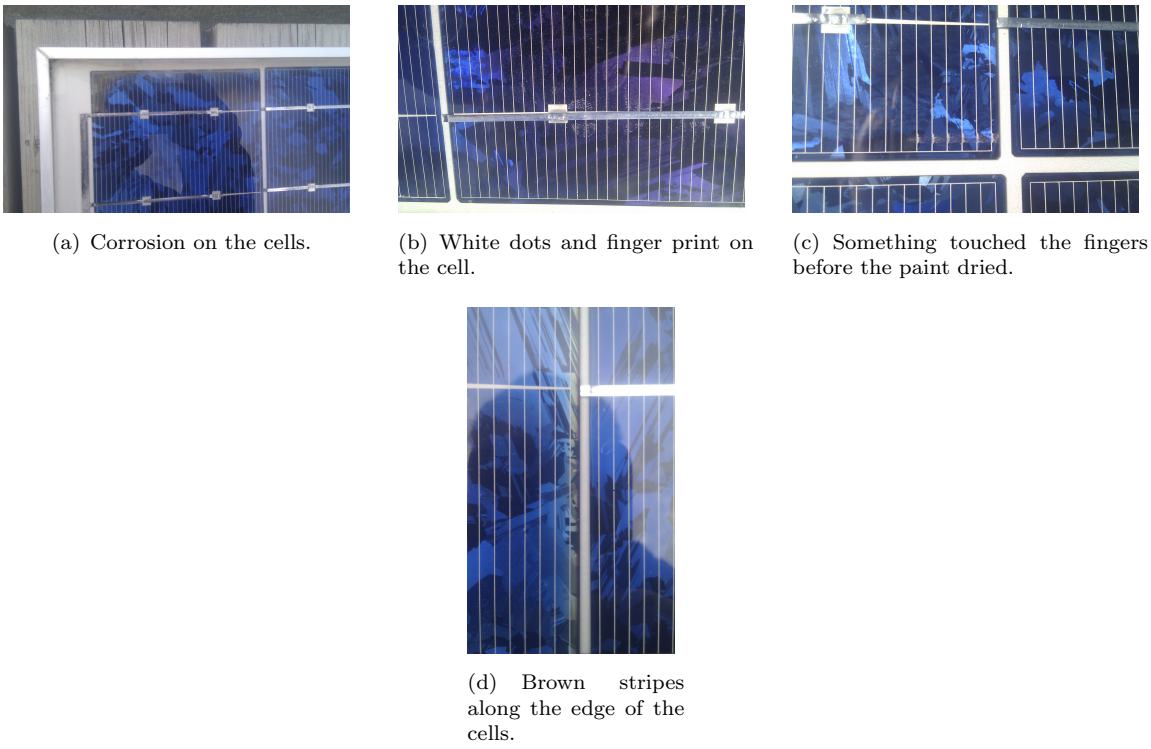

(a) Corrosion on the cells.

(b) White dots and finger print on the cell.

(c) Something touched the fingers before the paint dried.

(d) Brown stripes along the edge of the cells.

FIGURE 5.14: Faults found during visual inspection.

four and 6 points where it was possible. The holes in the supporting beam were not necessarily made for these modules, so new holes was needed to be drilled on the module frame making it possible to mount the modules and securely fasten them in the configuration given in Figure 5.4. As mentioned in Section 5.7.2, some of the PV modules had bent frames; this does not affect the overall strength of the module because a new hole was drilled where the structural integrity of the frame was still intact. Figure 5.15 illustrates the array after the installation of the PV modules.

5.7.4 Electrical Installation

Two students who are certified electricians did the installation of the inverter and the circuit breakers on April 22. Figure 5.16 illustrates the inverter and the junction box mounted on a plywood plate and then connected to two wall main supports. Figure 5.16(b) illustrates the DC cables marked with red and green insulating tape for + and −, respectively, coming in through the bottom of the junction box from the roof and elongated with MC3 connectors. The DC cable is then running through an Eaton DC circuit breaker and connected to the DC input of

FIGURE 5.15: Configuration of the PV array after the mechanical installation.

the inverter with two MC4 connectors. The connection diagram: "Unearthed system" on page one in Appendix D was used to connect the circuit breaker.

The AC cable from the wall socket is connected to an AC circuit breaker with one phase (brown cable) and one neutral (blue cable), the phase and neutral cable then exit the AC circuit breaker and is connected to the AC output of the inverter. Grounding between the two AC cables is connected to the earth bar (blue) on top of the fuse box indicating that the inverter is grounded on the AC side.

(a) Inverter and junction box installed on the plywood plate with the AC socket and user instructions.

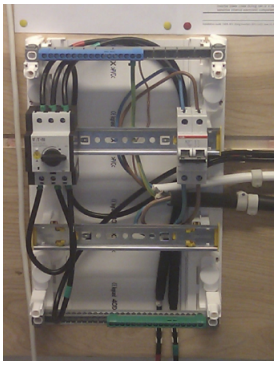

(b) Wire connection inside the junction box with the DC (left) and AC (right) circuit breakers.

FIGURE 5.16: The inverter installed on the wall along with the junction box and wire connections.

5.7.5 Inverter Start-Up Installation

Before the inverter could be started, two electricians from Agder El Installasjon inspected the system and the system wiring. The installation process could start after they inspected and implemented their suggestions and inputs to the system. Their Statement of Compliance, where Agder El Installasjon declare that the system is complying with the applicable Norwegian regulations is given in Appendix O. The start-up was done on 24 April, a cloudy day with a measured V_{OC} of 346 V_{DC}. The list of "Checks before start Up" listed in Section 4.3.7 in Theia HE-t User manual [53] was followed before the installation process started. This list ensured that all cables were properly sized and connected, as well as circuit breaker size, polarity and the inverter-mounting bracket. When these points had been checked out, Section 5.1.3 in the user manual was used to start the installation. A minimum voltage of 230 V_{DC} and 184 V_{AC}, and a minimum power of 7 W_{DC} needed to be present before the inverter would start. Measurements done before start-up indicated that these conditions were present. The circuit breakers were turned "ON" on the AC side first, then the DC side. The inverter's "start installation" program is a predetermined guide that is automatically initiated when the inverter is supplied with its minimum power. The parameters listed in Table 5.16 was set and installed.

The inverter power quality and protection values are predetermined according to European standard EN 50438:2007 and had most of the requirements from Agder Energi already preset. Two values were set at "Not Applicable" in the inverter; Slow trip values for "Voltage dip" and "Swell". The installer's password was needed to manually type these values.

5.7.6 Commissioning

Commissioning is described in [3] and [4] to control the cable cross-section, circuit breakers, polarity and grounding resistance before and during start-up. This is done because Australia and Germany have a requirement instructing that a commissioning certificate has to be issued containing certain measurements of V_{OC}, I_{SC}, grounding- and isolation resistance. However, this is a requirement that is not necessary in Norway, mostly because standards for commissioning PV systems has not been developed at this time. Any reports, documentation or information other than what is specified by Agder Energi is therefore not needed.

The inverter start up was done on a cloudy day at 15:00. The Australian manual specifies that commissioning should be done on sunny clear sky days when larger voltages, currents and power

TABLE 5.16: Start up parameters for the inverter [53].

Point	Parameter	Set value
2	Language	English
3	Time Format	24h
4	Date	24 Apr 2014
5	Time	15:00
6	Set Bus ID	99 (default)
7	Set as Master unit	No
8	Grid Configuration	TN/TT
9	Feed in phase	Unknown
10	Plant Apparent Power	3.8 kW
11	Grid Code	Norway
13	Reactive Power Setting	VDE 4105 0-13.8
14	Screen Timeout	99
15	Customer Name	UiA
16	Site	Grimstad
17	Unit Name	PV1
18	Owner password	****

can be recorded to test the PV system. To comply with this, measurements done on 27 April at clear sky was used to see how the system operated at these conditions. The result was an operating voltage of 340 V, operating current of 5.4 A and an internal isolation resistance of 65.5 $M\Omega$. The performance ratio of the system with regards to STC is calculated in Section 5.5.11 to be 0.80. Conditions at 27 April were ideal, which resulted in a better performance ratio at this day when the inverter recorded an output power of 1921 W at 12:00. It is of interest to study the temperature and irradiation data for that time, as Figure 5.17 illustrates, to see if the recorded power complies with the expected theoretical output power when no factors like shading and dirt was present.

The temperature of 32 $°C$ (A10156) was recorded as Figure 5.17(a) illustrates a drop in temperature just before 12:00, this could be a result of a wind gust cooling down the modules and resulting in a peak power at that time. This is also reasoned by Figure 5.17(b), at 0.975 suns, illustrating that the peak power did not occur at full sun with a temperature of 34 $°C$ but rather at an irradiance of approximately $975 W/m^2$.

When calculating if the theoretical power from the PV system corresponds with the actual AC energy being produced, it can be investigated how the inverter performs with regard to the calculated expected power. To find this, Equation 5.53 is used with the assumption that voltage

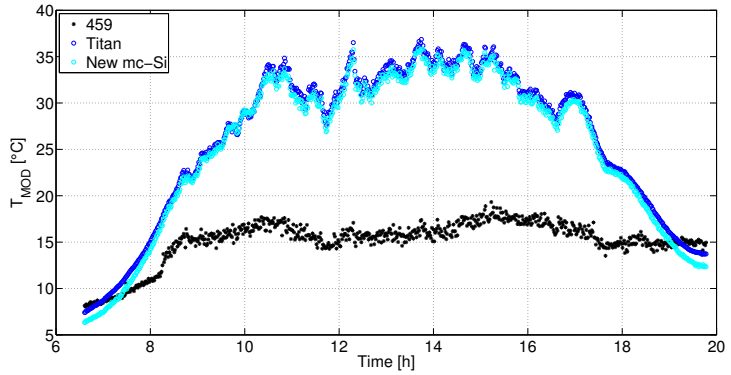

(a) Module temperature for the NESTE modules on 27 April. "459", "Titan" and "New mc-si" are different measuring points on the array.

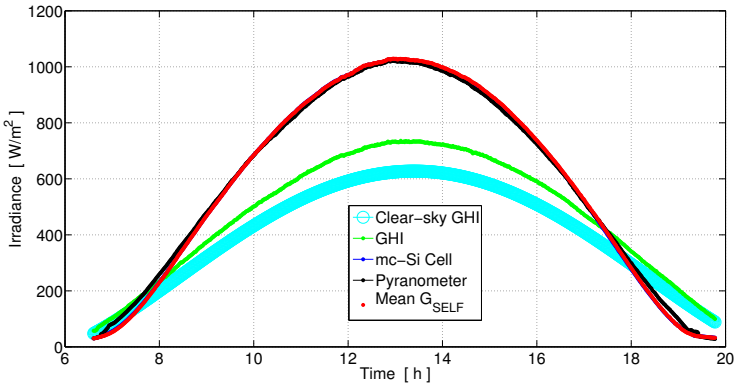

(b) Irradiation over Grimstad.

FIGURE 5.17: Temperature and irradiance measurements on 27 April 2014, the highest power was recorded at 12:00.

drop is 0.986 and the inverter at this time is operating at the euro efficiency (0.967).

$$P_{DC} = P_0 \cdot (T_{mod} - 25)^\circ C \cdot \gamma \cdot \frac{G}{G_0} + P_0 \tag{5.53}$$

$$P_{DC} = 2116\ W \cdot (32 - 25)^\circ C \cdot \frac{-0.44\ W/^\circ C}{92\ W} \cdot \frac{975\ W/m^2}{1000\ W/m^2} + 2116\ W = \mathbf{2046.9\ W} \tag{5.54}$$

Where P_0 is the array power at STC and γ is the temperature coefficient for P_{max} given in Table 5.11. T_{mod} is measured on the back of the modules and G is measured with the PV cells, which is assumed to include spectral effects and reflection losses. Equation 5.54 takes into account the loss due to temperature and irradiance. To see the AC output power, the cable loss and inverter efficiency need to be added, as calculated in Equation 5.55.

$$P_{AC} = 2046.9\ W \cdot 0.986 \cdot 0.967 = \mathbf{1951.6\ W} \tag{5.55}$$

The calculated expected AC power of 1951.6 W is subject to some uncertainties. P_0 has an uncertainty of ± 3%, the cable loss has an uncertainty and the inverter could operate at a different efficiency. It is therefore assumed that P_{AC} has an uncertainty of ± 5%. It was measured a maximum AC power of 1921 at this day, which is within a 5 % range of 1951.6 W. It has been shown that the inverter is operating as expected at clear sky days, which indicate that the MPPT manage to follow the MPP when the irradiance is not shifting rapidly, giving the inverter a good performance at these conditions.

5.7.7 Thermal Imaging

To inspect how the inverter, fusebox, cables and PV array work with regards to thermal heating during conditions with high currents and voltages, the system was inspected with a thermal imaging camera for any hot spots or overheating. The photos were taken on a sunny day when the PV system was operating at its maximal capacity. It was windy at this day, as it often is on the roof, and it is believed that the PV array is cooled by the wind at these days. Conditions on the PV array will therefore be different on days with no wind, it will be a lot warmer, but possible hot spots at thermal heating will still occur on these pictures.

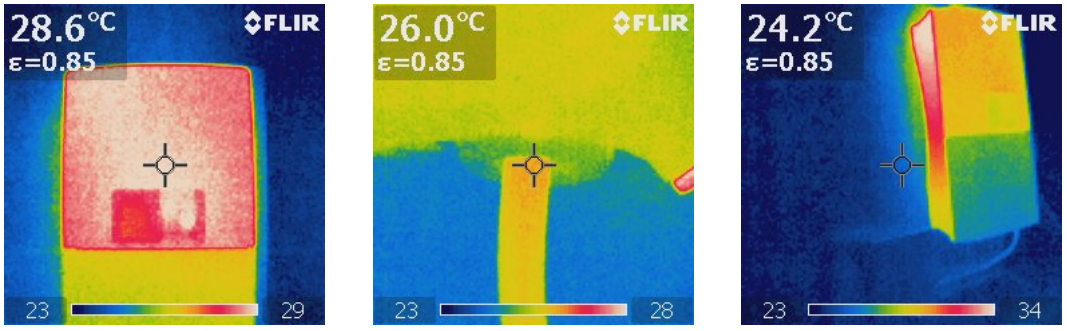

(a) Temperature and hot areas in the inverter.

(b) Temperature of the AC connection cable.

(c) Hot areas of the inverter.

FIGURE 5.18: Thermal images of the inverter taken when operating at a high power [19].

Figure 5.18(a) is taken over the top part of the inverter, where the transformer is located. The figure illustrates that the temperature is approximately 28.6 $°C$ when the array is operating at a relatively high power. Figure 5.18(b) illustrates the AC connection point of the AC cable in the inverter. This picture is taken to ensure that no hot spots occur at this point, indicating that the cable is not properly installed and must be reconnected. The picture indicates some red colour on the cable close to the connection point, but it is not a distinct red colour and the temperature is only 26 $°C$. It is therefore considered not to be a severe issue. Figure 5.18(c)

gives an overview of the warmest areas on the inverter. It is seen that the warmest spot is the ventilation on the side reaching up to 34 $°C$. This overview does not reveal any hot spots in the cables, junction box or inverter, except from the natural hot sources like transformer and ventilation.

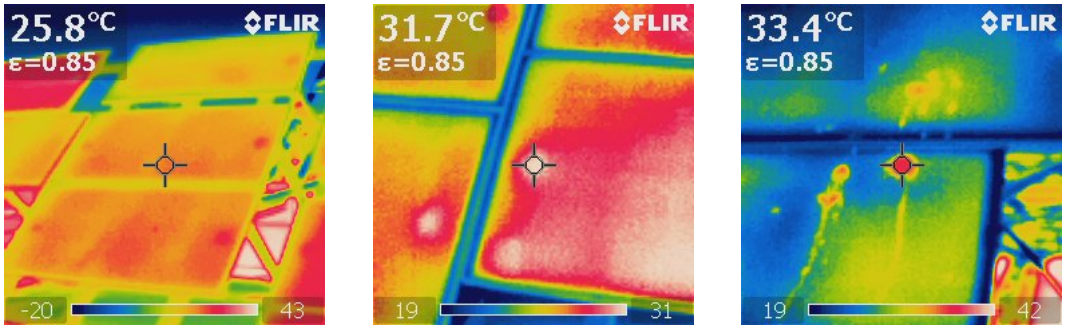

(a) Module 4,5 and 6.

(b) The junction box behind a module.

(c) Bird dropping on a module.

FIGURE 5.19: Thermal images of the array on a sunny day indicating that bird droppings and junction boxes are a heat source.

It is believed that the array was to a high extent cooled by the wind. The temperature is therefore not consistent to what it would be on days with no wind. Figure 5.19(a) is an overview of module 4,5 and 6 in the array showing that module 5 has a surface temperature of 25.8 $°C$. The picture does not reveal any large hot spots in these modules other than heat in the junction boxes, which is also illustrated in Figure 5.19(b), operating at a temperature of 31.7 $°C$.

Reflections from the sun was prominent on this day, which is also illustrated in Figure 5.19(b) which is seen by the large red and white surface. Figure 5.19(c) is illustrating something that could happen to all of the PV modules. Bird dropping on the glass will provide shading on the module cells causing mismatched cells within the module. This figure shows that the temperature at the bird dropping reaches 33.4 $°C$ which is more than the hot area created by the junction boxes. Factors like this will affect the shading loss of the array, as explained in Section 5.5.4, which can only be improved by physically washing the dirty modules or waiting for rain to do the job. It is, however, not given that rain will wash bird droppings since this can be quite sticky and is best removed by physical labour.

There are 23 points in the array where string cables are connected together to form a string of series connected PV modules. If these connectors are not connected properly, heat will evolve, which will increase the voltage drop and form thermal heating at these points. Too high temperatures will affect the cables and could, at worst case, cause a fire. Figure 5.20

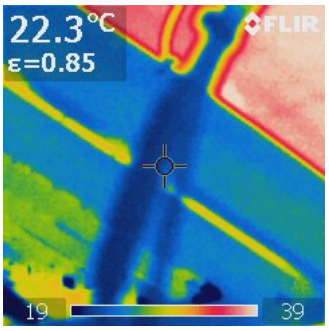

FIGURE 5.20: Thermal inspection of the cable MC3 connectors. It is seen that no heat is evolved at this point.

is illustrating one of these connection points. All of them were inspected with the thermal camera, but no thermal heating was observed. Figure 5.20 shows that the connectors are properly connected and does not show any abnormal temperatures.

5.8 Inverter Performance

With the included software it was only possible to extract 15 min data from the inverter. With a Python script received from Eltek and modified by our supervisor, we were able to extract one-second data from the web interface. Due to time limitations, only a few days of logged one-second data are analysed in this thesis. The data was used to analyse how the inverter is handling low irradiance and overirradiance conditions, in addition to calculating the performance ratio. The energy harvest was recorded from the "Theia Analyzer" and is based on 15 min data, which covers approximately one month. Screenshots of the "Theia Analyzer" pages and the Theia Service tool from where the inverter data was downloaded is given in Appendix I.

5.8.1 Analysis of Operating Data

From analysing Figure 5.21, two colours can be seen where the green line (P_{AC}) is almost consistently under the blue line (P_{PV}). The P_{PV} peak at almost 14:00 hours is recorded to be 2.065 kW, and the respective P_{AC} value is recorded to be 2.006 kW, illustrating that the inverter works at its full capacity and efficiency close to the expected PV output on days with close to STC conditions and little losses (Section 5.4.1).

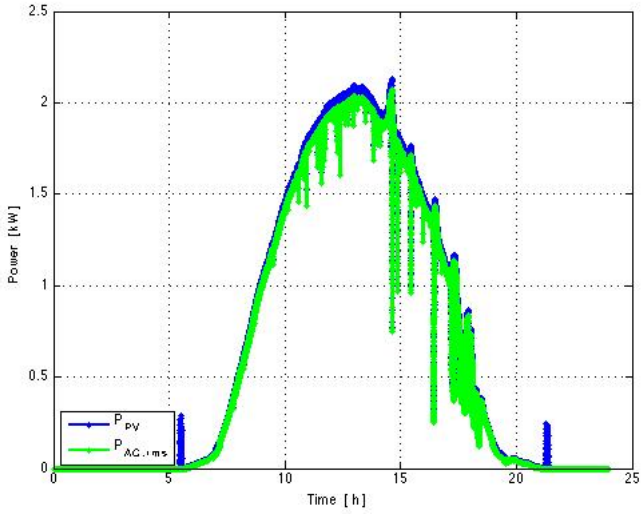

(a) PV and AC power entering and leaving the inverter, respectively.

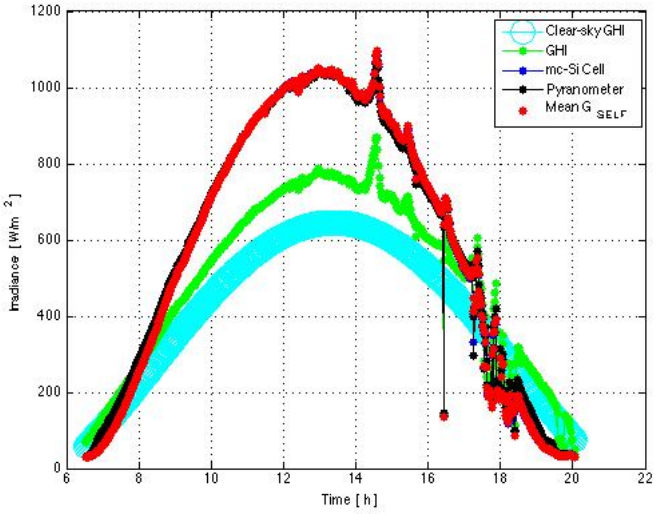

(b) Irradiance measured over Grimstad with a mc-Si Cell and pyranometer.

FIGURE 5.21: Irradiance in Grimstad and inverter power on 2 May 2014.

Before and after the inverter starts generating power there are several blue spikes from the PV array in Figure 5.21(a) and 5.27(a), of both DC current and power which lasts from approximately 6 to 11 minutes. These are generated between 05:16 and 05:27 in the morning and in the evening between 21:07 and 21:30, where they can range up to 300 W but are usually close to 200 W. Figure 5.21(b) shows that the pyranometer and mc-Si cell start recording at 6:30 in the morning and stop at 20:00. The peaks in Figure 5.21(a) occur earlier and later than this, it is assumed that this is diffuse or low irradiance on the PV array because of the early sunrise at approximately 4:30. The blue peaks are therefore power from the PV system not

being processed due to low irradiance and voltage.

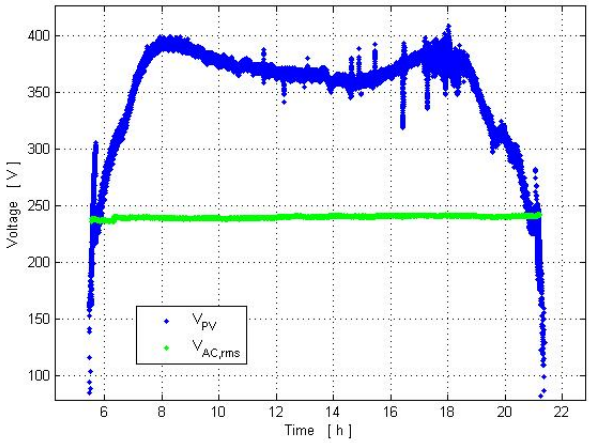

(a) PV and AC voltage over a sunny day.

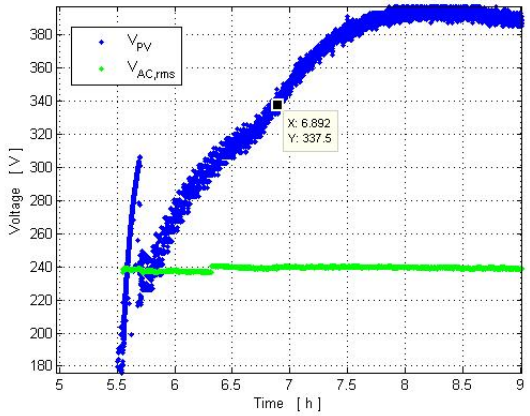

(b) PV and AC voltage with focus on the first hour of operation.

FIGURE 5.22: Inverter voltage on 2 May 2014.

Figure 5.22 show the first minutes when the PV voltage is under the minimum inverter PV voltage, between 5:24 and 5:36. Between 5:36 and 5:42, the inverter MPPT with a minimum voltage of 230 V_{DC} is searching for the array MPP, it is found at approximately 5:42 when the inverter is receiving the required 7 W_{DC} and Figure 5.21(a) start indicating that the inverter is producing power. The straight voltage line and spike in Figure 5.22(b) at approximately 5:30 occurs after the diffuse power spike in Figure 5.27(a) and indicate how the inverter is receiving an increased input voltage as it is searching for the required input power and MPP. From Figure 5.22(a) it is seen how the input voltage is dependent on temperature in Figure 5.23. In the morning, when the temperature is low, the voltage is high and reaches its morning peak at approximately 8:15 and 11.2 $°C$. It then decreases throughout the day as the temperature rises,

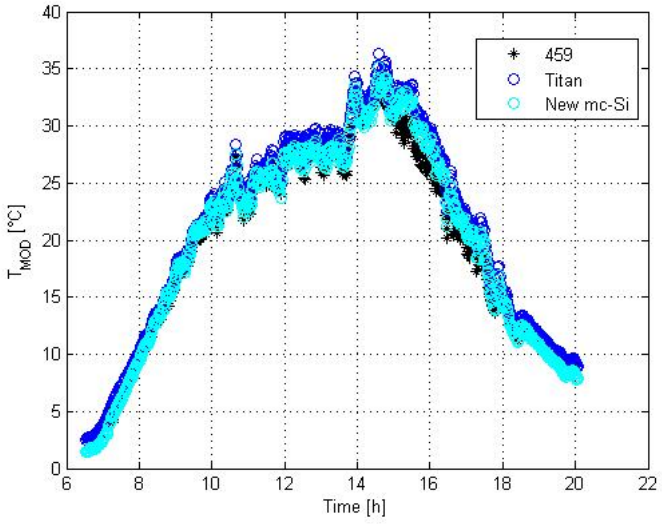

FIGURE 5.23: Module Temperature on 2 May 2014. "459", "Titan" and "New mc-Si" are different measuring points on the array.

and a new voltage peak appears at 18:00 when the temperature is approximately 14.4 $°C$. The voltage then decreases as the sun sets.

As the inverter start feeding power into the grid, the current in Figure 5.24(b) is not consistent. I_{AC} is oscillating between 0.06 A and 0.4 A for almost an hour, even though it can be seen that I_{PV} has a stable and close to linear increase. This oscillation can be seen more clearly on cloudy days when the array is exposed to low irradiance. When analysing Figure 5.25, it can be seen that oscillation starts when irradiance is low. This is seen in the morning and evening when the incident angle of the sun is low or the inverter is operating on diffuse irradiance. The efficiency during this time is illustrated in Figure 5.27(b). It is seen that the efficiency is not stable, but is increasing as the inverter is starting up and operates at better efficiencies. Figure 5.25(b) indicates that the inverter output does not only oscillate at these times, but also at times when Figure 5.25(c) indicate low irradiance over a long period of time, like at midday between 12:00 and 14:00. It would be interesting to investigate how oscillation over a long period of time, like in Figure 5.25(b) affects the power quality, but this is not investigated in this thesis. This oscillation could however, introduce harmonic currents and affect the power quality of the grid. It is required to keep these harmonics as low as possible or at least keep it within the limits stated in Tables 5.4 and 5.5.

The Theia HE-t datasheet in Appendix A explains that *"Early start-up and high efficiency at low irradiation gives longer operation time and higher energy yields"*. Figure 5.21(a) indicates

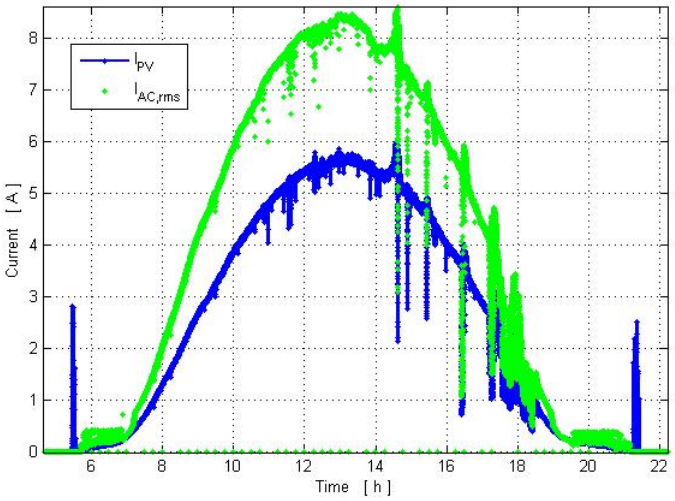

(a) PV and AC current on a sunny day and the PV power spikes before and after operation cased by low irradiance.

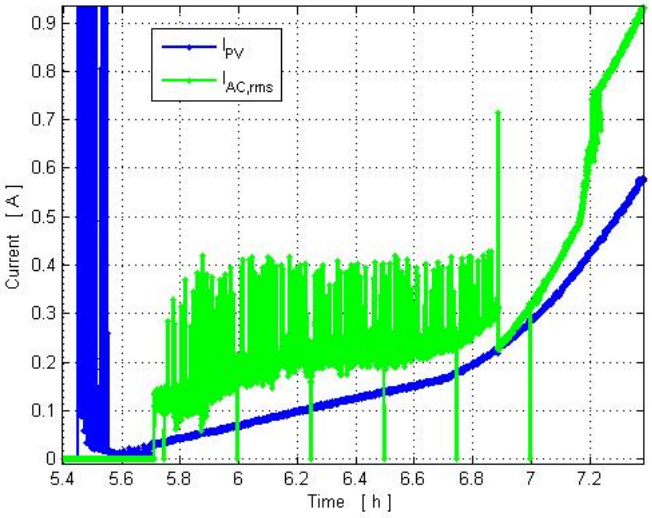

(b) PV and AC current with focus on the first hour of operation.

FIGURE 5.24: Inverter current with the oscillation at low irradiance on 2 May 2014.

a high power at high irradiance, and early start-up which results in longer operation time is consistent with the figures. As already explained, an early start-up at low irradiance results in more oscillation, which could affect the output power quality. Figure 5.25(a) indicates that the inverter has a good efficiency at low irradiance, but the efficiency is not consistent. It varies a lot, and drops as far down as 43 % at 12:35 and 22 % at 16:45 for conditions where Figure 5.25(c) indicate low irradiance. These drops can last from 5 minutes to one hour, dependent of the irradiance, before the inverter manage to increase the efficiency. This is also illustrated in Figure 5.26 where $P_{AC,rms}$ is at some times much lower than P_{PV}. Eltek has been informed about these results, but it is assumed that they are already aware of the oscillation effect at low

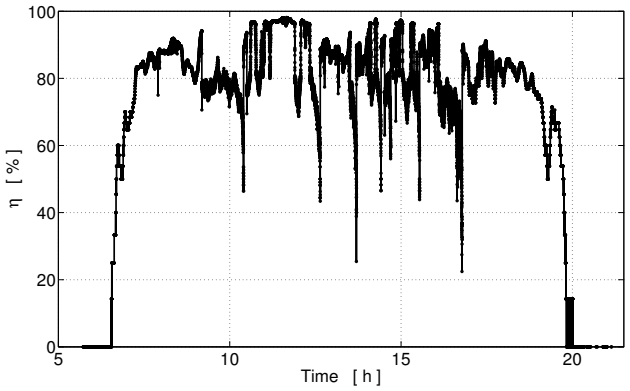

(a) Inverter efficiency on a cloudy day.

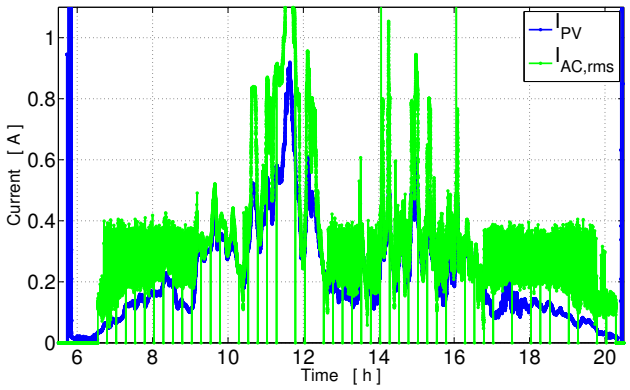

(b) Current on a cloudy day.

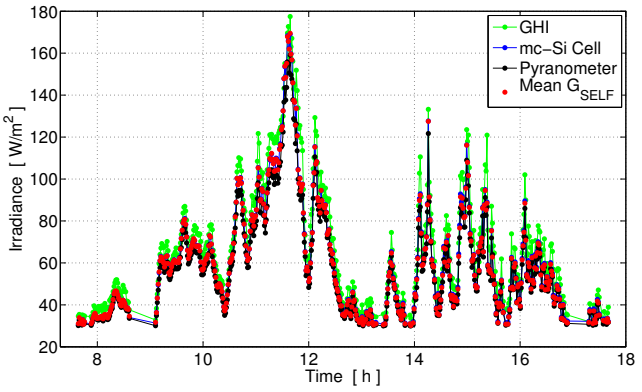

(c) Irradiance on a cloudy day.

FIGURE 5.25: Irradiance, inverter current and efficiency on 6 May 2014.

irradiance.

Figure 5.27 illustrates a phenomenon appearing every day. From 06:53 to 7:11, the efficiency drops suddenly despite of an almost exponential increase in input current (Figure 5.24(b) and an almost constant increase and less varying (i.e more dense) input voltage (Figure 5.22(b)). The drop lasts for 18 minutes or until the inverter manages to increase it back to the original

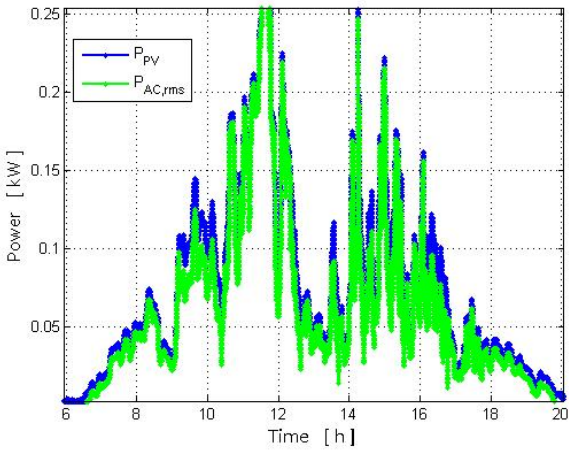

FIGURE 5.26: Inverter power on 6 May 2014.

course. The efficiency then reaches 96 % before it increases to the maximal efficiency of 98 %, when reaching this point it stop being stable, drops a few percentage and start varying. This drop in efficiency results in the power loss illustrated in Figure 5.27(a) of only 14 W to 29 W, a rather insignificant power loss appearing every morning and evening. The time range varies from 6:48 to 07:35 in the morning and 18:11 to 20:22 in the evening, for the period 2-6 May. It is consistent and is easiest to detect on clear sky mornings and evenings when the power drop can be easily read off the power curve, like in Figure 5.27(a). Even though a power drop can be easily detected by studying the efficiency curve in Figure 5.27(b), it is harder to detect on cloudy days like Figure 5.26 illustrates. By analysing Figures 5.25(a) and 5.25(b), it can be seen that the large drops in efficiency happens in a transition when the current stop oscillating and start producing a higher AC current. Since the input current and voltage is relative stable, i.e. not oscillating like the output current, it is believed that external influences, software or hardware programming or an algorithm design causes this.

The current efficiency curve in Figure 5.28(a) is studied for two different days, 2 May and 18 May. It was recorded a clear sunny day on 2 May with some thin clouds in the afternoon (Figure 5.21(b)), while 18 May was a more overcast day with varying sky conditions as illustrated in Figure 5.29. Figure 5.28(a) illustrates the efficiency versus input current on these days, showing a consistent drop in efficiency at currents between 0.3 A and 0.4 A and another consistent drop at 98 % efficiency and 0.8 A. The figure shows a more varying and less consistent efficiency for the clear day (2 May) between 0.8 A and 2 A, where the efficiency on the cloudy day is a lot more stable at this range. This changes above 2 A where the inverter manages to operate at a more stable efficiency. Every dot in Figure 5.28(a) illustrates one second of data, it is seen

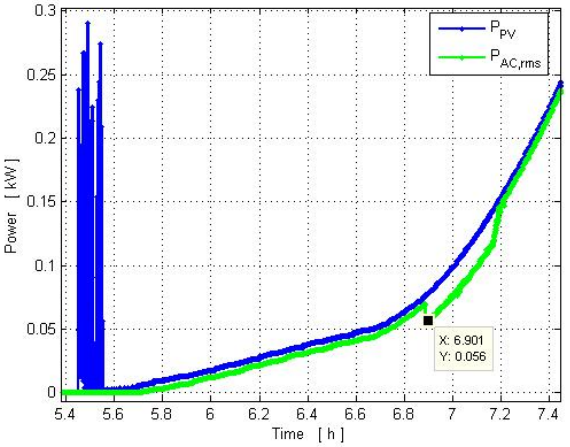

(a) Illustration of a power drop and blue power spikes at early morning.

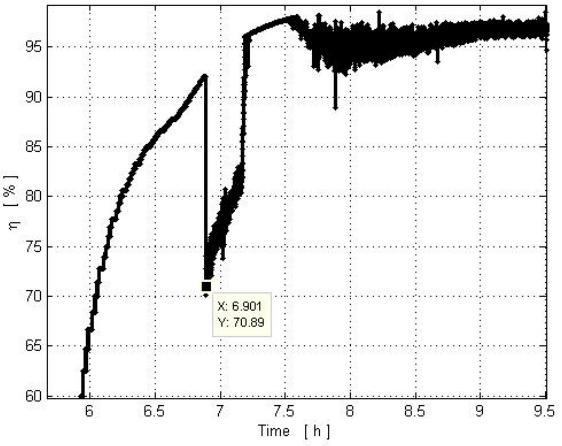

(b) Illustration of an efficiency drop.

FIGURE 5.27: A drop in power, illustrated with the efficiency on 2 May 2014.

that for a few seconds the efficiency drops down to 89 and 90 % and then it increases up to 98.5 %. An imaginary line can be interpolated between the steady efficiency of 98 % at 0.8 A and the maximum efficiencies, creating a theoretical maximum efficiency of 98.5 %. This is an efficiency only achieved for a few seconds at a time, but they form a line that is more prominent at currents between 3.5 A and 6 A. Since no specific pattern can be seen between the available days of measurements, no conclusion can be made of why the efficiency is more stable on a cloudy day at low currents and at sunny days at high currents. It is believed that this is a result of the varying irradiance on different days determining how the MPPT should operate. The MPPT is not perfect, Figure 5.28 shows how the MPPT is having difficulties to follow the MPP of the array as the current and irradiance changes. The I-V curve from Figure 5.28(b) shows the relation of the input voltage and current. It is seen that this curve have the same

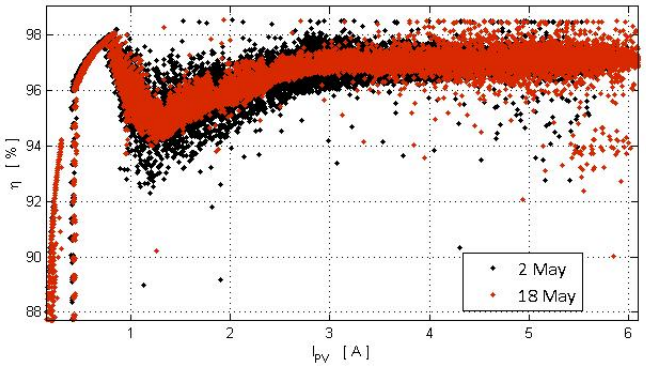

(a) Comparing I_{PV} efficiency curve on a clear day (2 May) and a cloudy day (18 May).

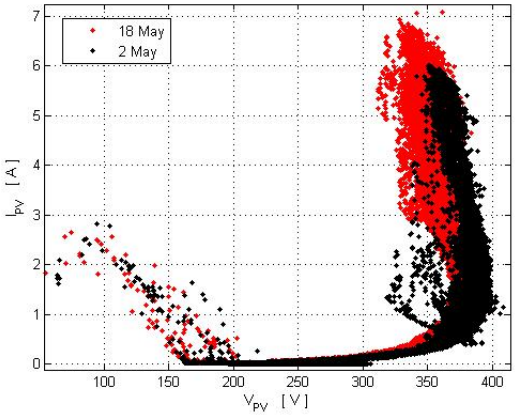

(b) I-V curve from a clear day (2 May) and a cloudy day (18 May).

FIGURE 5.28: Input current and voltage are compared on two days with different sky conditions.

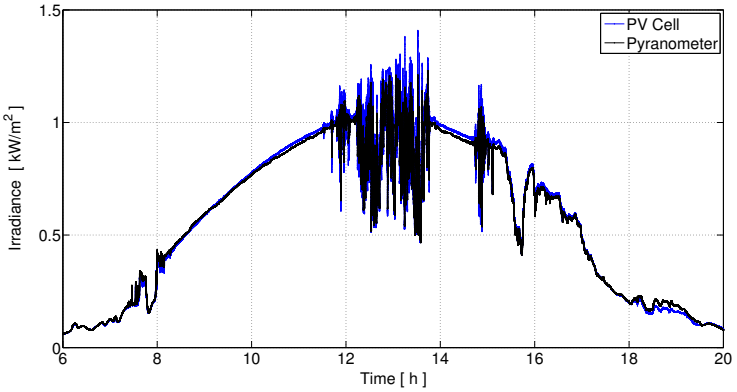

FIGURE 5.29: Irradiance on 18 May 2014, indicating varying irradiance at midday and in the afternoon [19].

tendencies as Figure 5.28(a), the voltage is varying at low currents on a sunny day and varying at high currents on cloudy days. It is also seen that at currents between 0.8 A and 2 A, the

voltage is high while the current efficiency drops. The efficiency in Figure 5.28(a) then increases at higher currents and slightly decreasing voltages.

FIGURE 5.30: Sky conditions during overirradiance on 9 May 2014 [19].

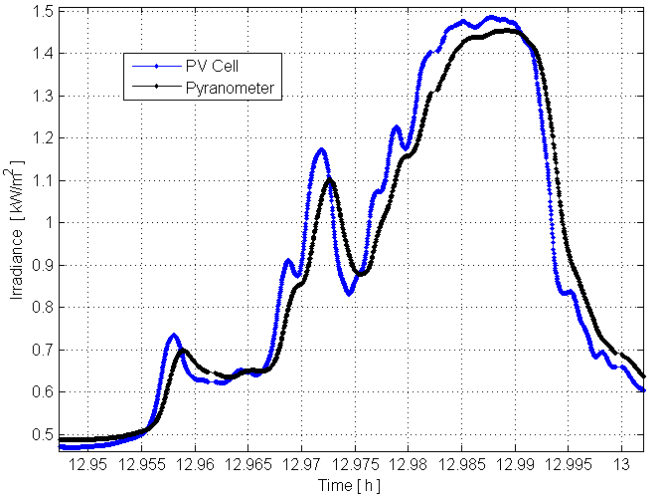

FIGURE 5.31: Overirradiance over Grimstad of almost 1.5 suns on 9 May 2014, the time values are approximate [19].

Overirradiance is a phenomenon affecting the output of the solar array and occur when clouds are boosting the existing irradiance to higher values. The irradiance increases when the spread of light is being magnified in optically thin clouds, like Figure 5.30 illustrates. These bursts of overirradiance is dependent of clouds and could last from a few seconds to minutes at a time [94]. In a climate with a high rate of clouds, it would be common and likely for the PV array to be exposed to overirradiance. It would therefore be of interest to analyse how the inverter works at these conditions, which occurred on 9 May. Figure 5.31 illustrates the overirradiance reaching 1.48 suns (1485 W/m^2) and lasts for approximately 30 seconds. During this time, the

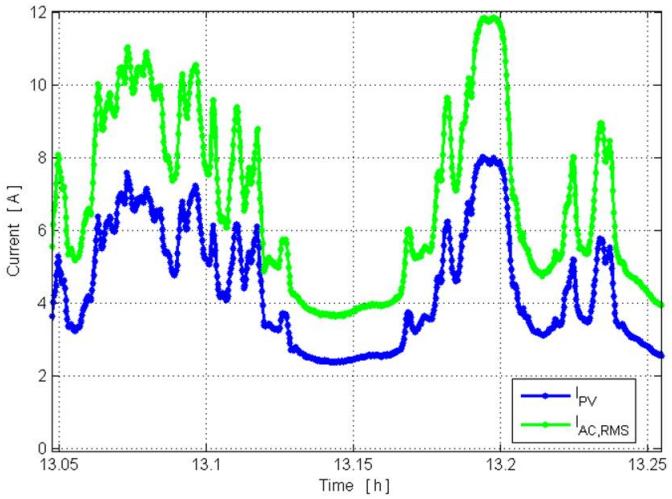

(a) PV and AC current produced at overirradiance, the time values are accurate.

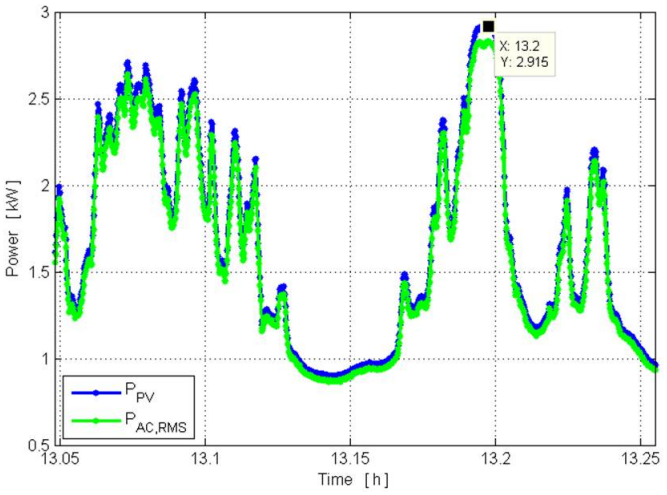

(b) PV and AC power produced at overirradiance.

FIGURE 5.32: Power and current produced during overirradiance on 9 May 2014 [19].

inverter records an input power of 2.9 kW_{DC} and input current of 8 A_{DC} while it produced a peak power of 2.8 kW_{AC} and a peak current of 11.8 A_{AC}, which is shown in Figures 5.32(b) and 5.32(a). The temperature on the back of the PV array at this time was 20-22 $°C$, the equivalent cell temperature is a few degrees higher than this and is assumed to be close to STC temperature. Meaning that the increase in power was caused by overirradiance and not a result of temperature effect on the PV power. These figures show how fast the inverter respond to sudden irradiance changes. No delay in increasing or decreasing power or current is noticeable, even small changes are almost identical between I_{PV} and I_{AC} in Figure 5.32(a) which allows the inverter to convert as much of the PV input as possible.

Figure 5.33(a) shows the maximum efficiency of 97 % achieved at the time of the overirradiance,

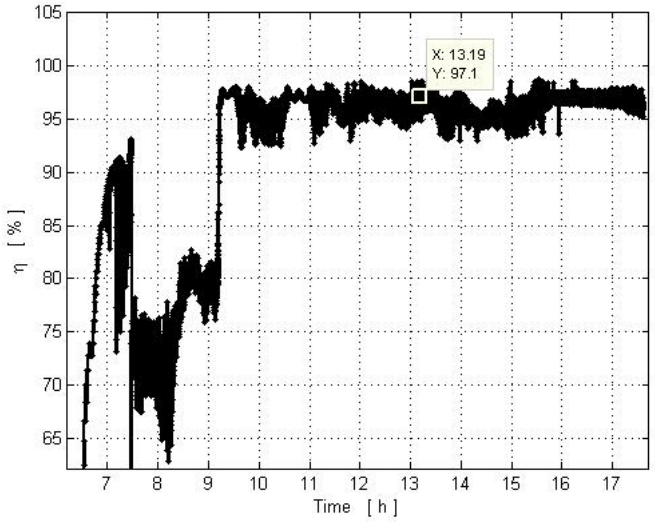

(a) Inverter efficiency over time.

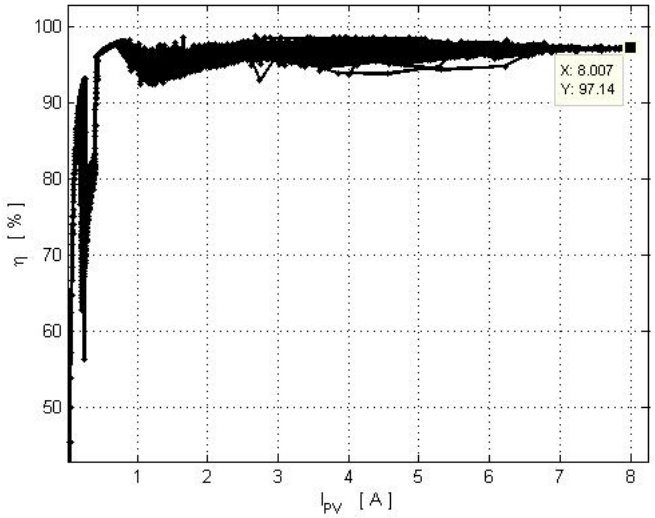

(b) PV current efficiency.

FIGURE 5.33: Inverter and Current efficiencies on 9 May 2014.

for a few seconds the efficiency even reaches 98.5 %. Even though the irradiance varies, the efficiency remains at a relatively stable value between 92 % and 97 % with an overall good efficiency. Better efficiencies at high currents are illustrated in Figure 5.33(b) showing that at almost 1.5 suns and an input current of 8 A_{DC}, an efficiency of 97 % is reached. The figure indicates that during this time, at a current between 7 and 8 A, the efficiency is much more consistent than at lower currents when the irradiance is also lower. Since this only happened for a few seconds, it shows that the MPPT operate better at higher input currents and higher irradiance when the efficiency is varying less.

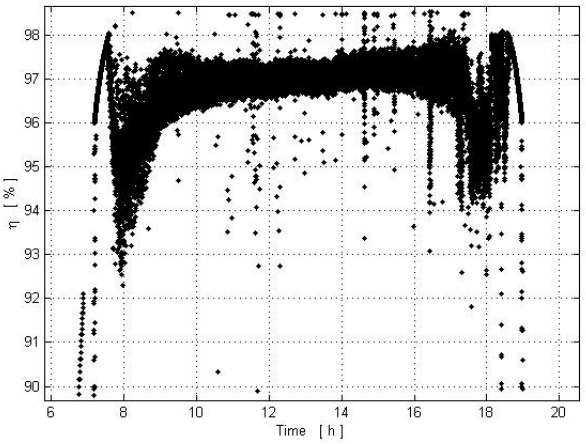

(a) Inverter efficiency over a whole sunny day, measured on 2 May.

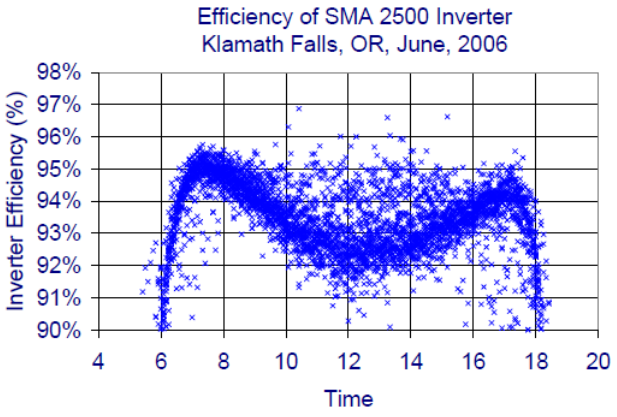

(b) Inverter efficiency for SMA 2500 inverter. Measured in Klamath Falls, Oregon in June 2006 [95].

FIGURE 5.34: Inverter efficiency of Theia HE-t compared to SMA 2500 on a sunny day in Grimstad and Klamath Falls, respectively.

Despite a few efficiency drops at low irradiance, the inverter has a good overall efficiency. Figure 5.34 compares the efficiency of Theia HE-t on 2 May 2014 to the SMA 2500 in June 2006. It shows how the efficiency of the SMA 2500 decreases with 2-3 % during midday at an average ambient temperature of 26 $°C$, compared to the efficiency of THEIA HE-t over the same time with a module temperature of 33 $°C$ at 14:00 [95]. The temperatures for the curves in Figure 5.34 are different, it is therefore hard to compare the two efficiency curves when the conditions are not the same. It is, however, observed that the module temperature does also increase in Grimstad from 11 $°C$ in the morning to 33 $°C$ at midday. While [95] explains how the SMA 2500 efficiency decreases as the solar radiation is increasing above the inverters optimum operating point of $400 - 600\ W/m^2$, the Theia HE-t manage to hold a relative stable efficiency varying within 1 % at the same time. The SMA 2500 does however; manage to hold a more stable

efficiency in the morning and evening than Theia HE-t.

Discussion

As mentioned, the inverter has a good overall efficiency varying at approximately 97 % measured on a sunny day as illustrated in Figure 5.34(a). It has a good performance, producing close to the rated power of 2.116 kW_p on days close to one sun and up to 2.8 kW on a day with overirradiance close to 1.5 sun.

Figures 5.27(b), 5.28(a) and 5.34(a) illustrate a phenomenon appearing every day under conditions where the input voltage is increasing and input current has an almost exponential increase without any peaks or drops. This phenomenon is only seen on the output current and power as well as on the efficiency curves and was therefore believed to be a result of a hardware issue, external influences or how the inverter algorithm is programmed. This suspicion was confirmed by Eltek [82]. At a power smaller than 200-300 W the Theia HE-t uses different algorithms for the inverter and the DC/DC-converter to ensure a high efficiency. When analysing Figure 5.27(b), this change of algorithm is seen by the very evident drop down to 70 %. The increase in efficiency before this drop is the result of one algorithm while the drop marks the spot where the inverter and DC/DC converter is changing to a different algorithm. It is seen that the inverter switches algorithm at 7:30, at a PV power of 77 W. This happens because the inverter has a hysteresis, which is dependent of irradiation and voltage. The inverter maintain the increase in efficiency until it reaches a point decided by the algorithm (77 W in Figure 5.27(a)) where the inverter start operating at "normal" mode and the efficiency drops. The variable efficiency occurring after 7:30 in Figure 5.27(b) is therefore a result of the inverter operating with another algorithm at "normal" mode.

This change of algorithm is also seen in Figure 5.28(a) and is believed to be the reason for the very evident drop in efficiency between 0.3 A and 0.4 A, a delay is then present when the inverter operates at an increasing efficiency between 0.4 A and 0.8 A before it indicates when the inverter is running at "normal" mode between 0.8 A and 2 A. The long efficiency drop in Figure 5.33(a) is also a result of that. The drop lasts for almost two hours because the irradiance decreased after the inverter switched algorithms and the efficiency was no longer optimal. If the irradiation had dropped more, then the inverter would have switched back to the other algorithm.

It is believed that the oscillation in Figure 5.24(b) is also a result of a "special" algorithm being used. It seems like one algorithm is programmed to reduce losses related to the inverter switches at low irradiance and power to maintain a good efficiency at these conditions. This algorithm is especially used on days with low irradiance like on 6 May in Figure 5.25(b) where some of the large drops in efficiency happens almost simultaneously to when the current start and stop oscillating. It is therefore assumed that the oscillation is a deliberate result of an algorithm designed to maintain a good efficiency at low irradiance, and that the resulting harmonics is within the requirements stated in IEC 61000-3-2 and IEC 61000-3-12.

During short bursts of overirradiance, both the current and power exceeds the expected power of 2.1 kW_p calculated in Chapter 5.4.1 and cable CCC of 7.81 A calculated in Chapter 5.4.2. This power is calculated for conditions at STC (1000 W/m^2), which is the average peak irradiance at local conditions [94]. As illustrated in Figure 5.32, both current and power is higher because of new conditions with a higher irradiance. It is therefore important to account for these overirradiance conditions when designing the PV system. The inverter must be large enough to handle overirradiance and to avoid loosing this extra power.

Both the Australian [3] and German manuals [4] state that the cable CCC should be calculated by using respectively 1.2 and 1.25 times array I_{SC}. The CCC for this PV system, calculated with guidelines from [4], is lower than the 8 A_{DC} produced during overirradiance. It indicates that if oversized cables were not used, the cable could be damaged over time as a result of repeatedly overirradiances. This could happen if more current than the CCC runs through the cable and is avoided by adding a circuit breaker. The circuit breaker would, however, have to be manually re-set for the inverter to start producing again. Some time could pass before this is done where the inverter would not be operating.

The Eaton circuit breaker is made for PV systems and has settings to allow for overcurrent to run through it for a short period of time and then allows the inverter to utilize the overirradiance. Overirradiance occurs mainly in the end of May, June and July and can happen quite often and rapidly, depending on the clouds. Since cables with larger cross section can only reduce the cable loss, the Australian and German manuals are considered to be too conservative when calculating the CCC and the cable cross section. Neither of these manuals mention overirradiance or how to handle this.

5.8.2 Performance Ratio

As mentioned in Section 5.5.11, performance ratio measures the quality of the PV system and describes the relation between the theoretical energy and the "real" energy output from the PV system. Usually one year of data is needed to perform an optimum PR analysis, but this is not possible to achieve in this thesis, and therefore only five days of data were used. Equation (5.56) was used to calculate the PR values [96].

$$PR = \frac{E}{A \cdot r \cdot H} \tag{5.56}$$

E is the electrical energy in kWh; H is the daily measured solar irradiation in kWh/m^2; A is the array area of 19.32 m^2; r is the efficiency factor of the PV modules, which is calculated to be $r = \frac{Max\ PV\ module\ power}{PV\ module\ area} = \frac{0.092\ kW}{0.84\ m^2} = 11\ \%$.

TABLE 5.17: Daily and total irradiation; electrical energy from inverter to grid and PR based on five days of data.

Date	**Irradiation [kWh/m^2]**	**El. energy to grid [kWh]**	**PR [%]**
02.05.14	7.94	15.40	92
03.05.14	6.16	11.91	91
04.05.14	6.71	12.87	91
05.05.14	1.32	1.87	67
06.05.14	0.58	0.88	72
Total	**22.71**	**42.93**	**89**

From Table 5.17 it can be seen that the PR was particular high at sunny days with high irradiation levels. The PR is lowest at 5 and 6 May when the irradiation is lower. However, the PR is higher on 6 May even if the irradiation is lower when compared with 5 May. Figure 5.35 shows the temperatures of 5 and 6 May. On 5 May the average array temperature was 11.56 $°C$ with a average peak temperature of 19.3 $°C$, and on the 6 May the average temperature was 9.24 $°C$ with a average peak temperature of 10.92 $°C$. In addition the temperature was for a longer period $>$ 1 hour higher than 14 $°C$ on May 5. The PV array is more efficient at lower temperatures and this could explain why the PV system was able to harvest more energy even though the irradiance was lower on the 6 May.

The total PR from five days of data is 89 %. This means that 11 % during this period were not converted to usable energy due to system losses. There are many factors that could influence the PR value. First of all the measurement period is too short and this gives insufficient measurements for calculating a reliable PR. After one year the system losses would probably be

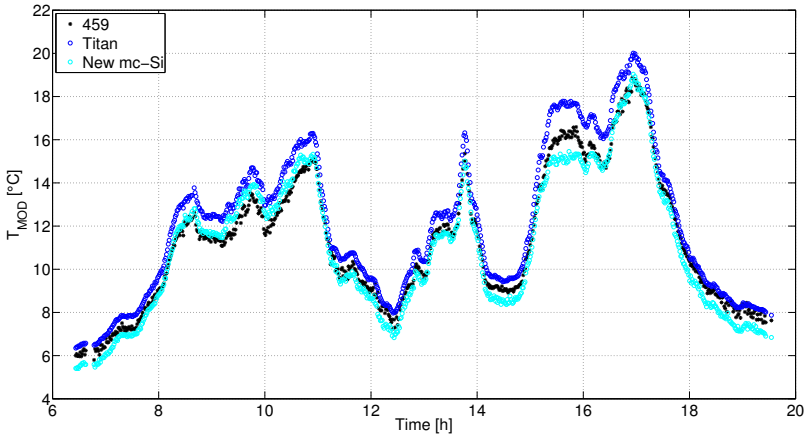

(a) Module Temperature on 5 May 2014. "459", "Titan" and "New mc-Si" are different measuring points on the array.

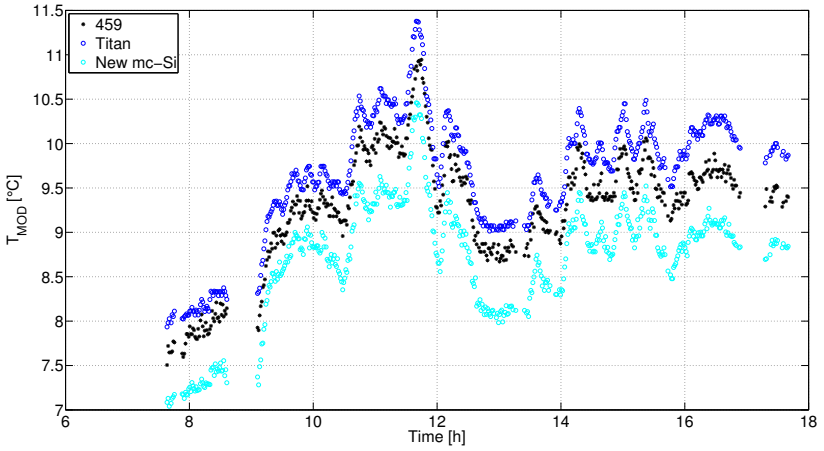

(b) Module Temperature on 6 May 2014. "459", "Titan" and "New mc-Si" are different measuring points on the array.

FIGURE 5.35: Array temperatures on 5 and 6 May.

closer to 20.4 %, which was calculated in Section 5.5.10. Temperature variations and temporary shading could have a larger effect on the calculated values if the measurement period is only a few days. At least one month of data should have been included in the calculations to minimise the effect from these factors. In addition to temperature and shading, conduction losses, efficiency factor of the PV modules and the inverter also affects the PR values [97].

5.8.3 Energy Harvest

From 24 April, when the inverter was installed and started commissioning to 26 May, the inverter has been operating for 493 hours. When using Equation 5.37 and the average irradiation for

May, calculated from Table 4.3 being 160.43 $\frac{kWh}{m^2}$, an estimated power output of 339.48 kWh is calculated with no losses added. When assuming the voltage drop, inverter efficiency, relative efficiency, spectral gain, angular reflectance effects and dirt losses from Section 5.5, and assuming no losses due to shading, tilt angle and manufacturer's tolerance, the estimated power in May is calculated to be 289 kWh. The expected power output will in reality be slightly smaller when considering that the inverter only operated for six days in April and 26 of 31 days in May (months with different average irradiation), an uncertainty of 5 % can also be added due to uncertainty in the system losses and varying temperature and irradiance during the operating hours. This varying irradiance is illustrated with Figure 5.36, showing the power output during the last week of operation. As seen on 19, 21, 22 and 23 May, clouds and varying irradiance varied the daily power production which resulted in lower power output on these days compared to 24 May.

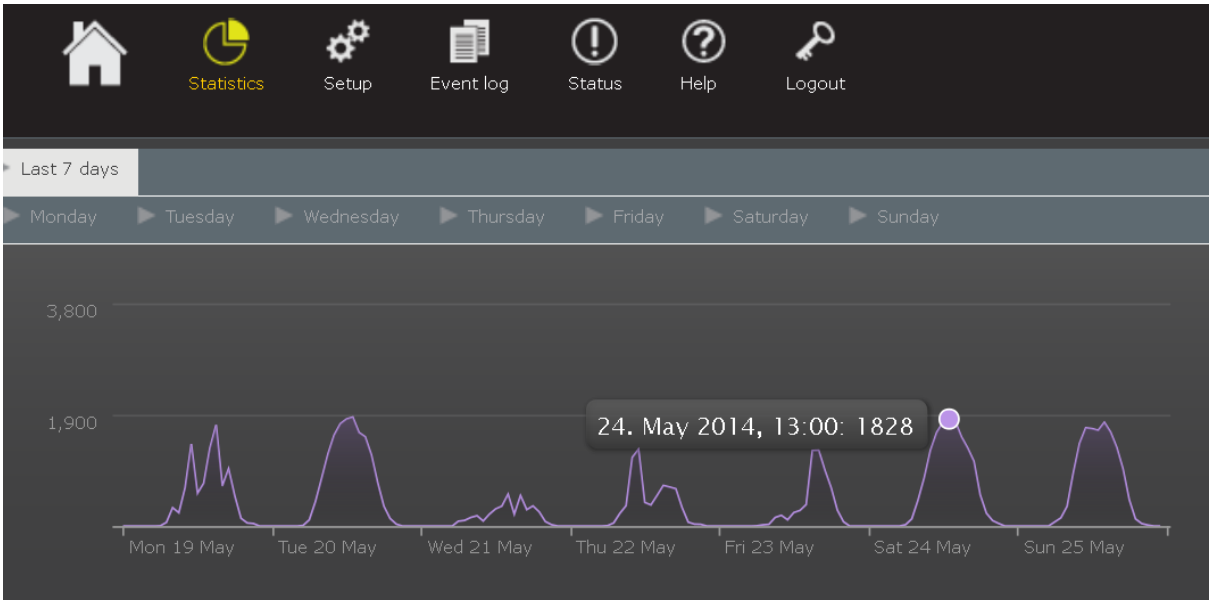

FIGURE 5.36: A screenshot of Theia Analyzer showing the inverter power output during the last 7 days, from 19 to 25 May. It indicates a varying power output due to irradiance, a very low production on 21 May and a production of 1828 W on 24 May.

The total produced power so far on 26 May, the month of May and year 2014 is showed in Figure 5.37. The total energy produced in April and May in Figure 5.37 c) is assumed to be "one month" to simplify the calculations above, resulting in an expected production in May of 289 kWh. It is seen in Figure 5.37 and Appendix I that the inverter produces more power than expected in the calculations, meaning that either the irradiation in May is higher than the average irradiation of the past three years, or the system losses at this period is smaller than expected.

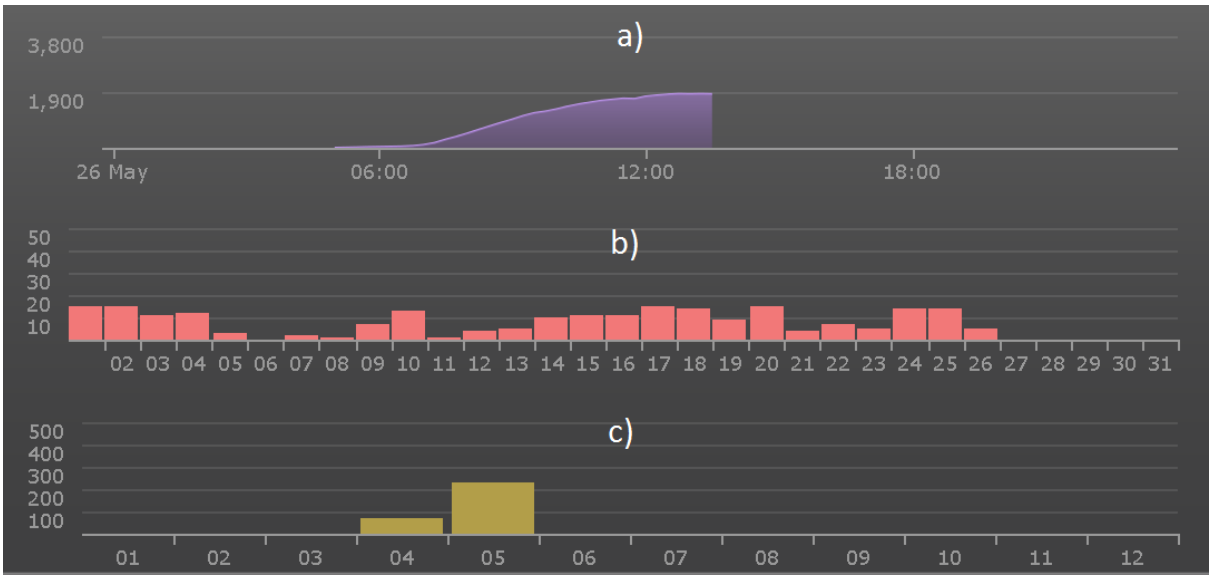

FIGURE 5.37: A screenshot of Theia Analyzer showing a) The total energy produced until 13:00 on 26 May of 8661 Wh, b) Energy produced every day in May, giving a total energy of 238 kWh this month, c) Energy produced so far this year, 313 kWh has been produced since the inverter started commissioning.

It is seen from Figure 5.37 b) that the inverter has a good average daily production, except from a few days with little or close to no production, like 6, 8 and 11 May. May was a sunny month, as Figure 5.37 b) indicate, and the inverter efficiency has been operating in average very close to its maximum capacity. This resulted in a good utilisation of the available irradiation on days with and without clouds. The 313 kWh produced in April/May is more than what is expected with the given assumptions in May, Figure 5.37 therefore shows a good production rate of the inverter on a daily, monthly and yearly basis. It is assumed that this good progression will continue to increase throughout May and the summer months as the irradiation increases, until it is expected to decrease in September. Assuming if the trend found by the production in May, shown in Figure 5.37 c), related to the irradiation in Table 4.3 is maintained throughout a whole year, the progression looks good with regards of producing the expected yearly energy yield calculated in Equation 5.39 of 2088 kWh or more. It is however, hard to predict a trend from Figure 5.37 c) and to conclude that the system will be operating accordingly when only one month is used as a reference. Ideally, two or three additional months should have been analysed to indicate a clear increase or decrease in the monthly production trend line.

Chapter 6

Conclusion

Renewable energy sources are now being implemented in a large scale in Europe. Large and small-scale hydro power plants, wind turbines and PV systems are built to reach the EU goal of getting 20 % of its energy from renewable sources by 2020. Energy from Grid Connected PV Systems is one way of reaching this goal when considering that only 0.01 % of the solar energy reaching the earth's surface is needed to cover the human energy need. As PV systems are covering more of the electricity demand on earth, at least 36.9 GW of them was installed all over the world in 2013. Europe, which has been a global leader on the PV market for many years, installed only 10.3 GW. This was a decrease of 6.7 GW from 2012. Germany, being number one in the European PV market, installed 3.3 GW of the European PV systems while Norway installed only 0.6 MW in 2013. When the average monthly irradiation found in Hamburg of 91.8 kWh/m^2 is compared to the average irradiation in Grimstad of 86.6 kWh/m^2, using PVGIS, it can be seen that the solar energy possibilities in the southern parts of Norway is worth investigating for future installations.

To examine these possibilities, a PV system was built at the University of Agder in Grimstad while making sure that the power produced and system components meets the required demands from the local utility company, Agder Energi. Theia HE-t 3.8, a string inverter from Eltek was found to be the most reasonable and compatible inverter, fulfilling all the power quality and protection requirements given from Agder Energi in addition to having good logging capabilities. It was calculated that the inverter could be connected to one string of 23 de-rated NAPS (NESTE) NP100G12 PV modules. The University provided 48 PV modules, which were tested with regards to I_{mp}, V_{mp} and P_{max} to find the best IV-curve characteristics so that the best 23

modules with the most similar and highest current ratings were used to constitute the system of 2.116 kW_p.

The PV array is made out of 0.83 m^2 sized modules, and should have to withstand a wind load of 1.26 kN each. SunTech modules available on the market can withstand wind loads of at least 2.4 kN/m^2. There is no available data for the NAPS (NESTE) modules used in this PV system, they are old and it is therefore unknown if they can withstand the same load as SunTech. Since the maximum expected wind load is much lower than the minimum wind load sustainable by the more modern PV modules, it was assumed that the older PV modules are capable of withstanding this maximum wind load.

For the practical examination of the solar energy possibilities, the PV system with an estimated total system loss of 20.4 % was installed and expected to produce 2088 kWh/year with a performance ratio (PR) of 80 %. Start-up of the PV system started on 24 April, when we got permission from Agder Energi to finalize the remaining agreements after the PV system had started commissioning. Data from the following days of operation were analysed to see how the inverter operated concerning efficiency. The first days of clear sky indicated that the inverter was operating at a good efficiency of 97 % and producing a maximum power of 2.065 kW_p at irradiance close to one sun. The inverter was operating close to its maximum efficiency and responded almost instantaneously to sudden changes in the irradiance.

It was observed that the inverter had problems producing a steady current when the system was exposed to very low irradiance at midday and at early operating hours. The current curves show a consistent oscillation at times with very low irradiance and a clear drop in efficiency- and power curves approximately at the same time in the morning and evening. It is also observed that when the current oscillates on days with low irradiance, the efficiency drops in the transition between oscillation and a steady current. Eltek was aware of these observations, which was caused by the inverter using two different algorithms for low- and high irradiance to ensure a good efficiency at these conditions. The inverter switches algorithms at a power less than 200-300 W which will cause a drop in efficiency at that time. The algorithms are operating with hysteresis, which is dependent of irradiance and voltage. The length of this efficiency drop therefore depends on the available PV power and could vary from 10 minutes to two hours.

One day of extreme overirradiance occurred during the time period, which resulted in a maximum peak power of 2.8 W at almost 1.5 suns and cell temperature of about 24 $°C$. During the few seconds of overirradiance, the inverter responded quickly and the MPPT managed to follow

the MPP of the array to a good extent. DC Current of 8 A was observed at a short time while the inverter kept operating at maximum efficiency, which indicates that the inverter manages to fully utilize the power from overirradiance conditions. However, this happens because the system is oversized to handle currents higher than what is possible for the system to achieve. If the system was not oversized, the circuit breaker would have different tripping times at currents with higher values than the rated. To avoid this, and to make sure that power from overirradiance is fully processed, it is recommended to size system cables and circuit breakers for the maximum overirradiance conditions of 1.6 suns in Grimstad.

During the time period of this thesis, the PV system was operational for 6 days in April and 26 days in May which was, for the sake of calculations, assumed to be approximately one month. The system produced 313 kWh during this time, which was more than the expected power of 288 kWh calculated for May. A PR of 89 % was calculated for the system during the first week of May. It was seen that the PV system has a good PR of 92 % on sunny days with high irradiation and a varying smaller PR on days with lower irradiation. It has good preconditions to meet the expected yearly production of 2088 kWh or more. However, it is hard to predict a trend line for how the system operates in the future when only one month is used as a reference.

For further work, we recommend the PV system to be operational for minimum one year. Several months of data makes it possible to compare energy output with estimations from tools such as PVGIS. In addition, it would be beneficial to see how much power a small sized PV system can generate throughout a year in Southern Norway.

Overirradiance and the resulting power gain should be studied. Furthermore, it should be determined how much harmonics are caused as a result of oscillation in the current when the inverter operates on the "low irradiance" algorithm. It would also be interesting to see how the power quality changes throughout the day. More studies should be done regarding the albedo effect. More research need to be done to see how the sea in the horizon and snow at the installation site is contributing with diffuse irradiance and how it affects the PV system. Another factor worthy of study is the shading effect on the PV array. A more precise loss factor due to shading can be determined if more research is done to see how shading from the telecom tower and fence affects the array.

Bibliography

[1] European Commision. Renewable energy. http://ec.europa.eu/energy/renewables/index_en.htm, Last accessed January 2014.

[2] IEA International Energy Agency. PVPS Report snapshot of Global PV 1992-2013 - Preliminary Trends Information from the IEA PVPS Programme. http://www.iea-pvps.org/index.php?id=3&eID=dam_frontend_push&docID=1924, Last accessed May 2014.

[3] G. Stapleton, S. Garrett, S. Neill, and B. McLean. *Grid-Connected PV Systems Design and Installation*. Global Sustainable Energy Solutions (GSES), 7th edition, December 2010.

[4] The German Solar Energy Society. *Planning and Installing Photovoltaic System. A guide for Designers, Installers, Architects and Engineers*. Routhledge, 2013.

[5] A. Ashfaq. *Power Electronics for Technology*. Prentice Hall, 1st edition, June 1998.

[6] Y. Chen and K. M. Smedley. A cost-effective single-stage inverter with maximum power point tracking. *IEEE Transactions on Power Electronics*, 19(5):1289–1294, September 2004.

[7] S.B. Kjaer, J.K. Pedersen, and F. Blaabjerg. A review of single-phase grid-connected inverters for photovoltaic modules. *IEEE Transactions on Industry Applications*, 41(5): 1292–1306, September 2005.

[8] S. Bergsmark. UiA. Private Communication, 2014.

[9] S. J. Chapman. Electric Machinery Fundamentals. http://www.mhhe.com/engcs/electrical/chapman/fundamentals/PWM.pdf, Last accessed May 2014.

[10] Fronius International GmbH. High Frequency Transformer with Transformer Switchover. http://www.fronius.com/cps/rde/xbcr/SID-17106601-1811CF4A/

fronius_international/SE_TA_High_Frequency_Transformer_With_Transformer_Switchover_EN_320487_snapshot.pdf, Last accessed February 2014.

[11] Schneider Electric. Description of Galvanic Isolation. http://www.schneider-electric.us/sites/us/en/support/faq/faq_main.page?page=content&country=US&lang=en&id=FA157465&redirect=true, Last accessed February 2014.

[12] V. W. Quinn. Scaling Design Methods To Improve Transformers. http://www.dalitech.com/Resources/Scaling%20Design%20Methods%20to%20Improve%20Transformers.pdf, Last accessed May 2014.

[13] E. Seymour. Design Characteristics of High-Power Photovoltaic Inverters. http://solarenergy.advanced-energy.com/upload/File/White_Papers/ENG-InverterDesign-270-02.pdf, Last accessed March 2014.

[14] B. Chen. Integration of Isolation for Grid-Tied Photovoltaic Inverters. http://www.analog.com/static/imported-files/tech_articles/Integration-of-Isolation-for-Grid-Tied-Photovoltaic-Inverters-MS-2356.pdf, Last accessed February 2014.

[15] D. Chiras. *Solar Electricity Basics: A Green Energy Guide*. New Society Publishers, July 2010.

[16] J. Worden and M. Z.-Martinson. How Inverters Work. http://pvdepot.com/media/resources/How-Solar-Inverters-Work.pdf, Last accessed March 2014.

[17] Y.-C-Kuo and T.-J. Liang. Novel maximum-power-point-tracking controller for photovoltaic energy conversion system. *IEEE Transactions on Industry Electronics*, 48(3):594–601, June 2001.

[18] G. Hering and C. Warren. Harvest time. *Photon International - The Solar Power Magazine*, (10), 2011.

[19] G. H. Yordanov. UiA. Private Communication, 2014.

[20] NVE. Håndtering av plusskunder og vedtak om dispensasjon fra forskrift 302 om økonomisk og teknisk rapportering m.v. http://www.nve.no/PageFiles/9733/Plusskunder.pdf, Last accessed March 2014.

[21] R. H. Josefsen. Agder Energi Nett. Private Communication, 2014.

[22] Dr J. Ravishankar. UNSW. Types of earthing systems. Lecture notes from the course ELEC9716 - Electrical Safety, 2013.

[23] Schneider Electric. Photovoltaic system: electrical equipments selection. http://www.electrical-installation.org/enwiki/Photovoltaic_system:_electrical_equipments_selection, Last accessed March 2014.

[24] Hafslund. 01-06-01 Tilknytning av Produksjonsanlegg 230 - 400 V. http://nettbiblioteket.hafslundnett.no/NettLib/Retningslinjer/01%20Tilknytning/06Tilknytning%20av%20produksjonsanlegg/01_06_01_Produksjon_230_400V.pdf, Last accessed March 2014.

[25] H. T. Bjørnstad. Vurdering av plusskunder sine rammebetingelser i framtidens distribusjonsnett (SmartGrid) - med fokus på AMS og produksjonsteknologi. Master's thesis, NTNU, http://www.diva-portal.org/smash/get/diva2:536457/FULLTEXT01.pdf, February 2012.

[26] M. E. Ropp, M. Begovic, and A. Rohatgi. Prevention of islanding in grid-connected photovoltaic systems. *Progress in Photovoltaics: Research and Applications*, 7(1):39–59, February 1999.

[27] Greenergy Research Group. Grid-Connected. http://grglab.blogspot.no/2012/11/grid-connected.html, April 2014.

[28] S. R. Wenham, M. A. Green, M. E. Watt, and R. Corkish. *Applied Photovoltaics*. Earthscan, 2nd edition, 2007.

[29] P. Emck and M. Richter. An upper treshold of enhanced global shortwave irradiance in the troposphere derived from field measurements in tropical mountains. *Journal of Applied Meterology and Climatology*, 47(11):2828–2845, November 2008.

[30] G. H. Yordanov, T. O. Sætre, and O.-M. Midtgård. Overirradiance studies require subsecond resolution; exclude thermopile pyranometers and commercial data loggers. *Proceedings of the 28th European Photovoltaic Solar Energy Conference and Exhibition (PVSEC)*, pages 3455–3459, 2013.

[31] Norsk solenergiforening. Om solenergi. http://www.solenergi.no/om-solenergi/, Last accessed January 2014.

[32] G. H. Yordanov. *Characterization and Analysis of Photovoltaic Modules and the Solar Resource Based on In-Situ Measurements in Southern Norway*. PhD thesis, NTNU, November 2012.

[33] A. Christensen. Lys framtid for solkraft i nord. http://forskning.no/artikler/2012/november/338931/, Last accessed March 2014.

[34] European Commision. Photovoltaic Geographic Information System. http://re.jrc.ec.europa.eu/pvgis/, Last accessed May 2014.

[35] D. Heinemann. Energy Meteorology. http://www.energiemeteorologie.de/team/dehe/Documents/Energy_Meteorology__%20Script.pdf, Last accessed February 2014.

[36] L. Wald M. Lefévre, M. Albuisson. Description of the software Heliosat-II for the conversion of images acquired by Meteosat satellites in the visible band into maps of solar radiation available at ground level. http://www.soda-is.com/heliosat/heliosat2_soft_descr.pdf, Last accessed March 2014.

[37] Kjeller Vindteknikk. Resource mapping of solar energy - an overview of available data in Norway. http://www.solenergi.no/wp-content/uploads/2010/01/KVT_OB_2013_R046_OREEC_Solressurskartlegging.pdf, Last accessed March 2014.

[38] M. Šúri, T. A. Huld, E. D. Dunlop, and H. A. Ossenbrink. Potential of solar electricity generation in the European Union member states and candidate countries. *Solar Energy*, 81(10):1295–1305, 2007.

[39] A. G. Imenes, G. H. Yordanov, O.-M. Midtgård, and T. O. Sætre. Development of a test station for accurate in situ I-V curve measurements of photovoltaic modules in southern Norway. *Proceedings of the 37th IEEE Photovoltaic Specialists Conference (PVSC)*, pages 003153–003158, 2011.

[40] R. Pitz-Paal, N. Geuder, C. H.-Klick, and C. Schillings. How to get bankable meteo data? - dlr solar resource assessment. http://www.nrel.gov/csp/troughnet/pdfs/2007/pitz_paal_dlr_solar_resource_assessment.pdf, Last accessed February 2014.

[41] Tradett.com. Poly Solar Panels. http://www.tradett.com/product/u75356p682283/poly-solar-panels.html, Last accessed March 2014.

[42] PLG Power Limited. I-V curve irradiance dependence. http://www.plgpower.com/images/graph.gif, Last accessed May 2014.

[43] Bioforsk AgroMetBase. Hent klimadata. http://lmt.bioforsk.no/agrometbase/getweatherdata.php, Last accessed March 2014.

[44] O.-M. Midtgård, T. O. Sætre, G. H. Yordanov, A. G. Imenes, and C. L. Nge. A qualitative examination of performance and energy yield of photovoltaic modules in southern Norway. *Renewable Energy An International Journal*, 35(6):1266–1274, 2010.

[45] T. Huld, R. Gottschalg, H. G. Beyer, and M. Topič. Mapping the performance of PV modules, effects of module type and data averaging. *Solar Energy*, 84(2):324–338, February 2010.

[46] R. Messenger and J. Ventre. *Photovoltaic Systems Engineering*. CRC Press LLC, 2000.

[47] A. B. W. Grimnes. UiA. Private Communication, 2014.

[48] SUNTECH. Global Installation Guide for Suntech Power Photovoltaic Module Version 20140101. http://file4.fanyacdn.com/imglibs/files/2014%20Installation%20Manual.pdf, Last accessed May 2014.

[49] L. Cohn. Safeguard Your RE Investment. http://www.homepower.com/articles/solar-electricity/design-installation/safeguard-your-re-investment, Last accessed March 2014.

[50] J. Althaus, K. Strohkendl, S. Menzler, and G. Mathiak. PV mounting system corrosion by salt mist - Experimental study with full size mounting systems. *Proceedings of the 28th European Photovoltaic Solar Energy Conference and Exhibition (PVSEC)*, pages 2893–2896, 2013.

[51] E. Weliczko. Galvanic Corrosion Considerations for PV Arrays. http://solarprofessional.com/articles/products-equipment/racking/galvanic-corrosion-considerations-for-pv-arrays?v=disable_pagination, Last accessed March 2014.

[52] SSINA. Stainless Steel Fasteners - A Systematic Approach To Their Selection. http://www.ssina.com/download_a_file/fasteners.pdf, Last accessed May 2014.

[53] Eltek. Theia HE-t - user manual. http://www.eltek.com/wip4/download_doc_647.epl?id=6851, Last accessed May 2013.

[54] Advanced Energy. Understanding Potential Induced Degradation. http://solarenergy.advanced-energy.com/upload/File/White_Papers/ENG-PID-270-01%20web.pdf, Last accessed March 2014.

[55] NEK 400:2010. *Elektriske lavspenningsinstallasjoner*. Norsk Elektroteknisk Komité (NEK), 4th edition, 2010.

[56] MCS. *Guide to the Installation of Photovoltaic Systems*. Microgeneration Certification Scheme (MCS), 2012.

[57] M. Shipp, C. Holland, D. Crowder, S. Pester, and J. Holden. Fire safety and solar electric/photovoltaic systems. http://www.bre.co.uk/page.jsp?id=3211, Last accessed March 2014.

[58] H. Laukamp, G. Bopp, R. Grab, C. Wittwer, H. Häberlin, B. van Heeckeren, S. Phillip, F. Reil, H. Schmidt, A. Sepanski, H. Thiem, and W. Vaassen. PV fire hazard - Analysis and assessment of fire incidents. *Proceedings of the 28th European Photovoltaic Solar Energy Conference and Exhibition (PVSEC)*, pages 4304–4311, 2013.

[59] ABB. ABB string inverters. http://new.abb.com/docs/librariesprovider22/technical-documentation/solar-inverter-pvs300-flyer.pdf?sfvrsn=2, Last accessed February 2014.

[60] ABB. Private Communication, 2014.

[61] SMA. SUNNY BOY 3000-US / 3800-US / 4000-US. http://www.sma.de/en/products/solar-inverters-with-transformer/sunny-boy-3000-us-3800-us-4000-us.html#Technical-Data-8733, Last accessed February 2014.

[62] SMA. Product Guide 2009/2010. http://getek.no/brosjyrer/SMAprodukter_2009-10.pdf, Last accessed March 2014.

[63] Eltek. Theia HE-t. http://www.eltek.com/detail_products.epl?id=1155461&cat=24675&k1=25509&k2=&k3=&k4=&close=1, Last accessed February 2014.

[64] Danfoss. Info Kit. ftp://software.danfoss.com/Global/InfoKit/Complete_Danfoss_Info_Kit_2013.pdf, Last accessed February 2014.

[65] Danfoss. The Danfoss DLX UL inverter series - Performance and flexibility in a user-friendly design. http://www.danfoss.com/nr/rdonlyres/

3769ba0a-9c73-455c-bb15-9e878b48139a/0/web_dksipfp203a122_dlx_factsheet_us.pdf, Last accessed February 2014.

[66] S. Madsen. Soltek. Private Communication, 2014.

[67] GETEK. Fronius IG Plus. http://www.getek.no/brosjyrer/FroniusIG_plus.pdf, Last accessed January 2014.

[68] Fronius International GmbH. Fronius IG Plus. http://www.fronius.com/cps/rde/xbcr/SID-C82B8BB3-7A0C9337/fronius_international/DBL_Fronius_IG_Plus_M_06_0008_EN_513_as13_low_156927_snapshot.pdf, Last accessed January 2014.

[69] Fronius International GmbH. Fronius Datamanager. http://www.fronius.com/cps/rde/xchg/fronius_international/hs.xsl/83_27954_ENG_HTML.htm#.Uym449xyfbM, Last accessed March 2014.

[70] GETEK. Private Communication, 2014.

[71] Agder Energi Nett. Tekniske funksjonskrav. http://www.aenett.no/PageFiles/622/PV_Vedlegg_3_Teknisk_34364a.pdf?epslanguage=no, Last accessed February 2014.

[72] LOVDATA. Forskrift om leveringskvalitet i kraftsystemet. http://lovdata.no/dokument/SF/forskrift/2004-11-30-1557, Last accessed May 2014.

[73] CESINEL (Compania Espanola de Instrumentos Electricos) Cee energiteknikk AS. *User Manual for MEDCAL Scope and MEDCALSetup for MEDCAL NT*, 1.1 edition, August 2006.

[74] H. Tranøy. Tekniske retningslinjer for tilknytning av plusskunder i lavspenningsnett. Master's thesis, NTNU, http://www.diva-portal.org/smash/get/diva2:566539/FULLTEXT01.pdf, July 2012.

[75] Eltek. Type Verification Test Sheet. http://midsummerwholesale.co.uk/pdfs/Eltek_G83-1_Theia%2044HE-t_and_38HE-t.pdf, Last accessed March 2014.

[76] SINTEF. Spenningskvalitet - fenomen for fenomen. http://dok.ebl-kompetanse.no/Foredrag/2008/Grunnlegg%20innforing%20spkv/02%20Fenomenbeskrivelse.pdf, Last accessed February 2014.

[77] SINTEF. Planleggingsbok for kraftnett - Spenningskvalitet. http://www.ren.no/c/document_library/get_file?uuid=

74190d68-f0bc-49a8-9fce-67eae2d73c1a&groupId=10206, Last accessed February 2014.

[78] Selectricity. Harmonic Distortion Analysis. http://selectricity.com/harmonicdistortionanalysis.html, Last accessed March 2014.

[79] standard.no. NEK IEC/TR 61000-3-6. http://www.standard.no/no/Nettbutikk/produktkatalogen/Produktpresentasjon/?ProductID=323818, Last accessed March 2014.

[80] standard.no. NEK IEC 61000-3-2. http://www.standard.no/no/Nettbutikk/produktkatalogen/Produktpresentasjon/?ProductID=378311, Last accessed March 2014.

[81] standard.no. IEC 61000-3-12 Ed. 2.0. http://www.standard.no/no/Nettbutikk/produktkatalogen/Produktpresentasjon/?ProductID=483603, Last accessed March 2014.

[82] E. Kristensen. Eltek. Private Communication, 2014.

[83] SINTEF. Håndbok Spenningskvalitet - Kortvarige underspenninger - Spenningsdipp. http://www.sintef.no/Projectweb/Handbok_Spenningskvalitet/Kort-innforing/Kortvarige-underspenninger---Spenningsdipp/, Last accessed March 2014.

[84] SINTEF. Håndbok Spenningskvalitet - Kortvarige overspenninger. http://www.sintef.no/Projectweb/Handbok_Spenningskvalitet/Kort-innforing/Kortvarige-overspenninger-eng-swell/, Last accessed March 2014.

[85] J. E. Ormbostad. *Montørhåndboka - NEK 400:2010*, volume 1. Elforlaget, 2010.

[86] National Instruments. Part II - Photovoltaic cell I-V Characterization Theory and LabVIEW Analysis Code. http://www.ni.com/white-paper/7230/en/, Last accessed May 2014.

[87] R. A. Matula. Electrical Resistivity of Copper, Gold, Palladium and Silver. *J. Phys. Chem. Ref. Data*, 8(4):1147–1298, 1979.

[88] T. M. Dauphnee and H. P.-Thomas. A Copper Resistance Temperature Scale. *The Review of Scientific Instruments*, 25(9):884–886, September 1954.

[89] G. H. Yordanov, M. Tayyib, O.-M. Midtgård, J.-O. Odden, and T. O. Sætre. Test of the European Joint Research Centre Performance Model for c-Si PV Modules. *Proceedings of the 38th IEEE Photovoltaic Specialists Conference (PVSC)*, pages 002382–002387, June 2012.

[90] T. Huld, M. Šúri, , and E. D. Dunlop. Geographical Variation of the Conversion Efficiency of Crystalline Silicon Photovoltaic Modules in Europe. *Progress in Photovoltaics: Research and Applications*, 16(7):595–607, November 2008.

[91] U. Jahn, W. Nasse, Th. Nordmann, L. Clavadetscher, and D. Mayer. Achievements of Task 2 of IEA PV Power Systems Programme: Final Results on PV System Performance. *Proceedings of the 19th European Photovoltaic Solar Energy Conference and Exhibition (PVSEC)*, pages 2813–2816, June 2004.

[92] R. Siddiqui, R. Kumar, G. K. Jha, and U. Bajpai. Performance Analysis of Polycrystalline Silicon PV Modules on the basis of Indoor and Outdoor Conditions. *International Journal of Current Engineering and Technology*, 4(1):340–349, February 2014.

[93] C. Honsberg and S. Bowden. Fill factor. http://pveducation.org/pvcdrom/solar-cell-operation/fill-factor, Last accessed April 2014.

[94] G. H. Yordanov, O.-M. Midtgård, T. O. Sætre, H. K. Nielsen, and L. E. Norum. Overirradiance (cloud enhancement) events at high latitudes. *IEEE Journal of Photovoltaics*, 3(1): 271–277, January 2013.

[95] F. Vignola, J. Krumsick, and F. Mavromatakis. Performance of PV Inverters. http://solardat.uoregon.edu/download/Papers/PerformanceofPVInverters.pdf, Last accessed May 2014.

[96] Photovoltaic-software.com. How to calculate the annual solar energy output of a photovoltaic system. http://photovoltaic-software.com/PV-solar-energy-calculation.php, Last accessed May 2014.

[97] SMA. Performance ratio - Quality factor for the PV plant. http://files.sma.de/dl/7680/Perfratio-UEN100810.pdf, Last accessed May 2014.

Appendix A

Theia 3.8 HE-t Datasheet

ELTEK

THEIA™ HE-t

The THEIA™ HE-t range defines a new level of efficiency, flexibility and user friendliness for isolated string inverters. Suitable for all PV cell technologies, and ready for use all over the world, the THEIA™ HE-t is the perfect choice for any PV installation.

THEIA™ HE-t

SOLAR INVERTERS: 2.0 kW – 4.6 kW

PERFORMANCE
- Maximum efficiency 97.3 % with galvanic isolation
- Suitable for use with all PV modules of any technology, with the ability to ground the positive or the negative terminal on the DC side
- Compliance with the highest international safety standards
- Early startup and high efficiency at low irradiation gives longer operation time and higher energy yields

EASE OF USE
- Lightweight and easy to install
- With or without DC Disconnect Switch
- Color screen with touch sense buttons
- Intuitive user interface

RELIABILITY
- High quality components, with a robust design
- Bespoke Maximum Power Point Tracking
- Stable operation under extremely dynamic irradiation conditions
- IP65 protection level

MONITORING AND COMMUNICATION
- Complete site overview from one single inverter
- Integrated webserver with easy-to-use monitoring software
- Multilanguage display

 Find your local office at: www.eltek.com Doc No: 357115.DS3 rev8

MODEL	2.0 HE-t	2.9 HE-t	3.8 HE-t	4.4 HE-t	4.6 HE-t
INPUT DATA					
Nominal DC power	2100 W	3000 W	4000 W	4600 W	4800 W
Max. PV power	2625 W_p	3750 W_p	5000 W_p	5750 W_p	6000 W_p
Max. DC voltage	600 V_{dc}				
Voltage range MPPT	230 to 480 V_{dc}	230 to 480 V_{dc}	230 to 480 V_{dc}	230 to 480 V_{dc}	230 to 480 V_{dc} [1]
Max. input current	9.5 A	13.5 A	18.0 A	21.0 A	21.0 A
Number of PV string inputs	3				
Number of MPP trackers	1				
Input features	Reverse polarity protection, Ground fault monitoring, Integral DC switch disconnector (optional), Integral DC fuses for string inputs (optional), Field configurable for positive or negative grounding, or ungrounded				
OUTPUT DATA					
Nominal output power	2000 W	2900 W	3800 W	4450 W	4600 W
Max apparent power	2000 VA	2900 VA	3800 VA	4450 VA	4600 VA
Nominal AC current	9.0 A	13.0 A	17.0 A	19.5 A	20.0 A
Max. AC current	10.5 A	15.2 A	19.7 A	23.0 A	23.0 A
Mains output voltage	230 Vac (+/-20 %) single or split phase				
Mains frequency	50 Hz / 60 Hz (+/-10 %)				
Cos Phi (power factor)	0.8i to 0.8c selectable				
PERFORMANCE DATA					
Maximum efficiency	97.2 %	97.2 %	97.2 %	97.3 %	97.3 %
CEC efficiency	96.8 %	96.8 %	97.0 %	97.0 %	97.0 %
EU efficiency	96.3 %	96.5 %	96.7 %	96.9 %	96.9 %
Power feed starts at	< 7 W				
Night mode power	< 1 W				
MECHANICAL DATA					
Protection degree (EN 60529)	IP 65				
Dimensions	610 H x 353 W x 154 D mm / 24.02 H x 13.90 W x 6.06 D inches				
Weight	< 19 kg / 42 lbs	< 19 kg / 42 lbs	< 21 kg / 46 lbs	< 21 kg / 46 lbs	< 21 kg / 46 lbs
Cable access	Bottom				
Input cable connection	MC3, MC4, Tyco, Screw terminals, Cable clamp, Others on request				
Output cable connection	Screw terminals, Cable clamp				
DESIGN STANDARDS					
EM compatibility	EN 61000-6-2, EN 61000-6-3				
CE marking	Yes				
Other standards	DIN VDE V 0126-1-1, G83/1, EN 50438, AS 4777, CEI 0-21, EN 61000-3-2, EN 61000-3-3, EN 61000-3-11, EN 61000-3-12, IEC 62109-2, IEC 61727, UTE C 15-712-1, C10/11, VDE AR-N 4105, RD1663, G59/2				
ENVIRONMENTAL DATA					
Operating temperature	- 25 °C to + 65 °C / - 13 to + 149 °F (possible power derating above + 45 °C / + 113 °F)				
Storage temperature	- 30 °C to + 80 °C / - 22 to + 176 °F				
Ventilation	Convection cooling				

ADDITIONAL FEATURES	
Topology	High frequency transformer, galvanic isolation
Protection class / Overvoltage category	I / III
Noise Emission	< 37 dB (A)
Communication	Graphical, color display with touch sense buttons, Embedded web-server, Ethernet, CAN and RS485 bus interface, 3x LEDs for visual status indication
Warranty	5 years, 10 years, 15 years, 20 years and 25 years options

1) Output power limitation 230 Vdc to 250 Vdc

EFFICIENCY CURVE THEIA 4.4 HE-t

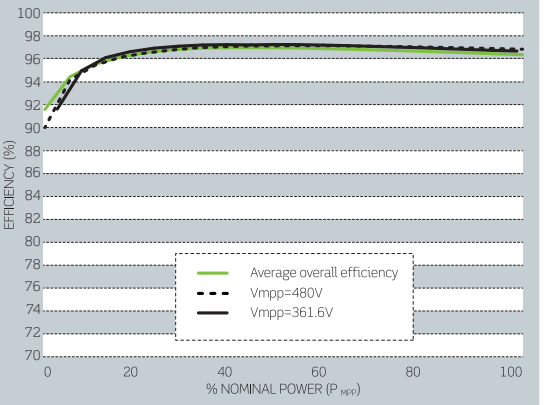

Appendix B

Application to Agder Energi

RENBLAD

REN blad 3004 – VER 1.3 / 2011

Kraftproduksjon - Søknad om nettilknytning.

Kontaktperson:	Kristen Leifsen
Adresse:	Campus Grimstad, Postboks 509, 4898 Grimstad
Telefon:	918 73 575
E-post:	kristen.leifsen@uia.no

Produksjonsenhet:

Navn:	UiA Campus Grimstad, solceller system nr. 1
Gårds- og bruksnr:	3/312
Anleggsadresse:	Jon Lilletunsvei 9
Postnummer:	4898
Kommune:	Grimstad
Status:	Ikke søkt NVE

Tekniske data:

Type produksjon:	Solceller
Generatortype:	THEIA HE-t Vekselretter
Antall generatorer:	1
Total innstallert effekt [kW]:	3,8
Produksjon sommer [GWh]:	3x10-3
Produksjon vinter [GWh]:	3x10-4
Utbyggingskostnad [kr/kWh]:	6,00

Legg ved kartskisse, målestokk 1:12500 for hele anlegget og 1:3125 for kraftstasjonen, se f. eks. www.statkart.no

Sted:	Dato:	Signatur:
Grimstad	1.24.2014	

Søknaden skal sendes til det nettselskapet som eier distribusjonsnettet der produksjonsenheten skal tilknyttes

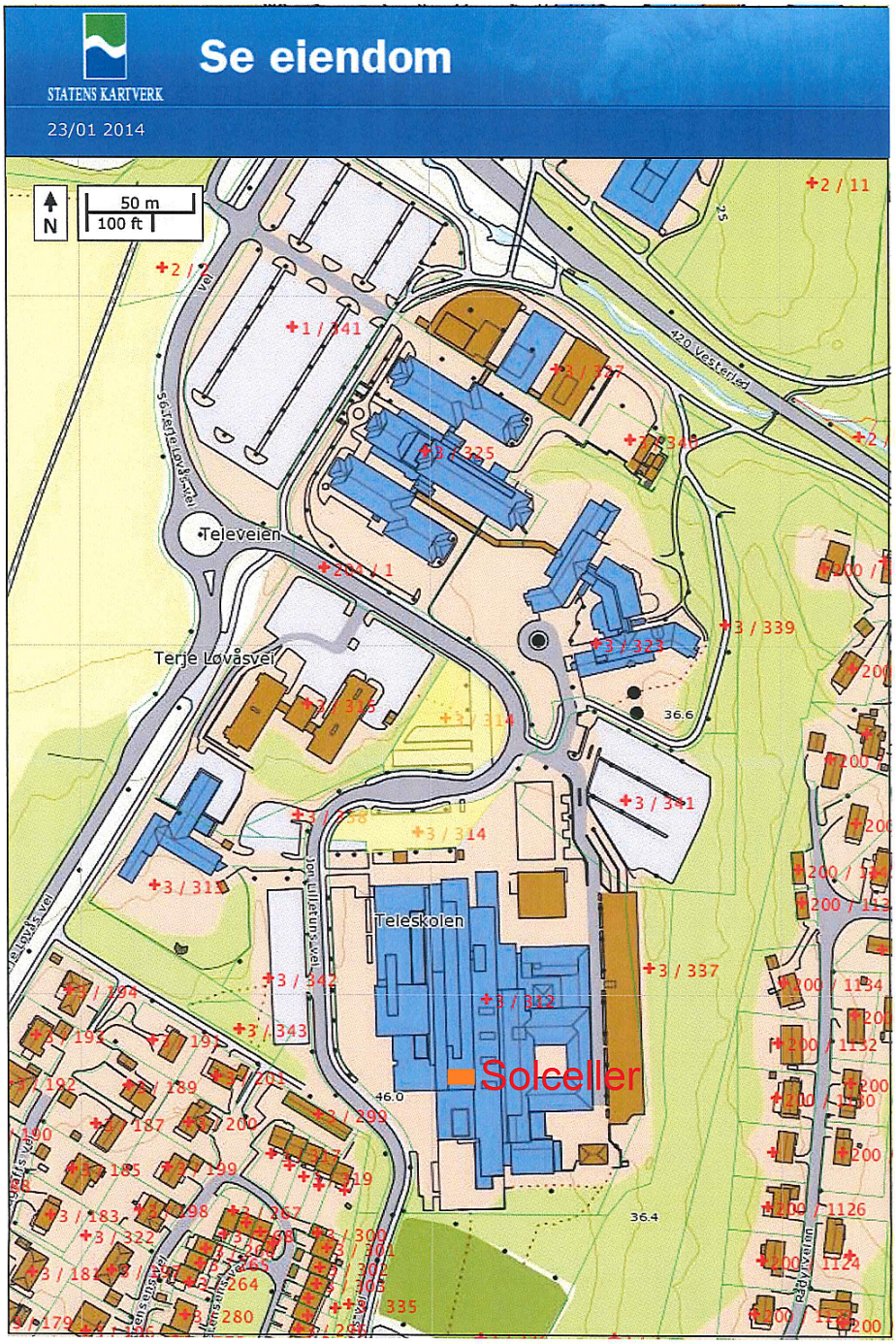
Se eiendom
STATENS KARTVERK
23/01 2014
N
50 m
100 ft
Televeien
Terje Løvåsvei
Teleskolen
Solceller
420 Vesterålsvei
Jon Lilletuns vei
Rådyrveien
46.0
36.6
36.4


sePlan
23/01 2014
N
100 m
500 ft

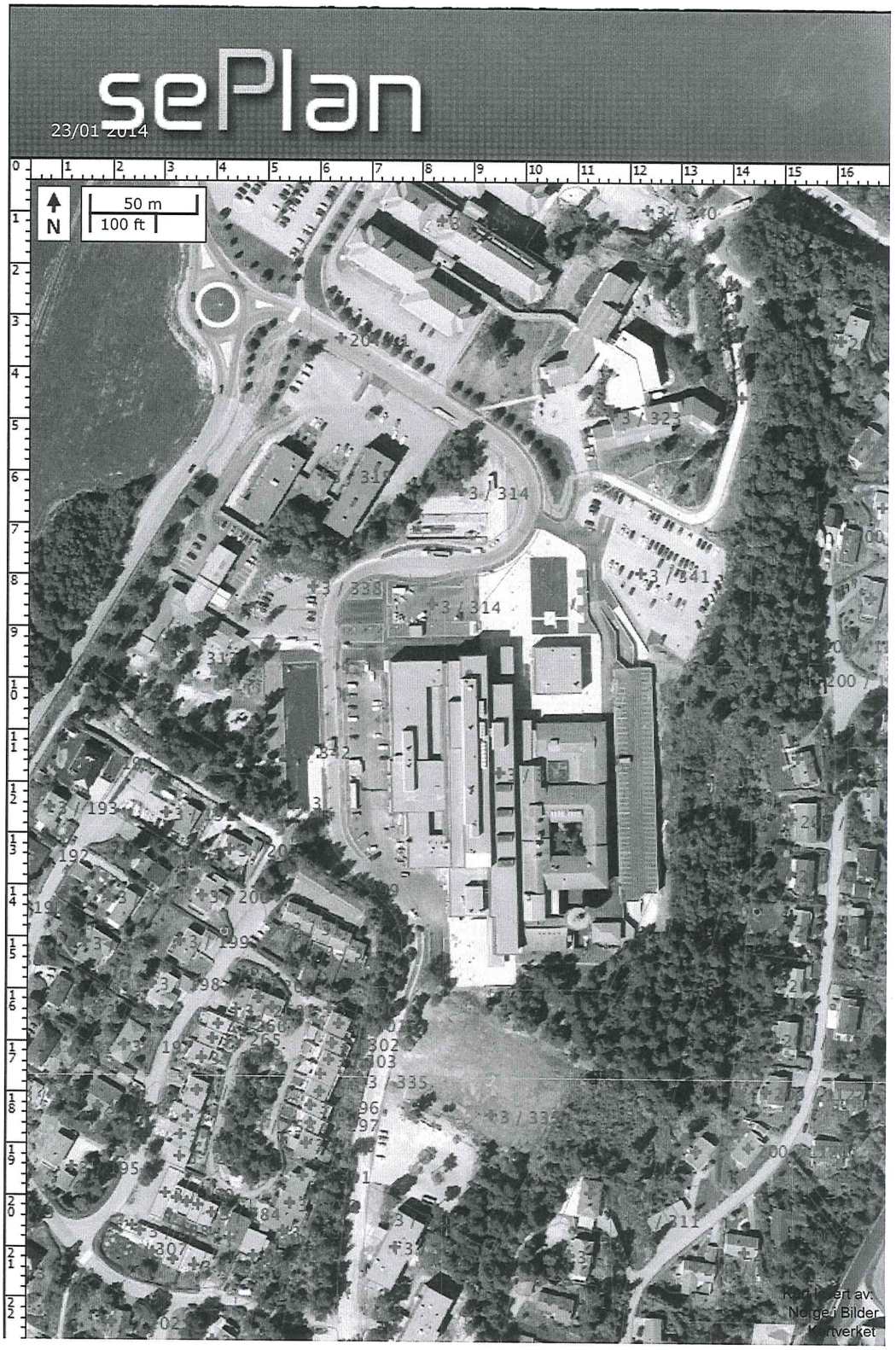
sePlan
23/01 2014
N
50 m
100 ft
Kartdata © Norgei Bilder
Kartverket

Appendix C

Specifications of Inverters

	Input (DC)				Output (AC)								
	Max PV power	MPP voltage range	Max voltage	Max current	Nom power	Nom current	Transformer	V/HZ	Euro efficiency	DC/AC connectors	PV strings	Communication	Weight
PVS300 TL 300	4500 Wp	335-800 V	900 V	14.6 A	4000 W	17.4 A	No	180-276 V/ 47-63 Hz	96.4 %	MC4	4	Ethernet, EIA-485, KNX	27 kg
SMA 3800-US	4040 Wp	250-480 V	600 V	18 A	3800 W	16 A	Yes	211-264 V/ 59.3-60.5 Hz	96 %	Screw	4	Bluetooth or RS485 is optional	38 kg
THEIA 3.8 HE-t	5000 Wp	230-480 V	600 V	18 A	3800 W	17 A	Yes	230 V/ 50 Hz/60 Hz	96.7 %	MC3, MC4, Screw, Clamp	3	Ethernet, Web-server, CAN, RS485	21 kg
DLX 3.8	5000 Wp	230-480 V	600 V	18 A	3800 W	17 A	Yes	230 V/ 45-55 Hz	96.7 %	Screw	3	Ethernet, CAN, RS485	23 kg
Fronius IG plus 35	3710 Wp	230-500 V	600 V	16.2 A	3500 W	N/A	Yes	230 V/ 50 Hz/60 Hz	95 %	Screw	6	WLAN, Ethernet, MODBUS TCP, Datalogger, Webserver	23.8 kg

Appendix D

Eaton DC Circuit Breaker Datasheet

DC string circuit-breaker

DC string circuit-breaker PKZ-SOL 2-poles

- Rated operational voltage 900 VDC
- Rated current In 4, 7, 12, 20, and 30 A
- For permissible string short-circuit currents Isc of 5 up to 22 A

wa_sg05409

Ie	Isc	Type designation	Article No.	Units per package
4A	1,6-3A	PKZ-SOL4	144069	1
7A	2,6-5A	PKZ-SOL7	144120	1
12A	5-9A	PKZ-SOL12	120937	1
20A	9-15A	PKZ-SOL20	120938	1
30A	15-22A	PKZ-SOL30	120939	1

Connection diagrams:

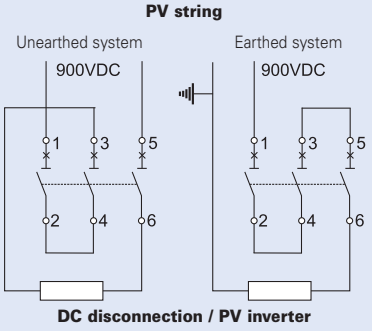

15

Photovoltaic - DC String Protection

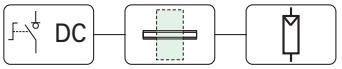

DC Switch-disconnector P-SOL

- Field of application:
  DC-Disconnection in photovoltaic systems between PV Array and Inverter to switch off the energy
- No polarity
- Any mounting position
- Spring work contacts
- Tested according to IEC/EN 60947-3, UL508
- Certificate TÜV-Rheinland
- Application acc. to IEC 60364-7-712 and IEC 62548

Connection diagram

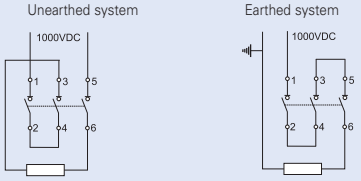

Technical Data

	P-SOL20	P-SOL30	P-SOL60
Electrical			
Number of poles	2	2	2
Rated operational voltage U_e	1000 VDC	1000 VDC	1000 VDC
Rated operational current I_e	20 A	30 A	63 A
Rated short-circuit making capacity I_{cm}	500 A	500 A	1500 A
Rated short-time withstand current 1sec. I_{cw}	700 A	700 A	1500 A
Utilization category	DC-21 A	DC-21 A	DC-21 A
Overvoltage category	III	III	III
Rated impulse withstand voltage U_{imp}	8 kV	8 kV	8 kV
Operating cycles electrical at U_e and I_e	1500	1500	1500
Internal resistance	6mΩ	5mΩ	3mΩ
Mechanical			
Width	58	58	55
Height	93	93	140
Depth	76	76	160
Weight	265 g	265 g	920 g
Mounting quick fastening on DIN rail acc. to IEC/EN 60517	35 mm	35 mm	35 mm
Screw fastening			2xM4x18
Degree of protection	IP20	IP20	IP20
Terminal capacity Flexible with end sleeve mm²	2x (1-6)	2x (1-6)	2x (1-35)
AWG	18-10	18-10	14-2
Tightening torque of terminal screws	1,7 Nm	1,7 Nm	3 Nm
Ambient temperature range	-25°C to +60°C	-25°C to +60°C	-25°C to +60°C
Climatic resistance acc. to IEC 60068-2-78	Damp heat, constant		
acc. to IEC 60068-2-30	Damp heat, cyclic		
Pollution degree2	2	2	
Operating cycles mechanical	100.000	100.000	100.000
Operating cycles mechanical per hour	≤120	≤120	≤120

Dimensions (mm)

P-SOL20
P-SOL30

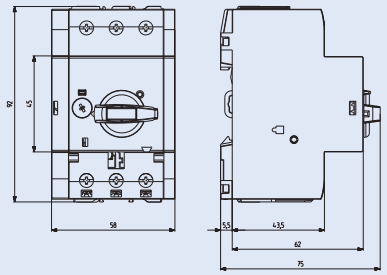

P-SOL60

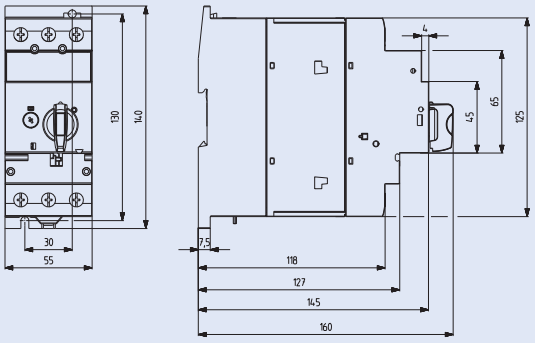

16

Photovoltaic - DC String Protection

DC Switch-disconnector SOL as pre-wired unit

- Field of application:
  DC-Disconnection in photovoltaic systems between PV Array and Inverter to switch off the energy
- Pre-wired unit ready for connection
- Lock-able in OFF-position with a padlock
- Any mounting position
- Spring work contacts
- Tested according to IEC/EN 60947-3, UL508
- Certificate TÜV-Rheinland

Connection diagram

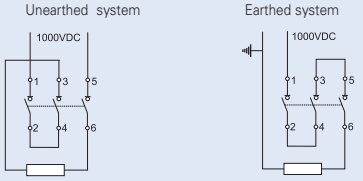

Technical Data

	SOL20	SOL30
Electrical		
Number of poles	2	2
Rated operational voltage U_e	1000 VDC	1000 VDC
Rated operational current I_e	20 A	30 A
Rated short-circuit making capacity I_{cm}	500 A	500 A
Rated short-time withstand current 1sec. I_{cw}	700 A	700 A
Utilization category	DC-21 A	DC-21 A
Overvoltage category	III	III
Rated impulse withstand voltage U_{imp}	8 kV	8 kV
Operating cycles electrical at U_e and I_e	1500	1500
Internal resistance	8mΩ	5mΩ
Mechanical		
Weight	420 g	420 g
Degree of protection	IP65	IP65
Ambient temperature range	-25°C to +60°C	-25°C to +60°C
Climatic resistance acc. to 60068-2-78	Damp heat, constant	
acc. to 60068-2-30	Damp heat, cyclic	
Pollution degree	3	3
Operating cycles mechanical	100.000	100.000
Operating cycles mechanical per hour	≤120	≤120

Dimensions (mm)

SOL20(30)	a [mm]
MC4	234
MV	224

SOL20
SOL30

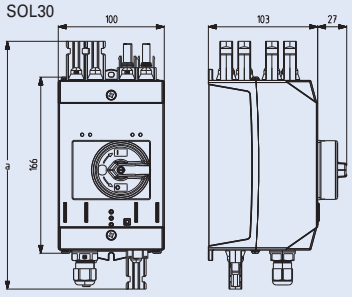

SOL20/2MC4
SOL30/2MC4

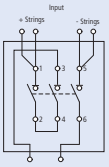

SOL20/2MV
SOL30/2MV

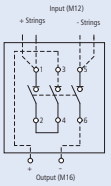

SOL20/4MC4
SOL30/4MC4

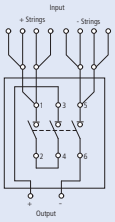

17

Photovoltaic - DC String Protection

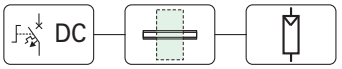

DC-String Circuit Breaker PKZ-SOL

- Field of application:
  DC-Circuit breaker for string protection
  in photovoltaic systems
- No polarity
- Spring work contacts
- Tested according to IEC/EN 60947-2
- Certificate TÜV-Rheinland

Connection diagram

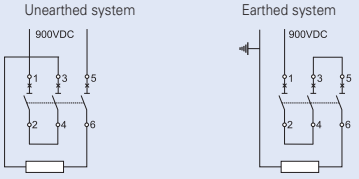

Technical Data

	PKZ-SOL4 PKZ-SOL7 PKZ-SOL12 PKZ-SOL20 PKZ-SOL30
Electrical	
Number of poles	2
Rated operational voltage U_e	900 VDC
Rated current I_n	4 / 7 / 12 / 20 / 30 A
Thermal tripping characteristic	1.05 to 1.3 x I_n
Electromagnetc tripping characteristic	6 x In
Rated ultimate short-circuit breaking capacity I_{cu}	5 kA
Rated service short-circuit breaking capacity I_{cs}	1.5 kA
Overvoltage category	III
Rated impulse withstand voltage U_{imp}	8 kV
Operating cycles electrical at U_e and I_n	1500
Internal resistance	138 / 60 / 32 / 14 / 9 mΩ
Mechanical	
Width	58
Height	93
Depth	76
Weight	265 g
Mounting quick fastening on DIN rail acc. to IEC/EN 60517 Screw fastening	35 mm
Degree of protection	IP20
Terminal capacity Flexible with end sleeve mm²	2x (1-6)
AWG	18-10
Tightening torque of terminal screws	1,7 Nm
Ambient temperature range	-25°C to +60°C
Climatic resistance acc. to IEC 60068-2-78	Damp heat, constant
acc. to IEC 60068-2-30	Damp heat, cyclic
Pollution degree	2
Operating cycles mechanical	100.000
Operating cycles mechanical per hour	≤120

Mounting position

PKZ-SOL4
PKZ-SOL7
PKZ-SOL12
PKZ-SOL20
PKZ-SOL30

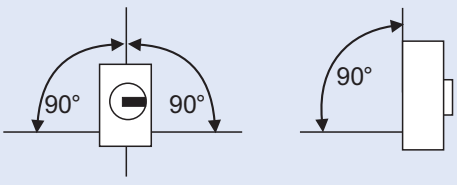

DC-String Circuit Breaker PKZ-SOL

Characteristic curve setting value - Short-circuit current

According to the design for IEC 62548-1, the tripping current for the circuit breaker must fall within a range of 1.4 to 2 times the value of the short-circuit current of the PV modules, in order to protect the PV modules.

Since only the current values for the built-in overload tripping device can be plotted on the setting scale of the circuit breaker1), the correlation between the tripping current for the safety device and the short-circuit current for the PV modules must be properly indicated for every point of the scale.

Tripping characteristic curve
String circuit breaker PKZ-SOL

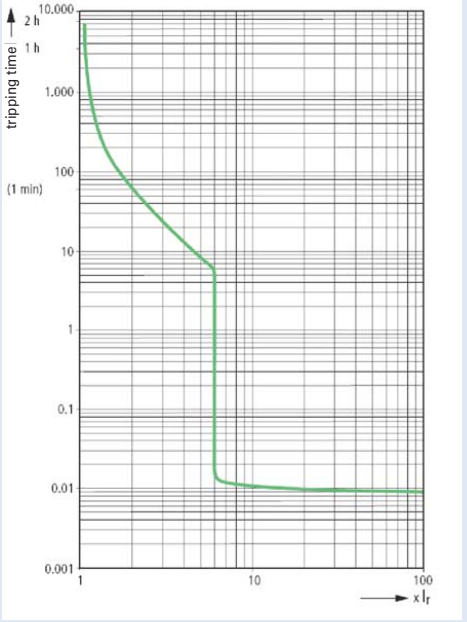

Adjustment tool for string circuit breaker PKZ-SOL

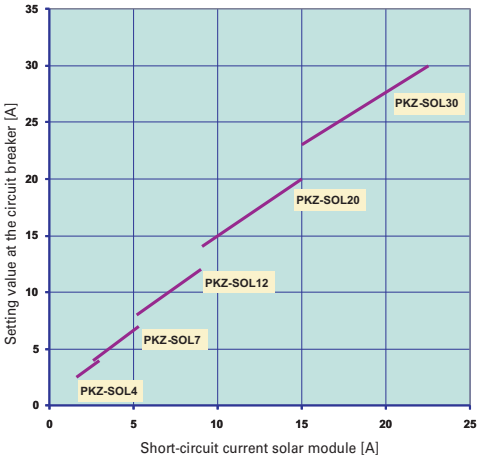

1) Norm IEC/EN 60947-2 (section 4.7.3) prohibits a direct specification of the PV short-circuit current on the circuit breaker's setting scale, whereby only the setting value for the response current may be entered.

Dimensions (mm)

PKZ-SOL4
PKZ-SOL7
PKZ-SOL12
PKZ-SOL20
PKZ-SOL30

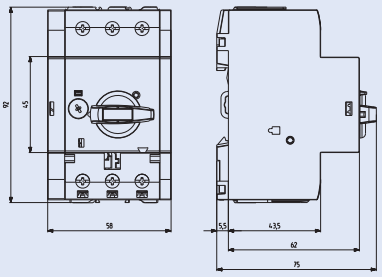

Appendix E

PV Module Ranking

	Isc			Im			Voc			Vm			Rs			Pm			Pm-Im*Vm	V'=Vmp+ΔV	P'=V'*Imin	FF
Module	Mean	Median	StdDev	Mean	Median	StdDev	Mean	Median	StdDev	Mean	Vmp_Me	StdDev	Mean	Median	StdDev	Mean	Median	StdDev				
1	6.405	6.385	0.147	5.761	5.755	0.092	20.975	20.968	0.035	15.692	15.689	0.146	0.327	0.329	0.076	90.398	90.302	0.86	0.0	16.255	89.013	0.674
18	6.386	6.389	0.038	5.710	5.706	0.041	21.381	21.382	0.021	16.575	16.567	0.041	0.297	0.295	0.059	94.635	94.644	0.52	0.1	17.011	93.149	0.692
19	6.294	6.295	0.009	5.690	5.690	0.015	21.292	21.262	0.085	16.655	16.622	0.077	0.275	0.266	0.055	94.759	94.643	0.45	0.1	17.071	93.480	0.707
3	6.341	6.344	0.025	5.668	5.672	0.052	21.282	21.281	0.022	15.279	15.278	0.080	0.480	0.405	0.283	86.593	86.619	0.57	0.0	15.689	85.909	0.642
37	6.288	6.287	0.008	5.646	5.646	0.018	21.241	21.231	0.066	16.438	16.431	0.052	0.306	0.301	0.054	92.800	92.701	0.46	-0.1	16.788	91.929	0.695
22	6.252	6.245	0.019	5.612	5.610	0.028	21.414	21.378	0.115	17.015	16.978	0.116	0.258	0.254	0.060	95.484	95.430	0.67	0.2	17.260	94.514	0.713
29	6.227	6.226	0.013	5.609	5.606	0.023	21.375	21.339	0.112	16.824	16.786	0.120	0.280	0.268	0.057	94.358	94.312	0.58	0.2	17.069	93.466	0.708
35	6.178	6.217	0.204	5.594	5.575	0.096	21.399	21.384	0.087	16.726	16.712	0.103	0.310	0.293	0.067	93.573	93.132	1.9	0.0	16.927	92.689	0.701
30	6.181	6.186	0.021	5.570	5.570	0.026	21.305	21.255	0.118	16.664	16.611	0.132	0.270	0.278	0.076	92.821	92.708	0.58	0.2	16.822	92.117	0.704
38	6.268	6.259	0.019	5.564	5.561	0.024	21.381	21.356	0.073	17.232	17.211	0.068	0.239	0.233	0.072	95.874	95.595	0.7	-0.1	17.379	95.167	0.716
23	6.138	6.182	0.194	5.620	5.555	0.162	21.330	21.296	0.113	16.651	16.695	0.235	0.303	0.295	0.948	93.563	92.761	2.64	0.0	16.872	92.392	0.704
14	6.188	6.188	0.011	5.551	5.550	0.020	21.156	21.126	0.097	16.588	16.557	0.104	0.281	0.285	0.054	92.079	91.862	0.5	0.0	16.720	91.555	0.703
40	6.190	6.186	0.021	5.530	5.541	0.091	21.159	21.161	0.081	16.793	16.799	0.078	0.257	0.257	0.057	92.868	92.991	1.54	-0.1	16.940	92.764	0.711
20	6.226	6.224	0.017	5.539	5.534	0.031	21.372	21.360	0.074	16.633	16.627	0.057	0.324	0.322	0.054	92.127	92.000	0.77	0.0	16.750	91.722	0.692
28	6.112	6.116	0.016	5.535	5.533	0.017	21.370	21.325	0.121	16.722	16.675	0.129	0.278	0.281	0.065	92.550	92.353	0.65	0.1	16.810	92.053	0.707
36	6.223	6.226	0.008	5.530	5.530	0.017	21.071	21.071	0.024	16.798	16.802	0.033	0.254	0.244	0.064	92.901	92.831	0.35	-0.1	16.913	92.614	0.708
42	6.164	6.164	0.017	5.527	5.524	0.022	21.281	21.266	0.093	16.857	16.844	0.094	0.258	0.266	0.075	93.166	93.060	0.72	0.0	16.951	92.824	0.710
21	6.200	6.203	0.014	5.509	5.514	0.029	21.236	21.204	0.108	16.758	16.726	0.102	0.286	0.286	0.063	92.320	92.106	0.87	-0.1	16.806	92.030	0.701
5	6.155	6.155	0.014	5.511	5.510	0.018	21.129	21.153	0.093	16.149	16.181	0.105	0.350	0.350	0.052	88.993	88.982	0.53	-0.2	16.259	89.034	0.685
43	6.099	6.098	0.021	5.496	5.496	0.028	21.254	21.216	0.108	16.731	16.692	0.105	0.271	0.274	0.069	91.956	91.725	0.9	0.0	16.740	91.665	0.709
15	6.122	6.119	0.018	5.490	5.492	0.028	21.171	21.156	0.048	16.513	16.495	0.054	0.290	0.295	0.058	90.651	90.766	0.53	0.9	16.532	90.527	0.700
34	6.149	6.144	0.022	5.492	5.487	0.236	21.194	21.194	0.029	16.487	16.480	0.034	0.305	0.304	0.056	90.541	90.537	0.37	0.1	16.506	90.386	0.695
31	6.159	6.161	0.115	5.485	5.486	0.018	21.344	21.328	0.065	16.661	16.647	0.083	0.292	0.298	0.068	91.384	91.357	0.47	0.0	16.669	91.280	0.695
32	6.110	6.108	0.015	5.487	5.485	0.020	21.339	21.321	0.054	16.628	16.605	0.074	0.278	0.281	0.047	91.234	91.201	0.528	0.1	16.626	91.040	0.699
27	6.130	6.129	0.011	5.488	5.482	0.026	21.305	21.273	0.092	16.827	16.791	0.096	0.272	0.281	0.064	92.343	92.338	0.615	0.3	16.806	92.028	0.706
24	6.124	6.113	0.049	5.421	5.481	0.489	21.286	21.243	0.150	16.747	16.708	0.146	0.288	0.292	0.104	90.724	91.487	8.011	-0.1	16.719	91.554	0.705
16	6.073	6.077	0.019	5.478	5.480	0.020	21.594	21.466	0.293	16.965	16.837	0.309	0.275	0.275	0.045	92.936	92.288	1.485	0.0	16.848	92.256	0.707
41	6.057	6.054	0.023	5.478	5.476	0.032	21.223	21.202	0.079	16.794	16.770	0.083	0.253	0.252	0.066	91.998	91.966	0.425	0.1	16.770	91.830	0.716
6	6.143	6.143	0.021	5.469	5.476	0.029	21.048	21.044	0.053	16.123	16.117	0.057	0.351	0.357	0.043	88.181	88.290	0.417	0.0	16.117	88.251	0.683
4	6.108	6.112	0.030	5.458	5.462	0.034	21.243	21.245	0.033	16.562	16.568	0.048	0.291	0.294	0.039	90.399	90.450	0.461	0.0	16.537	90.328	0.697
8	6.091	6.089	0.018	5.454	5.458	0.023	21.323	21.282	0.157	16.496	16.453	0.160	0.327	0.342	0.070	89.975	89.918	0.804	0.1	16.410	89.570	0.693
12	6.123	6.119	0.019	5.453	5.447	0.025	21.012	21.001	0.114	16.680	16.672	0.118	0.270	0.268	0.062	90.952	90.904	0.723	0.1	16.606	90.449	0.707
47	5.997	5.995	0.012	5.418	5.416	0.017	21.997	21.262	0.103	16.494	16.446	0.112	0.310	0.316	0.050	89.359	89.122	0.661	0.1	16.285	88.191	0.699
33	6.095	6.093	0.012	5.388	5.392	0.035	21.226	21.169	0.135	16.738	16.677	0.134	0.289	0.294	0.074	90.190	90.250	0.465	0.3	16.486	88.887	0.697
48	6.071	6.071	0.017	5.389	5.388	0.023	21.055	21.028	0.096	16.606	16.575	0.105	0.286	0.286	0.056	89.489	89.463	0.457	0.1	16.373	88.223	0.700
2	6.299	6.212	0.630	5.393	5.371	0.180	20.971	20.940	0.213	16.257	16.278	0.540	0.336	0.303	0.134	91.755	89.530	9.98	2.1	16.073	86.323	0.707
7	6.124	6.119	0.029	5.376	5.369	0.029	21.093	21.130	0.085	16.751	16.786	0.093	0.296	0.296	0.061	90.043	90.042	0.297	-0.1	16.556	88.890	0.697
25	6.063	6.067	0.019	5.357	5.356	0.027	21.199	21.154	0.096	16.966	16.919	0.101	0.264	0.272	0.074	90.881	90.746	0.546	0.1	16.647	89.162	0.706
46	6.002	6.002	0.018	5.365	5.354	0.025	21.029	21.101	0.137	16.673	16.748	0.142	0.268	0.267	0.070	89.449	89.547	0.713	-0.1	16.444	88.034	0.708
44	5.996	5.996	0.013	5.351	5.353	0.020	21.070	21.051	0.106	16.658	16.636	0.108	0.305	0.282	0.143	89.139	89.013	0.604	0.0	16.327	87.404	0.706
39	6.064	6.064	0.010	5.344	5.348	0.024	21.185	21.140	0.116	16.889	16.843	0.114	0.276	0.280	0.058	90.261	90.159	0.743	0.1	16.553	88.523	0.703
9	6.099	6.098	0.019	5.346	5.343	0.022	20.702	20.697	0.054	16.471	16.467	0.057	0.282	0.283	0.043	88.054	88.023	0.326	0.0	16.179	86.451	0.697
45	5.898	5.895	0.012	5.343	5.343	0.025	21.054	21.065	0.092	16.413	16.425	0.097	0.296	0.289	0.063	87.688	87.692	0.471	-0.1	16.030	85.650	0.707
11	6.000	6.001	0.022	5.330	5.329	0.024	21.035	21.055	0.142	16.679	16.705	0.145	0.275	0.283	0.058	88.905	88.819	0.78	-0.2	16.345	87.111	0.705
10	6.062	6.054	0.020	5.318	5.315	0.021	21.150	21.152	0.190	16.724	16.730	0.194	0.311	0.318	0.065	88.930	88.983	1.04	0.1	16.360	86.955	0.694
26	6.010	6.011	0.011	5.311	5.311	0.017	21.201	21.185	0.055	16.939	16.925	0.054	0.291	0.274	0.069	89.962	89.923	0.426	0.0	16.532	87.794	0.706
13	5.996	5.992	0.011	5.309	5.305	0.018	21.142	21.135	0.096	17.041	17.035	0.097	0.253	0.244	0.045	90.476	90.290	0.652	-0.1	16.623	88.183	0.714
17	6.024	6.039	0.031	5.276	5.280	0.031	21.387	21.249	0.334	17.197	17.052	0.361	0.226	0.261	0.045	90.721	90.337	1.473	0.3	16.614	87.717	0.702
49	4.965	4.963	0.056	2.205	2.214	0.133	20.845	20.795	0.199	53.465	53.417	1.419	-10.661	-10.892	1.483	117.905	117.765	7.931	-0.5	BROKEN!	BROKEN!	BROKEN!

Appendix F

Visual Inspection of PV Modules

Code	
1	White dots
2	Light discoloration (brown line) around the edge of cell
3	Corrosion on the cell
4	Uneven lines on the cell fingers
5	Bent/damaged frame
6	Scratch on the glass
7	Dislamination/leakage

Severity values	
1	Acceptible
2	Acceptible
3	Moderate
4	Significant
5	Extreme

Module Nb	Comments	Severity
14	1, 4	1
16	1, 2, 4, 7	1
18	2 (many cells), 3, 1, 5	2
19	1, 4, 3, 2	1
20	6, 4, 1, 2	2
21	1, 4	1
22	1	1
23	1	1
24	1, 2	1
27	1, 4	1
28	1	1
29	1, 4, 6	1
30	4, 1, 2	2
31	3, 2, 5	2
32	1, 2, 4	1
35	1, 4	1
36	1, 2	1
37	1	1
38	1, 4	1
40	1, 2, 4, 5	1
41	1, 3, 4	2
42	1, 3 (whole corner)	2
43	1, 3	2

Appendix G

Single Line Diagram

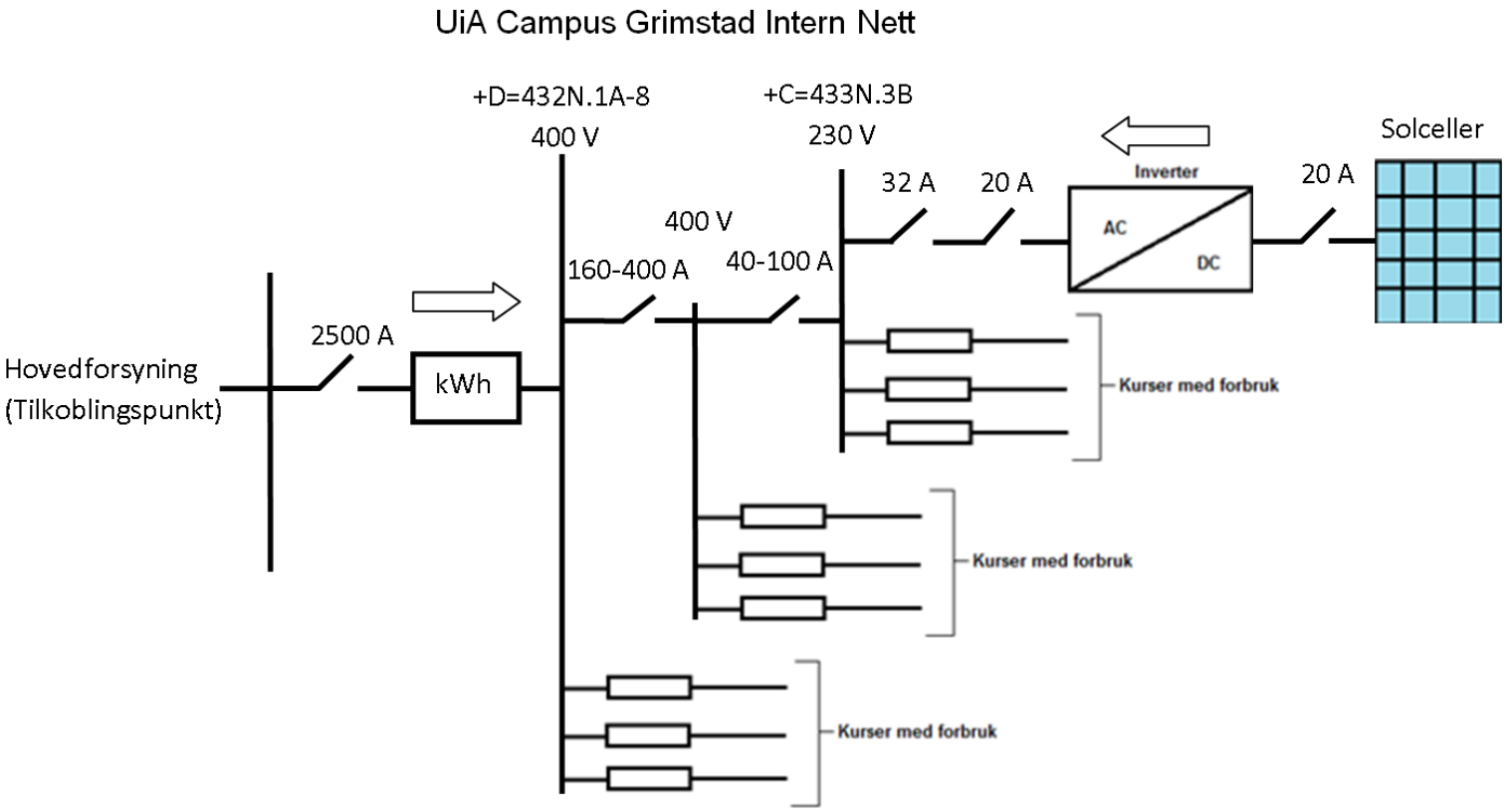
UiA Campus Grimstad Intern Nett
+D=432N.1A-8
400 V
+C=433N.3B
230 V
Solceller
Inverter
32 A
20 A
20 A
AC
DC
400 V
160-400 A
40-100 A
2500 A
Hovedforsyning
(Tilkoblingspunkt)
kWh
Kurser med forbruk
Kurser med forbruk
Kurser med forbruk

Appendix H

Price Quotation from Eltek

General commercial conditions & pricing

PN# incl DC switch and connection box, no fuse board	Product	Description	Power rating AC (W)	Price EXW Drammen
RTSCGT3K8.1043	Theia 3.8HE-t	Theia 3.8HE-t ROW DC 3xMC4 G2	3800	NOK 6840

Further conditions for the offer:

Delivery terms:

- MVA ekskl.
- Frakt fra Drammen vil tilkomme
- Standard 1 week delivery lead time within forecast

Payment terms:

- Fri lev. mnd + 30 dager

Warranty:

- Standard warranty conditions

Validity: This quotation is valid until 31st January 2014

We hope that you find this quotation according to your expectations, and look forward to hearing your response.

Best regards

Espen Kristensen

ELTEK RENEWABLE
Eltek, Andøyfaret 33, 4623 Kristiansand, Norway
MOBILE 90055248
Email espen.kristensen@eltek.com

Appendix I

Logging Capabilities of the Chosen Inverter

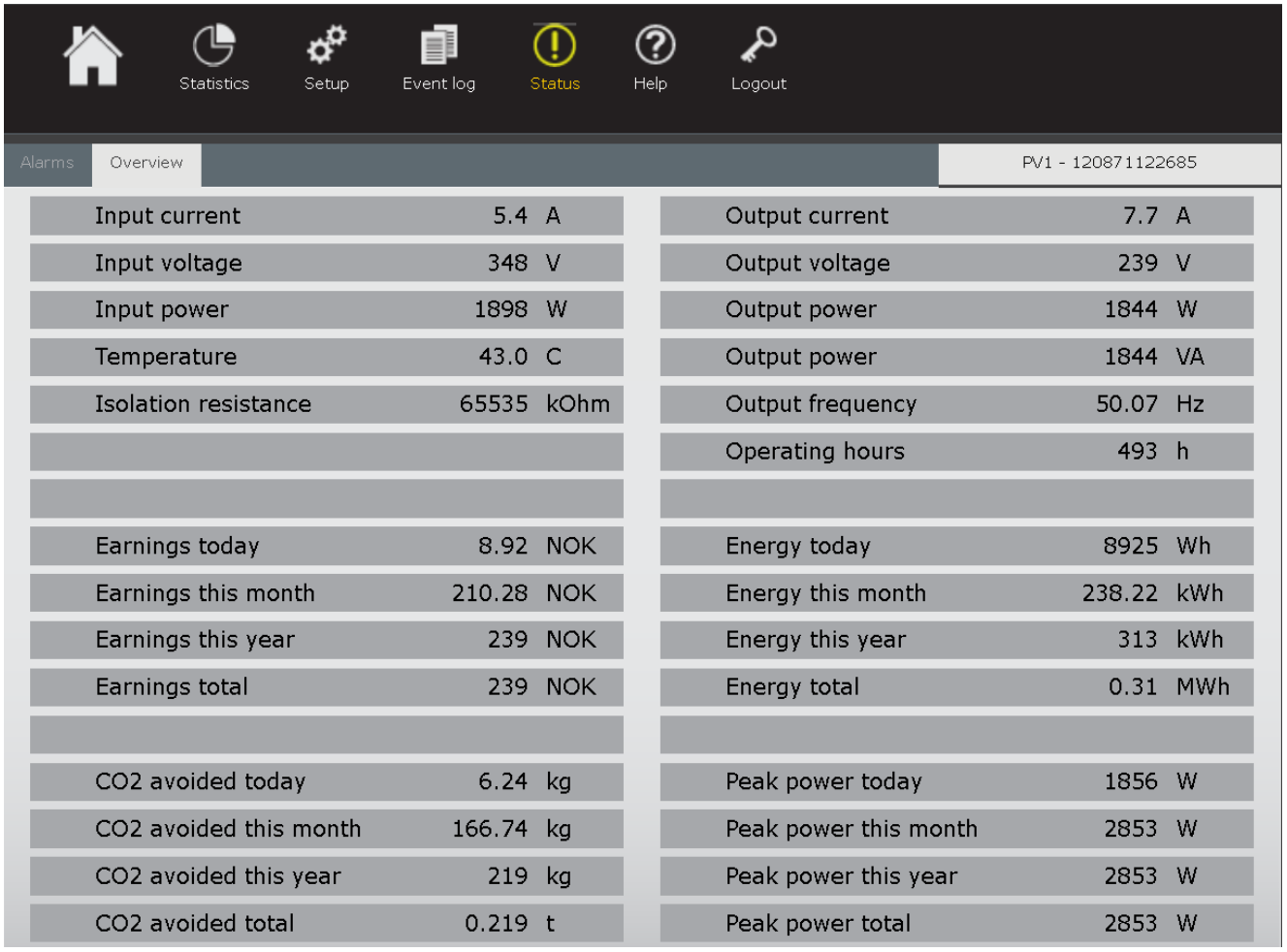
Statistics
Setup
Event log
Status
Help
Logout
Alarms
Overview
PV1 - 120871122685
Input current 5.4 A
Input voltage 348 V
Input power 1898 W
Temperature 43.0 C
Isolation resistance 65535 kOhm
Earnings today 8.92 NOK
Earnings this month 210.28 NOK
Earnings this year 239 NOK
Earnings total 239 NOK
CO2 avoided today 6.24 kg
CO2 avoided this month 166.74 kg
CO2 avoided this year 219 kg
CO2 avoided total 0.219 t
Output current 7.7 A
Output voltage 239 V
Output power 1844 W
Output power 1844 VA
Output frequency 50.07 Hz
Operating hours 493 h
Energy today 8925 Wh
Energy this month 238.22 kWh
Energy this year 313 kWh
Energy total 0.31 MWh
Peak power today 1856 W
Peak power this month 2853 W
Peak power this year 2853 W
Peak power total 2853 W


Statistics
Setup
Event log
Status
Help
Logout
THEIA | Analyz
System Status
Site: Grimstad
Site Time: 13:38
26 May 2014
Status:
Normal
Mode:
Running
System Overview:
PV1 - 120871122685
Input DC:
Current: 5.5 A
Voltage: 340 V
Power: 1880 W
Output AC:
Current: 7.6 A
Voltage: 239 V
Power: 1826 W
Operating Hours: 493 h
Current Power Production:
0 W
3800 W
Production Status
Today's Energy
3,800
1,900
26 May
06:00
12:00
18:00
8661 Wh
This Month's Energy
50
40
30
20
10
02 03 04 05 06 07 08 09 10 11 12 13 14 15 16 17 18 19 20 21 22 23 24 25 26 27 28 29 30 31
238.0 kWh
This Year's Energy
500
400
300
200
100
01 02 03 04 05 06 07 08 09 10 11 12
313 kWh

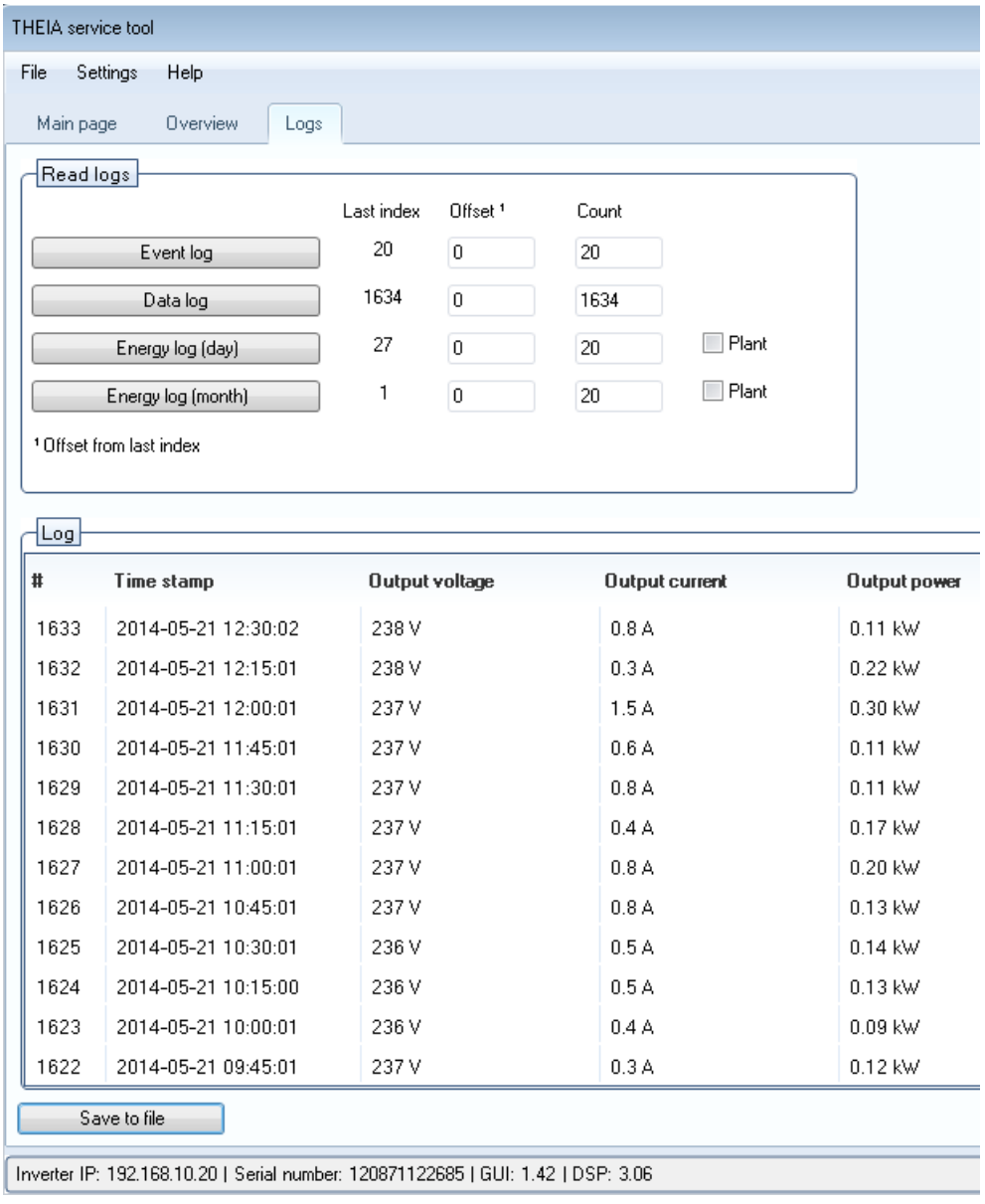
THEIA service tool
File
Settings
Help
Main page
Overview
Logs
Read logs
Last index
Offset ¹
Count
Event log
20
0
20
Data log
1634
0
1634
Energy log (day)
27
0
20
Plant
Energy log (month)
1
0
20
Plant
¹ Offset from last index
Log
Time stamp Output voltage Output current Output power
1633 2014-05-21 12:30:02 238 V 0.8 A 0.11 kW
1632 2014-05-21 12:15:01 238 V 0.3 A 0.22 kW
1631 2014-05-21 12:00:01 237 V 1.5 A 0.30 kW
1630 2014-05-21 11:45:01 237 V 0.6 A 0.11 kW
1629 2014-05-21 11:30:01 237 V 0.8 A 0.11 kW
1628 2014-05-21 11:15:01 237 V 0.4 A 0.17 kW
1627 2014-05-21 11:00:01 237 V 0.8 A 0.20 kW
1626 2014-05-21 10:45:01 237 V 0.8 A 0.13 kW
1625 2014-05-21 10:30:01 236 V 0.5 A 0.14 kW
1624 2014-05-21 10:15:00 236 V 0.5 A 0.13 kW
1623 2014-05-21 10:00:01 236 V 0.4 A 0.09 kW
1622 2014-05-21 09:45:01 237 V 0.3 A 0.12 kW
Save to file
Inverter IP: 192.168.10.20 | Serial number: 120871122685 | GUI: 1.42 | DSP: 3.06

Appendix J

Technical Guidelines (Attachment 3 from the Agreement between Agder Energi Nett and UiA)

Tekniske funksjonskrav for lavspent tilknytning av PV-anlegg

Vedlegg 3

til Tilknytnings- og
nettleieavtale for lavspente PV-enheter.

Innholdsfortegnelse

1 Krav til spenningskvalitet

1.1 Innledning

Den kraft som mates inn på Nettselskapets nett skal overholde de til enhver tid gjeldende krav til spenning og effektflyt som følger av Avtaleforholdet, med mindre Nettselskapet stiller strengere krav i det aktuelle Tilknytningspunktet. Det gjøres oppmerksom på at kravene i Avtaleforholdet er planleggingsgrenser som skal sikre at summen av flere enheter ikke fører til at kraven i forskriften oveskrides. Gjeldende offentligrettslige krav til Nettselskapets leveringskvalitet fremkommer for tiden i første rekke i *FOR-2004-11-30-1557: Forskrift om leveringskvalitet i kraftsystemet.* (Se kapittel 3 - Krav til leveringspålitelighet og spenningskvalitet.)

1.2 Tillatt Spenningsbånd

For å unngå uakseptable stasjonære spenningsvariasjoner hos sluttbrukere, skal PV - enheten ved drift ikke føre til avvik fra tillatt Spenningsbånd:

Tabell 1: Tillatt spenningsbånd i Tilknytningspunktet.

Spenningsnivå [U_n] :	Tillatt Spenningsbånd i Tilknytningspunktet:
230 V	207 V – 253 V
400 V	360 V – 440 V

1.3 Tillatte spenningssprang

PV-enheten skal ikke forårsake større antall spenningssprang i Tilknytningspunktet enn angitt i tabell 2 nedenfor. Kravene gjelder spenningssprang der spenningsstigningen er større enn 0,5 % av U_n per sekund. Grensene er oppgitt i prosent av nettets Nominelle spenning [U_n]:

Tabell 2: Spenningssprang i Tilknytningspunktet.

Spenningssprang i Tilknytningspunktet:	Tillatt antall per døgn:
$\Delta U_{\text{Stasjonær}}$ (Maksimalt 3 %)	24
ΔU_{Max} (Maksimalt 5 %)	24

1.4 Hurtige spenningsvariasjoner (flimmer)

PV-enheter skal ikke føre til at kort- eller langtidsflimmerintensitet i Tilknytningspunktet overstiger grenser gitt i tabell 3 nedenfor.

Tabell 3: Tillatt flimmerintensitet i Tilknytningspunktet.

Intensitet:	0,23 kV ≤ U_n ≤ 35 kV	Tidsintervall:
Korttidsintensitet av flimmer, P_{st} [pu]	1,0	95% av uken
Langtidsintensitet av flimmer, P_{lt} [pu]	0,8	100% av tiden

1.5 Grenseverdier for overharmoniske spenninger

1.5.1 Total overharmonisk spenning

PV-enheten skal ikke føre til at total overharmonisk forvrenging (THD) av spenning i Tilknytningspunktet overstiger grenseverdier gitt i Tabell 4.

Tabell 4: Grenseverdier for tillatt total harmonisk forvrengning.

Gjennomsnitt over:	THD [% av U_N]
1 uke (langtid)	4,5 %
10 minutter (korttid)	6 %

1.5.2 Individuelle harmoniske spenninger

PV-enheten skal ikke bidra til at de individuelle grensene i Tabell 5 for overharmoniske spenninger i Tilknytningspunktet overskrides. Alle verdier er gjennomsnittsverdier over 10 minutter.

Tabell 5: Grenseverdier for tillatte individuelle harmonisk spenninger i tilknytningspunktet.

Orden h:	[% av U_n]
5	5.4
7	4,5
11	3,2
13	2,7
17	1,8
19	1,4
23	1,4
25	1,4
>25	0,9

Orden h:	[% av U_n]
3	4,5
9	1,4
15	0,5
21	0,5
>21	0,5
2	1,8
4	0,9
6	0,5
>6	0,3

1.6 Grenseverdier for overharmoniske strømmer

PV-enhetens generatorinstallasjon skal tilfredsstille grenseverdier i Tabell 6 for relativ overharmonisk strøm som angitt i IEC 61000-3-6.

I_h er total overharmonisk strøm av orden h, forårsaket av PV - enheten, og I_i er rms-verdien av 50 Hz merkestrøm:

Tabell 6: Grenseverdier for relativ overharmonisk strøm fra PV-enheten.

Overharmonisk orden h	5	7	11	13	$\sqrt{(\sum i_h^2)}$
Overharmonisk strøm $i_h=I_{hi}/I_i$ [%]	5 – 6	3 - 4	1,5 – 3	1 – 2,5	6 - 8

1.7 Innmating av DC-strøm

PV-enheten skal ikke mate inn DC-strøm til lavspenningsnettet.

2 Krav til vern

2.1 Overordnede krav

PV-enhetens vern- og kontrollsystem skal tilfredsstille krav gitt i Avtaleforholdet og i de til enhver tid gjeldende offentligrettslige regler.

PV-enheten skal Utkobles umiddelbart dersom:

- PV-enheten forårsaker forstyrrelse i tilknyttet avgang som f.eks. effektpendlinger og spenningsavvik.
- Det oppstår utilsiktet Øydrift (frakobling skal skje innen 1 sekund etter at Øydrift har oppstått).
- Det oppstår feil internt i PV-enheten, inkludert DC-anlegg, kontrollanlegg, vern, brytere, bryterutspoler eller lignende.

2.2 Respons på over- eller underspenning

Ved over- eller underspenning i Tilknytningspunktet skal PV-enheten automatisk frakobles i henhold til krav gitt i Tabell 7 nedenfor.

Det gjøres oppmerksom på at med frakoblingstid menes tiden fra over- eller underspenning oppstår til innmating fra PV-enheten opphører.

Tabell 7: Krav til vernrespons ved over- eller underspenning i Tilknytningspunktet.

Spenningsområde i % av Nominell spenning (U_n)	Tillatt forsinkelse [s]
U >> 115	0,2
U > 110	60
U < 90	60
U << 85	0,2

2.3 Respons på unormal frekvens

Ved unormal frekvens i Målepunktet skal PV-enheten automatisk frakobles i henhold til kravene angitt i Tabell 8 nedenfor. Det gjøres oppmerksom på at med frakoblingstid menes tiden fra unormal frekvens oppstår til innmating fra PV-enheten opphører.

Tabell 8: Krav til vernrespons ved unormal frekvens i Målepunktet.

Frekvensområde [Hz]	Maksimum frakoblingstid [s]
f > 50,2	0,2
f < 47	0,2

2.4 Gjeninnkobling etter feil

For PV-enheter tillates det automatisk gjeninnkobling etter feil i nettet. Se Tabell 9 nedenfor for krav til forsinkelse.

Tabell 9: Krav til forsinkelse for gjeninnkobling etter feil.

Feilvarighet [s]	Tillatt gjeninnkobling etter: [s]
< 3s	5s
> 3s	30s

2.5 Øydriftsvern

Alle PV-enheter skal være utformet på en slik måte at innmating ved øydrift ikke kan forekomme. Ved øydrift skal PV-enheten frakobles innen 1s.

3 Krav til inverter

3.1 Respons ved feil på PV-enhetens DC-side

Invertere uten galvanisk skille (transformatorløse invertere) skal være utstyrt med RCMU. Hvis det detekteres feilstrøm på AC eller DC side som er større enn 30 mA skal inverteren koble seg fra nettet momentant. Det skal være to brytere i serie slik at det er redundans.

Det anbefales at det benyttes inverter med galvanisk skille.

3.2 Isolasjonsnivå

Isolasjonsnivået skal være større enn 1 kOhm/V for invertere uten galvanisk skille.

Appendix K

Documentation (Attachment 5 from the Agreement between Agder Energi Nett and UiA)

agder energi

Dokumentasjon

Vedlegg 5

til Tilknytnings- og
nettleieavtale for lavspente PV-enheter.

UiA Campus Grimstad PV System 1

agder energi

Innholdsfortegnelse

agder energi

1 Installatør

Det skal gis informasjon om hvem som har installert de delene av anlegget som krever godkjent el-installatør:

El-installatør:
Bjørn Håkon Lindemann Even Evensen Marius Waage Agder El. Installasjon

2 Enlinjeskjema

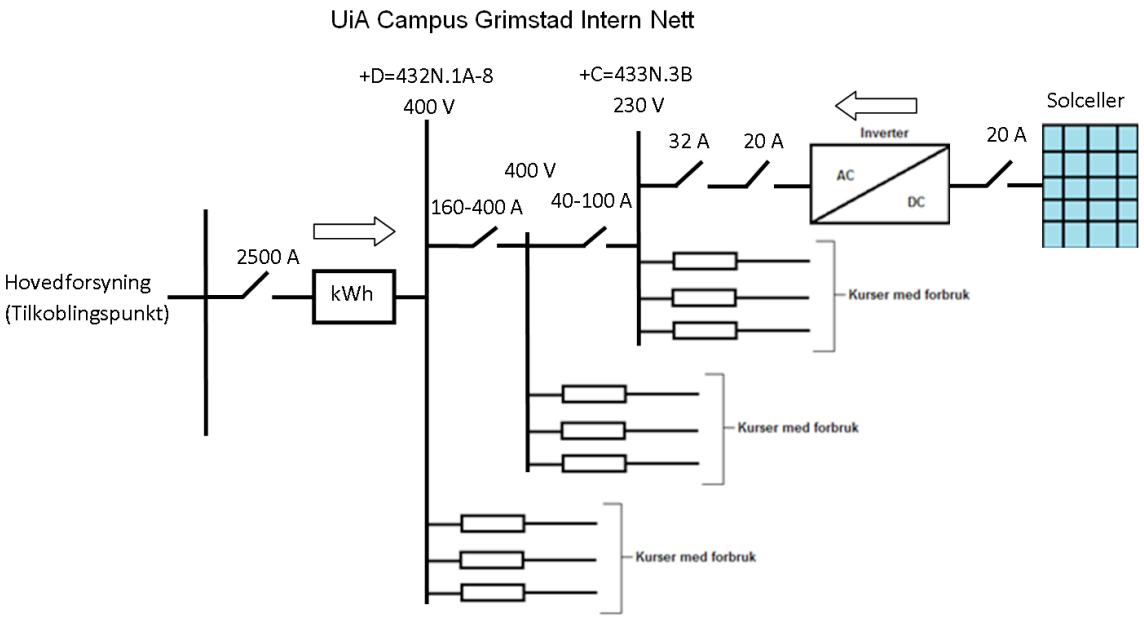

agder energi

3 Verninnstillinger

3.1 Frekvens og spenning

Tabell for innstilte verdier skal fylles ut. Disse skal være innenfor maksimale verdier bestemt av Nettselskapet. Vernene kan være plassert i inverteren og/eller i effektbryter.

Vernfunksjon	Maksimal verdi	Maksimal frakoblingstid [s]	Innstilt verdi	Innstilt frakoblingstid
Overspenning, momentan	**264,5 V**	**0,2 s**	264,5 V	0,20 s
Overspenning, forsinket	**253,0 V**	**60 s**	253,0 V	60,0 s
Underspenning, momentan	**207,0 V**	**60 s**	207,0 V	60,0 s
Underspenning, forsinket	**195,5 V**	**0,2 s**	195,5 V	0,20 s
Overfrekvens, momentan	**50,2 Hz**	**0,2 s**	50,2 Hz	0,20 s
Underfrekvens, momentan	**47,0 Hz**	**0,2 s**	47,0 Hz	0,20 s

3.2 Vern mot uønsket øydrift

Beskriv type øydriftsvern (kryss av for aktivert funksjonalitet) og fyll inn innstilt verdi:

Funksjonalitet øydriftsvern	Aktivert?	Innstilling
Rate of Change of Frequency (ROCOF) - df/dt	Ikke kjent	Ikke kjent
Voltage phase jump detection (Vector Shift) - dφ/dt	Ikke kjent	Ikke kjent
Impedance measurement	Ikke kjent	Ikke kjent
Annet (anvend merknadsfelt under for beskrivelse)		

Merknad:

3.3 Automatisk gjeninnkobling etter feil

Tabell for innstilte verdier skal fylles ut. Disse skal være innenfor minimale verdier bestemt av Nettselskapet.

Feilvarighet [s]	Minimal forsinkelse [s]	Innstilt forsinkelse [s]
< 3 s (Mindre enn 3 s)	**5 s**	5 s
> 3 s (Mer enn 3 s)	**30 s**	30 s

Appendix L

General Agreement (Main Document between Agder Energi Nett and UiA)

agder energi

Tilknytnings- og nettleieavtale for lavspente PV-enheter.

(Rammeavtalen)

mellom
Agder Energi Nett AS (Nettselskapet)
på den ene siden

og

Universitetet i Agder (Innmatingskunden)
på den andre siden

(i fellesskap Partene)

UiA Campus Grimstad PV System 1

agder energi

1 Partene

Partene i avtaleforholdet er:

Nettselskapet	
Firmanavn	Agder Energi Nett AS
Org nr.	NO 982 974 011 MVA
Postadresse	Postboks 794 Stoa, 4809 Arendal
Kontaktperson	Rolf Håkan Josefsen

Innmatingskunden	
Firmanavn	Universitetet i Agder
Org nr. / Fødselsnr.	970546200
Postadresse	Jon Lilletunsvei 9, 4879 Grimstad
Kontaktperson	Kristen Leifsen
Stilling	Driftsleder
Tlf. kontaktperson	37233031
E-post kontaktperson	kristen.leifsen@uia.no

Dersom Partene endrer sin respektive representant skal den andre parten varsles om dette skriftlig.

Partenes eventuelle endring av kontaktperson skal skje i tråd med bestemmelsene i vedlegg 2.

2 Avtaledokumenter

Tilknytnings- og nettleieavtalen mellom Nettselskapet og Innmatingskunden består av herværende dokument (Rammeavtalen) med følgende vedlegg (samlet betegnet som Avtaleforholdet):

Vedlegg 1	Definisjoner
Vedlegg 2	Tilknytnings- og nettleievilkår for lavspente PV - enheter
Vedlegg 3	Tekniske funksjonskrav
Vedlegg 4	Individuelle forhold

agder energi

Vedleggene 1-3 er i tillegg til del av Rammeavtalen, også Nettselskapets gjeldende vilkår for tilknytning og nettleie for Innmatingskunder. Dersom det foreligger saklig grunn kan Nettselskapet endre vilkårene innenfor det til enhver tid gjeldende offentligrettslige regelverk. Nettselskapet skal informere på hensiktsmessig måte om endringer som er vesentlige for Innmatingskunden. Innmatingskunden har plikt til å etterkomme endringene, selv om disse er omstridt. De til enhver tid gjeldende vilkår er tilgjengelig på Nettselskapets hjemmeside. Innmatingskunden forplikter seg til å holde seg oppdatert.

Ved uttak av kraft i Tilknytningspunktet gjelder Nettselskapets til enhver tid gjeldende vilkår for tilknytning og nettleie for privatkunder på uttakstidspunktet. Når det mates inn kraft i nettet gjelder Avtaleforholdet på innmatingstidspunktet. I tilfellet av motstrid gis Avtaleforholdets bestemmelser forrang.

Prioritetsrekkefølgen mellom Avtaleforholdets ulike deler fremgår av vedlegg 2 - Tilknytnings og nettleievilkår for innmatingskunder i distribusjonsnettet.

3 Kort beskrivelse av avtaleforholdet

Innmatingskunden mater inn elektrisk kraft til det lavspente Distribusjonsnettet i Tilknytningspunktet. Nettselskapet er leverandør av nettjenester til Innmatingskunden og eier av Distribusjonsnettet som Innmatingskundens PV-enhet er tilknyttet.

4 Identifikasjon, omfang og beskrivelse av installasjon

PV - enhetens navn	UiA Campus Grimstad PV System 1
PV - enhetens adresse og kommune	Jon Lilletuns vei 9, 4879 Grimstad
Maksimal tillatt innmatet aktiv effekt [kW]	3,8 kW
Planlagt idriftsatt [yyyy-mm]	2014-04

Sted/dato:

Svein Are Folgerø
Agder Energi Nett AS

Sted/dato:

Kristen Leifsen
Universitetet i Agder

Appendix M

Datasheet of the PV modules

NP series modules

- Electrically-matched, polycrystalline silicon solar cells for efficient conversion of both direct and diffuse light.
- Cells chemically coated for reduced reflection.
- Double redundant contacts on each cell for greater circuit reliability.
- Low iron content 3mm tempered glass cover provides mechanical protection and high light transmission.
- Circuit laminated between layers of ethylene vinyl acetate (EVA) for moisture resistance, UV stability, and electrical isolation.
- Tough, multi-layered polymer backsheet for resistance to abrasion, tears and punctures.
- Rugged, lightweight anodised aluminium frame with one or two sets of mounting holes and central holes for grounding screws.
- One or two junction boxes, designed for easy field wiring, safety and environmental protection.
- Wired-in bypass diodes reduce potential loss of power or damage from partial array shading.
- Normal Operating Cell Temperature (NOCT) 41°C (800 W per sq m, 20°C ambient).
- Laboratory tested for wide range of operating conditions (-40°C to + 85°C).
- Designed to meet or exceed the environmental requirements of IEC1215 and Ispra CEC503.

Mounting hole positions
(NP50G illustrated)
See table below

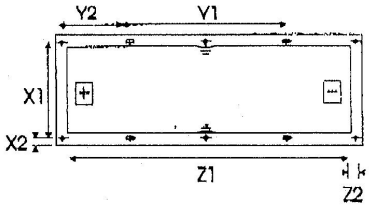

Power Specifications

	NP50G	NP50GK	NP100G12	NP100G24	
Maximum Power (± 10%)	50	50	100	100	Wp
Current (typical at max power)	3.0	3.0	6.0	3.0	A
Voltage (typical at max power)	16.7	16.7	16.7	33.3	V
Short Circuit Current (typical)	3.35	3.35	6.70	3.35	A
Open Circuit Voltage (typical)	21.6	21.6	21.6	43.1	V

The above values refer to standard test conditions of 1000 Wm-2 solar irradiance, 25°C cell temperature, Air Mass 1.5.

Physical Characteristics

	NP50G	NP50GK	NP100G12	NP100G24	
Length	1293	985	1293	1293	mm
Width	330	440	650	650	mm
Depth	34	34	34	34	mm
Depth including junction box(es)	34	37	34	37	mm
Weight	5.2	5.0	9.1	9.1	kg
Number of junction boxes	2	1	2	1	
Mounting holes (see diagram)					
Dimensions X1, X2	287, 21.5	409, 15.5	607, 21.5	607, 21.5	mm
Inner slots 7x12mm, Y1, Y2	643, 325	505, 240	643, 325	643, 325	mm
Outer holes, 7mm d, Z1, Z2	1265, 14	none	1265, 14	1265, 14	mm

Specifications may change without notice due to NAPS policy of continuous product improvement

GB-SE-PI45-1-04/98

NAPS INTERNATIONAL
Head Office
P.O.Box 3,
FIN-02151 Espoo, Finland
Tel. int +358-204-501
Telefax +358-204-505797
Internet www.neste.com

Customer Service Centre
Sähkötie 8
FIN-01510 Vantaa, Finland
Tel. int +358-204-501
Telefax +358-204-505744
Email: solar.shop@neste.com

NAPS SWEDEN AB
Måsholmstorget 2
P.O.Box 26
S-12721 Skärholmen
Tel. int +46-8-449-5930
Telefax +46-8-740 5001

NAPS NORWAY
NAPS NORWAY A/S
Strandvn. 50, N- 1324 Lysaker
Telefax [illegible]

NAPS KENYA
P.O.Box 19533
Nairobi
Tel. int +254-2-561 096
Telefax +254-2-561 098

NAPS FRANCE
Le Luzard 3
35, Allée du 12 février 1934
Noisiel
F-77437 Marne-la-Vallée cédex
Tel. int +33-1-60 373 560
Telefax +33-1-60 378 411

NESTE
Advanced Power Systems

Appendix N

Performance of Grid-connected PV from PVGIS

Performance of Grid-connected PV

PVGIS estimates of solar electricity generation

Location: 58°20'3" North, 8°34'36" East, Elevation: 47 m a.s.l.,
Solar radiation database used: PVGIS-classic

Nominal power of the PV system: 2.1 kW (crystalline silicon)
Estimated losses due to temperature and low irradiance: 7.4% (using local ambient temperature)
Estimated loss due to angular reflectance effects: 3.1%
Other losses (cables, inverter etc.): 14.0%
Combined PV system losses: 22.8%

	Fixed system: inclination=39 deg., orientation=-7 deg.			
Month	**Ed**	**Em**	**Hd**	**Hm**
Jan	1.19	36.9	0.67	20.8
Feb	2.70	75.5	1.53	42.9
Mar	4.39	136	2.57	79.7
Apr	6.54	196	3.97	119
May	7.82	242	4.90	152
Jun	8.08	243	5.18	155
Jul	7.66	238	4.95	154
Aug	6.40	198	4.11	127
Sep	4.97	149	3.08	92.4
Oct	2.97	92.2	1.77	54.7
Nov	1.50	45.0	0.86	25.7
Dec	0.87	27.1	0.49	15.2
Year	4.60	140	2.85	86.6
Total for year		1680		1040

Ed: Average daily electricity production from the given system (kWh)

Em: Average monthly electricity production from the given system (kWh)

Hd: Average daily sum of global irradiation per square meter received by the modules of the given system (kWh/m2)

Hm: Average sum of global irradiation per square meter received by the modules of the given system (kWh/m2)

Appendix O

Statement of Compliance from Agder El Installasjon

Elsikkerhetsdokumentasjon

Sluttkontroll

Agder
El·Installasjon
Tlf 37 25 80 70

Rapport fra sluttkontroll etter arbeid på elektriske anlegg

Kunde	Fra	
100159 - UNIVERSITETET I AGDER FAKTURAMOTTAK POSTBOKS 383 ALNABRU 0614 OSLO	**AGDER EL INSTALLASJON AS** Saksbehandler: Helge Rindli	
Ordre / dato	**Arbeidssted**	**Kontakt**
Ordre nr: 21233 16. mai 2014	UIA GRIMSTAD 4879 GRIMSTAD	BJØRN LINDEMANN

Anleggsbeskrivelse			
Gjelder for		Utvidelse	
Type anlegg		Barnehager/skoler	
Utført i henhold til		NEK 400:2010	
Måler nr.			
Byggeår			
Senere utbedret			
Risikovurdering			
Er det foretatt risikovurdering av anlegget?	Ikke aktuelt		
Måling/prøving			
Er det målt kontinuitet i beskyttelsesledere og utjevningsforbindelser?	Ikke utført		
Er det utført isolasjonsmåling? (Måles mellom hver spenningsførende leder og jord.)	Ikke utført		1 megaohm
Er det målt eller beregnet overgangsmotstand på jordelektroden? Angi metode og verdi.	Ikke aktuelt		
Er det kontrollert at kursene har automatisk utkobling?	Ikke aktuelt		
Er det målt atskillelse ved SELV- og PELV-kretser?	Ikke aktuelt		
Er det målt gulv- og veggresistans?	Ikke aktuelt		
Er det kontrollert spenningsfall?	Ikke aktuelt		
Er anlegget funksjonstestet?	Ja	Agder El Installasjon var tilstede ved igangkjøring av solcelleanlegg. Det ble sjekket tilkoblinger av ledningsklemmer. Videre fulgte AEI igangkjørings prosedyrene og så at dette ble utført riktig.	
Er det foretatt polaritetskontroll?	Ja	AEI utførte polaritetskontroll, fase og nøytralleder var byttet plass. Dette ble rettet! Driftsspenning var korrekt.	
Visuell kontroll			
Er utstyret CE-merket og montert i henhold til monteringsanvisning?	Ikke aktuelt		
Er kabler og utstyr betryggende festet?	Ja		
Er alle spenningsførende deler beskyttet av IP2X-kapsling eller bedre?	Ja		
Er jordelektroden tilkoblet, og har du sjekket at det ikke er blandet jordet og ujordet utstyr i samme rom?	Ja		
Er alle gjennomføringer i brannvegger tettet?	Ikke aktuelt		
Er kabeltverrsnitt valgt riktig med hensyn til spenningsfall og strømføringsevne?	Ja		
Er effektbrytere/motorvernbrytere riktig justert?	Ja		
Er jordfeilbrytere riktig valgt i forhold til type og utløsestrøm?	Ja		
Er det valgt nødvendig frakobling, sikkerhetsbryter, nødstopp og nullspenningsutløser?	Ja		
Har tilkoblet utstyr IP-grad tilpasset omgivelsene? (støv/fukt etc.)	Ja		
Er merking av PEN-, PE- og N-leder utført?	Ikke aktuelt		
Er anlegget tilstrekkelig merket?	Ja		
Er alle tilkoblinger riktig utført?	Ja		
Er skjult varme dokumentert og eier informert?	Ikke aktuelt		
Er det nødvendig adgang for drift og vedlikehold?	Ikke aktuelt		
Er selektiviteten i anlegget kontrollert (dersom dette er et krav)?	Ikke aktuelt		
Er advarselstekster montert og nødvendig dokumentasjon/informasjon overlevert til eier/bruker?	Ikke aktuelt		

Denne dokumentasjonen er i samsvar med NELFOs standardiserte sjekklister og dokumentasjonsskjema.

ELSIKKERHETSDOKUMENTASJON

Samsvarserklæring

Agder
El·Installasjon
Tlf 37 25 80 70

KUNDE	FRA
100159 - UNIVERSITETET I AGDER FAKTURAMOTTAK POSTBOKS 383 ALNABRU 0614 OSLO	**AGDER EL INSTALLASJON AS** Saksbehandler: Helge Rindli

ORDRE / DATO	ARBEIDSSTED	KONTAKT
Ordre nr: 21233 16. mai 2014	UIA GRIMSTAD 4879 GRIMSTAD	BJØRN LINDEMANN

ARBEIDSBESKRIVELSE	Kst	Prj
ARBEIDER MED SOLCELLEANLEGG VED UIA GRIMSTAD.		

Anleggsbeskrivelse			
Gjelder for		Utvidelse	
Type anlegg		Barnehager/skoler	
Utført i henhold til		NEK 400:2010	
Måler nr.			
Byggeår			
Senere utbedret			
Risikovurdering			
Er det foretatt risikovurdering av anlegget?	Ikke aktuelt		

Erklæring om samsvar skal i følge § 13 i Forskrift om Elektriske Lavspenningsanlegg oppbevares av eier av anlegget i hele anleggets levetid. Dette er et verdipapir og en garanti på at installasjonen er kontrollert og prøvet for å sikre at forskriftens krav er fulgt.

Vi erklærer at planlegging/utførelse av installasjonen er i samsvar med sikkerhetskravene i forskrift om elektriske lavspenningsanlegg. Dokumentasjonen i henhold til gjeldende regelverk er overlevert eier av anlegget.

Dato: 16.05.2014

Underskrift, installatør:

